In compliance with the
Canadian Privacy Legislation
some supporting forms
may have been removed from
this dissertation.

While these forms may be included
in the document page count,
their removal does not represent
any loss of content from the dissertation.

University of Alberta

Parametric Study of a Catalytic Flow Reversal Reactor for the Combustion of Lean Methane Emissions

by

Amika Kushwaha

A thesis submitted to the Faculty of Graduate Studies and Research in partial fulfillment of the requirements for the degree of **Master of Science**.

Department of Chemical and Materials Engineering

Edmonton, Alberta
Fall 2003

National Library of Canada
Acquisitions and Bibliographic Services
395 Wellington Street
Ottawa ON K1A 0N4
Canada

Bibliothèque nationale du Canada
Acquisisitons et services bibliographiques
395, rue Wellington
Ottawa ON K1A 0N4
Canada

Your file Votre référence
ISBN: 0-612-87805-8
Our file Notre référence
ISBN: 0-612-87805-8

The author has granted a non-exclusive licence allowing the National Library of Canada to reproduce, loan, distribute or sell copies of this thesis in microform, paper or electronic formats.

The author retains ownership of the copyright in this thesis. Neither the thesis nor substantial extracts from it may be printed or otherwise reproduced without the author's permission.

L'auteur a accordé une licence non exclusive permettant à la Bibliothèque nationale du Canada de reproduire, prêter, distribuer ou vendre des copies de cette thèse sous la forme de microfiche/film, de reproduction sur papier ou sur format électronique.

L'auteur conserve la propriété du droit d'auteur qui protège cette thèse. Ni la thèse ni des extraits substantiels de celle-ci ne doivent être imprimés ou aturement reproduits sans son autorisation.

Canada

University of Alberta

Library Release Form

Name of Author: Amika Kushwaha

Title of Thesis: Parametric Study of a Catalytic Flow Reversal Reactor for the Combustion of Lean Methane Emissions

Degree: Master of Science

Year this Degree Granted: 2003

Permission is hereby granted to the University of Alberta Library to reproduce single copies of this thesis and to lend or sell such copies for private, scholarly or scientific research purposes only.

The author reserves all other publication and other rights in association with the copyright in the thesis, and except as herein before provided, neither the thesis nor any substantial portion thereof may be printed or otherwise reproduced in any material form whatever without the author's prior written permission.

Date: September 24, 2003

University of Alberta

Faculty of Graduate Studies and Research

The undersigned certify that they have read, and recommend to the Faculty of Graduate Studies and Research for acceptance, a thesis entitled **Parametric Study of a Catalytic Flow Reversal Reactor for the Combustion of Lean Methane Emissions** submitted by Amika Kushwaha in partial fulfillment of the requirements for the degree of **Master of Science**.

Dr. Robert E. Hayes
Supervisor

Dr. Lary W. Kostiuk
External Examiner

Dr. William C. McCaffrey

Date: September 23, 2003

Abstract

Methane emissions are an important source of greenhouse gas emissions that can be reduced by conversion to carbon dioxide and water. Lean emissions can be oxidized catalytically, although relatively high temperatures are required because of the stability of the methane molecule.

To achieve auto-thermal operation of a methane combustion reactor with ambient feed, the reverse flow "heat trap" effect can be used. Furthermore, because a reverse flow reactor can achieve high temperatures, the possibility exists for extraction of the useful energy.

The internal reactor configuration, which comprises inert and catalytically active sections, determines the reactor performance. In this work, three types of inerts were studied; (1) ceramic monoliths, (2) metal monoliths, and (3) packed Denstone balls. An experimental pilot scale reactor was used to gather data at different inlet conditions, with and without hot gas withdrawal. The experimental results were used to verify a numerical model to simulate the behaviour of the reverse-flow reactor.

It is shown that physical properties of the inerts affect performance. Inerts with low thermal mass (metal monoliths) exhibit the fastest movement of temperature fronts, thus require shorter cycle times. Inlet methane concentration is key to stable performance. High methane concentrations require heat extraction to avoid overheating. The time history of the reactor is critical for the performance. Extraction of hot gas from the centre causes significant change in the temperature profile.

A two-space-dimensional numerical simulator is able to capture the critical aspects of the reactor. Correct imposition of the initial conditions is key to a good simulation.

"My pen is at the bottom of a page,
which being finished, here the story ends;
'Tis to be wished it had been sooner done,
But stories somehow lengthen when begun."
Byron

I dedicate this work to my parents, sister,
sister-in-law, brother, and my many wonderful friends.
Their love, support and patience is rarely seen in this world.

Acknowledgements

I would like to acknowledge the people, without whom, this project would not have been possible.

- My M.Sc. supervisor, Dr. Robert E. Hayes provided a wonderful opportunity for me to discover, learn and become a better researcher. Through his knowledge and support, he guided me through this academic path. I thank him for the time, patience, wisdom and encouragement that he showed during these years.
- I am greatful to Dr. Michel Poirier and Dr. Hristo Sapoundjiev at the CANMET Energy Technology Centre (Varenne, Québec). They were extensively involved with the experimental work of this project. I appreciate their patience, knowledge, and the many hours they spent in the laboratory. I also thank Vincent Simoneau for all of this help with the technical setup required for this work.
- Thank you to COURSE and NSERC for financially supporting this project.
- A sincere thank you to my collegues, Stephen Salomons, Joe Mmbaga, Sam Mukadi, Rajab Litto, and Ben Liu, who were wonderful to work with and greatly helped me along the way. A special thanks to Stephen Salomons who was patient with my many project querries.
- Thanks to the Department of Chemical and Materials Engineering (Univeristy of Alberta) for helping me become a better engineer. The Computer and Network Services for providing the computing resources, specifically Bob Barton, for helping with my computer issues.
- Last but not the least, I am extremely thankful to my wonderful family and all of my dear friends for being by my side during all obstacles great and small. Their love, support, and encouragement remains my pillar of strength in life.

Contents

1 Introduction 1

2 Background 3
- 2.1 Environmental Concerns . . . 3
  - 2.1.1 Greenhouse Gas Problem . . . 3
  - 2.1.2 Fugitive Emissions . . . 4
- 2.2 Reduction of Emissions . . . 5
  - 2.2.1 Homogeneous Combustion . . . 5
  - 2.2.2 Catalytic Combustion . . . 5
- 2.3 Flow Reversal Reactor Concept . . . 7
- 2.4 Inert Sections . . . 10
- 2.5 Modeling of the Reactor . . . 11
- 2.6 Objective . . . 13

3 Experimental and Modeling Methodology 14
- 3.1 Experimental Setup . . . 14
  - 3.1.1 Reactor Internals . . . 14
  - 3.1.2 Overall Operation . . . 18
  - 3.1.3 Control and Data Acquisition . . . 19
- 3.2 Numerical Model . . . 21
  - 3.2.1 Initial Conditions . . . 23
  - 3.2.2 Boundary Conditions . . . 24
  - 3.2.3 Conservation Equations . . . 24
  - 3.2.4 Reaction Kinetics . . . 26
  - 3.2.5 Physical Properties of the Fluid . . . 27
  - 3.2.6 Heat and Mass Transfer Coefficients . . . 27

4 Experimental Results 29
- 4.1 Fractional Conversion of Methane . . . 30
- 4.2 Inert Ceramic Monolith . . . 30
  - 4.2.1 Inert Ceramic Monolith with Heat Extraction . . . 36
- 4.3 Inert Metal Monolith . . . 38
  - 4.3.1 Inert Metal Monolith with Heat Extraction . . . 42
- 4.4 Packed Denstone Ball Inert . . . 46
  - 4.4.1 Denstone Ball Inert with Heat Extraction . . . 49

4.5 Radial Gradients of the Inert Types 52
4.6 Discussion 57

5 Simulation Model Validation **61**
5.1 Ceramic Monolith Inert 62
5.2 Metal Monolith Inert 70
5.3 Packed Denstone Ball Inert 75
5.4 Sensitivity Analysis - heat extraction 85
5.5 Parameter Analysis 86
5.5.1 Cycle Time and Velocity 86
5.5.2 Methane Concentration 88
5.6 Discussion 90

6 Conclusions and Recommendations **92**
6.1 Experimental Conclusions 92
6.2 Heat Extraction Conclusions 93
6.3 Simulation Conclusions 94
6.4 Recommendations and Future Work 95
6.4.1 Experimental 95
6.4.2 Simulator suggestions 96

Bibliography **98**

A List of Experiments and Simulations **101**
A.1 List of Experiments 101
A.2 List of Simulations Conducted 103

B Calculations used during experiments **105**
B.1 Heat extraction calculation 105
B.2 Calculating air velocities 106

List of Figures

2.1 Reverse-flow reactor mechanism 7
2.2 Heat trap effect cause by flow reversal 9

3.1 Schematic of reactor internals and thermocouple locations. Use of ceramic monoliths is illustrated. 15
3.2 Photograph of ceramic monolith seen from the top of the reactor. Reactor diameter of $0.2m$ 16
3.3 Photograph of Denstone balls from the top of the reactor . . . 17
3.4 Schematic of reactor valves and thermocouple locations. Radially placed thermocouples are shown in the circles, and the gas withdrawal system is also shown 22
3.5 Locations of the centreline thermocouples placed in the reactor shown on a numerical scale 23

4.1 Ceramic monolith: Experimental axial forward flow temperature profiles. Multiple forward flow profiles for $0.2\%CH_4$ and $0.3m/s$ superficial velocity 32
4.2 Ceramic monolith: Experimental axial forward flow temperature profiles. Multiple forward flow profiles for $0.2\%CH_4$ and $0.7m/s$ superficial velocity 32
4.3 Ceramic monolith: Experimental axial forward flow temperature profiles. Multiple forward flow profiles for $0.6\%CH_4$ and $0.7m/s$ superficial velocity 33
4.4 Ceramic monolith: Experimental axial temperature profile for one full cycle. Profile for cycle one at $0.6\%CH_4$ and $0.3m/s$ superficial velocity with switch time of $300s$ 34
4.5 Ceramic monolith: Experimental axial temperature profile for one full cycle. Profile for cycle one at $0.6\%CH_4$ and $0.7m/s$ superficial velocity with switch time of $100s$ 35
4.6 Ceramic monolith: Multiple experimental axial temperature profiles with heat extraction at $0.6\%CH_4$ and $0.3m/s$ superficial velocity with switch time of $350s$ 36
4.7 Ceramic monolith: Multiple experimental axial temperature profiles with heat extraction at $0.6\%CH_4$ and $0.7m/s$ superficial velocity with switch time of $130s$ 37

4.8 Ceramic monolith: Forward flow profiles showing heat extraction progression with 0.6%CH_4 and 0.3m/s superficial velocity with switch time of 350s 38
4.9 Metal monolith: Experimental axial temperature profile for one full cycle. Profile for cycle one at 0.6%CH_4 and 0.7m/s superficial velocity with switch time of 150s 39
4.10 Metal monolith: Experimental axial temperature profile for one full cycle. Profile for cycle one at 0.2%CH_4 and 0.7m/s superficial velocity with switch time of 150s 39
4.11 Metal monolith: Multiple experimental reverse flow axial temperature profiles at 0.6%CH_4 and 0.3m/s superficial velocity with switch time of 400s 40
4.12 Metal monolith: Multiple experimental reverse flow axial temperature profiles at 0.6%CH_4 and 1m/s superficial velocity with switch time of 60s 41
4.13 Metal monolith: Multiple experimental reverse flow axial temperature profiles at 0.2%CH_4 and 1.2m/s superficial velocity with switch time of 60s 42
4.14 Metal monolith: Multiple experimental reverse flow axial temperature profiles with heat extraction at 0.6%CH_4 and 1.2m/s superficial velocity with switch time of 60s 43
4.15 Metal monolith: Forward flow profiles showing heat extraction progression with 0.6%CH_4 and 0.7m/s superficial velocity with switch time of 150s 44
4.16 Metal monolith: Multiple experimental reverse flow axial temperature profiles with heat extraction at 0.6%CH_4 and 0.7m/s superficial velocity with switch time of 150s 44
4.17 Metal monolith: Experimental axial temperature profile for one full cycle with heat extraction. Profile for first cycle at 0.6%CH_4 and 0.7m/s superficial velocity with switch time of 150s . . . 45
4.18 Metal monolith: Experimental axial temperature profile for one full cycle with heat extraction. Profile for 8^{th} cycle at 0.6%CH_4 and 0.7m/s superficial velocity with switch time of 150s . . . 46
4.19 Denstone balls: Multiple experimental reverse flow axial temperature profiles at 0.6%CH_4 and 0.7m/s superficial velocity with a cycle switch time of 150s 47
4.20 Denstone balls: Multiple experimental forward flow axial temperature profiles at 0.2%CH_4 and 1m/s superficial velocity with a cycle switch time of 60s 48
4.21 Denstone balls: Multiple experimental reverse flow axial temperature profiles at 0.2%CH_4 and 0.3m/s superficial velocity with a cycle switch time of 150s 48
4.22 Denstone balls: Multiple experimental forward flow axial temperature profiles at 0.6%CH_4 and 0.7m/s superficial velocity with a cycle switch time of 130s 49

4.23 Denstone balls: Multiple experimental forward flow axial temperature profiles with heat extraction at $0.6\%CH_4$ and $1.2m/s$ superficial velocity with a cycle switch time of $100s$ 50
4.24 Denstone balls: Multiple experimental reverse flow axial temperature profiles with heat extraction at $0\%CH_4$ and $0.7m/s$ superficial velocity with a cycle switch time of $150s$ 50
4.25 Denstone balls: Experimental axial temperature profiles for first cycle with heat extraction at $0\%CH_4$ and $0.7m/s$ superficial velocity with a cycle switch time of $150s$ 51
4.26 Denstone balls: Experimental axial temperature profiles for the 10^{th} cycle with heat extraction at $0\%CH_4$ and $0.7m/s$ superficial velocity with a cycle switch time of $150s$ 52
4.27 Experimental radial temperature profiles in the inert ceramic monolith in the left-hand-side reactor during experimental conditions of $0.6\%CH_4$ and $0.7m/s$ superficial velocity 53
4.28 Experimental radial gradients in the inert ceramic monolith in the left side reactor for one full cycle during experimental conditions of $0.6\%CH_4$ and $0.7m/s$ superficial velocity 54
4.29 Experimental radial gradients in the inert ceramic monolith in the left side reactor for three full cycles during experimental conditions of $0.6\%CH_4$ and $0.7m/s$ superficial velocity 55
4.30 Experimental radial temperature profiles in the inert metal monolith of the left-hand-side reactor during experimental conditions of $0.6\%CH_4$ and $0.7m/s$ superficial velocity 55
4.31 Experimental radial temperature profiles for one half cycle in the inert metal monolith in both reactors during experimental conditions of $0.2\%CH_4$ and $0.7m/s$ superficial velocity 56
4.32 Experimental radial temperature profiles in the inert Denstone balls in the left-hand-side reactor during experimental conditions of $0.6\%CH_4$ and $0.7m/s$ superficial velocity 57

5.1 Ceramic monolith: Model and Experimental results for axial reverse flow temperature profile at $0.2\%CH_4$ and $0.7m/s$ superficial velocity. Profiles shown for the beginning and end of the simulation 62
5.2 Ceramic monolith: Model and Experimental results for axial reverse flow temperature profile at $0.6\%CH_4$ and $0.7m/s$ superficial velocity. Profiles shown for the beginning and end of the simulation 63
5.3 Ceramic monolith: Model results for multiple axial reverse flow temperature profiles at $0.6\%CH_4$ and $0.3m/s$ superficial velocity. 64
5.4 Ceramic monolith: Model and Experimental results for axial forward flow temperature profile at $0.2\%CH_4$ and $0.3m/s$ superficial velocity. Profiles shown for the beginning and end of the simulation 64

5.5 Ceramic monolith: Simulated axial forward flow temperature profiles. Multiple forward flow profiles for $0.2\%CH_4$ and $0.3m/s$ superficial velocity 65
5.6 Ceramic monolith: Simulated axial forward flow temperature profiles. Multiple forward flow profiles for $0.6\%CH_4$ and $0.7m/s$ superficial velocity 66
5.7 Ceramic monolith: Simulated and experimental axial reverse flow temperature profiles for $0.6\%CH_4$ and $0.7m/s$ superficial velocity, switch time $100s$ 66
5.8 Ceramic monolith: Simulated axial forward flow temperature profiles with heat extraction. Multiple forward flow profiles for $0.6\%CH_4$ and $0.3m/s$ superficial velocity 67
5.9 Ceramic monolith: Simulated axial reverse flow temperature profiles. Multiple reverse flow profiles for $0.6\%CH_4$ and $0.3m/s$ superficial velocity 68
5.10 Ceramic monolith: Model results for axial reverse flow temperature profile at $0.6\%CH_4$ and $0.3m/s$ superficial velocity with heat extraction. 69
5.11 Ceramic monolith: Model results for axial forward flow temperature profile at $0.6\%CH_4$ and $0.3m/s$ superficial velocity with heat extraction. 69
5.12 Ceramic monolith: Model results for axial reverse flow temperature profile at $0.6\%CH_4$ and $0.7m/$ superficial velocity with heat extraction 70
5.13 Metal monolith: Model results for axial forward flow temperature profile at $0.6\%CH_4$ and $0.3m/$ superficial velocity 71
5.14 Metal monolith: Multiple simulated reverse flow axial temperature profiles at $0.2\%CH_4$ and $1.2m/s$ superficial velocity . . . 72
5.15 Metal monolith: Multiple simulated axial temperature profile with heat extraction. Forward flow profiles at $0.6\%CH_4$ and $0.3m/s$ superficial velocity with switch time of $400s$ 73
5.16 Metal monolith: Multiple experimental axial temperature profile with heat extraction. Forward flow profiles at $0.6\%CH_4$ and $0.3m/s$ superficial velocity with switch time of $400s$ 73
5.17 Metal monolith: Comparison of experimental and simulated axial temperature profiles for the forward flow direction at the beginning and end of the run. Profiles for cycle one at $0.6\%CH_4$ and $0.3m/s$ superficial velocity with switch time of $400s$ . . . 74
5.18 Metal monolith: Comparison of experimental and simulated reverse flow axial temperature profiles with heat extraction at $0.6\%CH_4$ and $1.2m/s$ superficial velocity 75
5.19 Denstone balls: Comparison of experimental and simulated reverse flow axial temperature profiles at $0.2\%CH_4$ and $0.7m/s$ superficial velocity 76

5.20 Denstone balls: Multiple experimental forward flow axial temperature profiles at 0.2%CH_4 and 0.7m/s superficial velocity with a cycle switch time of 150s 76
5.21 Denstone balls: Multiple simulated forward flow axial temperature profiles at 0.2%CH_4 and 0.7m/s superficial velocity and cycle switch time of 150s 77
5.22 Denstone balls: Comparison of experimental and simulated reverse flow axial temperature profiles at 0.2%CH_4 and 1m/s superficial velocity 78
5.23 Denstone balls: Multiple simulated forward flow axial temperature profiles at 0.2%CH_4 and 0.7m/s superficial velocity and cycle switch time of 60s 78
5.24 Denstone balls: Multiple experimental reverse flow axial temperature profiles at 0.6%CH_4 and 1.2m/s superficial velocity with a cycle switch time of 100s 79
5.25 Denstone balls: Multiple simulated reverse flow axial temperature profiles at 0.6%CH_4 and 1.2m/s superficial velocity and cycle switch time of 100s 80
5.26 Denstone balls: Comparison of experimental and simulated reverse flow axial temperature profiles at 0.6%CH_4 and 1.2m/s superficial velocity 81
5.27 Denstone balls: Comparison of experimental and simulated reverse flow axial temperature profiles at 0.6%CH_4 and 0.3m/s superficial velocity 81
5.28 Denstone balls: Multiple simulated reverse flow axial temperature profiles at 0.6%CH_4 and 0.3m/s superficial velocity and cycle switch time of 400s 82
5.29 Denstone balls: Multiple experimental reverse flow axial temperature profiles at 0.6%CH_4 and 0.3m/s superficial velocity with a cycle switch time of 400s 83
5.30 Denstone balls: Comparison of experimental and simulated reverse flow axial temperature profiles with heat extraction at 0.6%CH_4 and 1.2m/s superficial velocity with a cycle switch time of 100s 84
5.31 Denstone balls: Multiple simulated forward flow axial temperature profiles at 0.6%CH_4 and 1.2m/s superficial velocity and cycle switch time of 100s 85
5.32 Comparison of different heat extraction ratios at the 5^{th} cycle. Experimental and simulated forward flow axial temperature profiles with heat extraction at 0%CH_4 and 1.2m/s superficial velocity with a cycle switch time of 100s 86
5.33 Comparison of different heat extraction ratios at the 10^{th} cycle. Experimental and simulated forward flow axial temperature profiles with heat extraction at 0%CH_4 and 1.2m/s superficial velocity with a cycle switch time of 100s 87

5.34 Comparison of different cycle switch times at the 5^{th} cycle. Simulated reverse flow axial temperature profiles at $0.6\%CH_4$ and $0.7m/s$ superficial velocity 88
5.35 Comparison of different superficial velocities at the 5^{th} cycle. Simulated reverse flow axial temperature profiles at $0.6\%CH_4$ and switch time of $100s$ 89
5.36 Comparison of different methane concentrations at the 5^{th} cycle. Simulated reverse flow axial temperature profiles at a superficial velocity of $0.7m/s$ and switch time of $100s$ 89

List of Tables

3.1 Characteristics of Inert Materials 17

A.1 **Experiments conducted without heat extraction** 101
A.2 **Experiments conducted with heat extraction** 102
A.3 **Simulations conducted with ceramic monoliths** 103
A.4 **Simulations conducted with metal monoliths** 104
A.5 **Simulations conducted with Denstone balls** 104

...

List of Symbols

symbol	units	description
A	m^2	area
a_v	m^2/m^3	surface area per unit volume
C	mol/m^3	gas molar density
C_p	J/kgK	heat capacity
D_C	m	characteristic diameter of a particle
D_H	m	hydraulic diameter
D_K	m^2/s	Knudsen diffusion coefficient
D_R	m	reactor internal diameter
$\dot{E}$	kJ/hr	rate of energy flow
G		radial conduction factor of a monolith
ΔH_n	kJ/g	enthalpy of combustion of methane
ΔH_R	J/mol	enthalpy of reaction of methane
h	W/m^2K	heat transfer coefficient
k	W/m^3	thermal conductivity
k_m	m/s	mass transfer coefficient
k_R	s^{-1}	first order rate constant
L_C	m	characteristic length of a particle
M	g/mol	molecular mass
$\bar{M}$	g/mol	average molecular mass
$\dot{m}$	kg/hr	mass flow-rate
P	Pa	pressure
Pr		Prandtl number
Q_{CH_4}	L/hr	volumetric flow-rate of methane
r_p	m	mean radius of catalyst pores
R_e		Reynolds number
R_g	$J/mol\ K$	ideal gas constant
Sc		Schmidt number
T	$K, ^oC$	temperature
V	m^3	volume
v	m/s	interstitial velocity
v_s	m/s	superficial velocity
$\dot{v}$	m^3/hr	volumetric flow-rate
Y		gas phase mole fraction

Greek Letters

symbol	units	description
ϵ		porosity
η		effectiveness factor
ρ	kg/m^3	density
μ	$Pa\,s$	viscosity
ϕ		Thiele modulus
τ		tortuosity factor

Subscripts and Superscripts

symbol	description
a	axial direction
eff	effective value in composite medium
f	fluid properties
r	radial direction
s	solid properties

Chapter 1

Introduction

The continual and increased emissions of harmful greenhouse gases through human activity has become a concern for improvement and maintenance of the environment, as well as human health. By ratifying the Kyoto protocol in 2003, Canada committed to reduce its levels of harmful greenhouse gas emissions by 6% below 1990 levels by 2010. It has been suggested that greenhouse gases are the cause for global warming.

Methane is one of the most harmful greenhouse gases, and reducing methane levels can significantly reduce the number of equivalent carbon dioxide emissions. Major sources of methane emissions are coal mining and conventional oil and gas processing facilities. These emissions are often lean ($0.1-1.5\%v/v$) in concentration and ambient in temperature. To reduce emission levels, the combustion of this gas has been proposed [1].

Two options for combustion exist; (1) homogeneous combustion and (2) catalytic combustion. This study focuses on catalytic combustion, which is a flameless combustion process that uses a catalyst to promote the reaction. A catalytic reverse flow reactor (CFRR) has been successful in converting lean methane feeds to carbon dioxide in experiments conducted on a pilot-plant reactor. The reverse flow technology allows for cool and lean inlet gases to be catalytically converted through an auto-thermal process.

This reactor consists of inert and active beds. The inert beds serve as heat traps as they retain the thermal energy being produced in the reactor. The cool inlet gas is sufficiently heated as it passes through the inert beds, such

that by the time it reaches to the active beds, the combustion reaction is led to completion. This study focuses on three different types of inert beds; (1) ceramic monoliths, (2) metal monoliths, and (3) packed Denstone balls. Each having different physical properties show somewhat different behaviour as lean methane is combusted in the fixed packed bed reactor.

To alleviate the costs and energy requirements associated with multiple experimental operations, numerical modeling has become an important tool for the investigation of such complex systems. Many models have been proposed for reverse-flow reactors. This study validates a two dimensional, continuous heterogeneous model with the aid of experimental data obtained from the pilot-plant catalytic reverse flow reactor.

The remainder of the thesis is structured as follows. Background and details about the reverse flow technology is presented in Chapter 2. Chapter 3 describes the experimental and modeling methodologies used for the study. Experimental apparatus and operating procedures are described, along with an introduction to the numerical model used to simulate the reactor system. Chapter 4 presents the experimental results obtained from the various operating conditions used for this study. The validation and comparison of the numerical model with the experimental results is found in Chapter 5. Chapter 6 presents the conclusions and recommendations gathered from this work, along with suggestions for future work. Appendices A and B present the operating conditions tested, and important calculations used for this study, respectively.

Chapter 2

Background

2.1 Environmental Concerns

Concerns about the impact of increased pollution and climate change, along with Canada's ratification of the Kyoto protocol, has focused much attention on the reduction of greenhouse gases (GHG's) in the atmosphere. It is believed that the release of GHG's is a cause for global warming via the greenhouse effect. Emissions such as carbon dioxide, methane, and nitrous oxide from human activity have become a primary concern for the well being of the environment.

2.1.1 Greenhouse Gas Problem

In 1997 Canada joined 164 countries that committed to improve the global environment, and reduce greenhouse gas emissions. Canada agreed to reduce its GHG emissions to 6% below 1990 levels by the year 2008-2012. Presently, Canada contributes about 2% of the world's total global GHG emissions, and is the highest per capita emitters owing to its resource-based economy, climate and size [2].

Excessive levels of GHG in the air has led to global warming, increased health problems, and environmental risks. The reduction of harmful GHG's has become an increasingly important issue over the years. The primary GHG's that are of main concern are carbon dioxide (CO_2), methane (CH_4) and nitrous oxide (N_2O), which are abundant throughout the world [2]. In 2002, CO_2 accounted for 78% of Canada's total greenhouse gasses, CH_4 ac-

counted for 12.6%, and N_2O accounted for 7.4%. Therefore methane is the second most important GHG. When methane is completely combusted it has 1 : 1 molar ratio with carbon dioxide through the following chemical equation:

$$CH_4 + 2O_2 \longrightarrow CO_2 + 2H_2O \tag{2.1}$$

Methane has a global warming potential of about 23 times that of carbon dioxide [2], that is, one tonne of methane has the GHG warming potential of 23 tonnes of CO_2 based on a 100 year life analysis. The reduction of methane emissions would have more positive impact in the atmosphere and will reduce surface air-pollution [3]. Therefore, research and implementation of methods for reducing equivalent carbon dioxide emissions through the reduction of methane emissions have become increasingly important [4].

2.1.2 Fugitive Emissions

Canada's primary sources of methane gas emissions are fugitive sources, which are underground coal mining, and natural gas and petrochemical production and transmission. In 2001, Canada produced a total of 54 800 kilotonnes CO_2 equivalent of methane. Coal mining produced 990 kilotonnes of CO_2 equivalent of methane, and the rest was from oil and gas production. Nearly 5% of Canada's total emissions for that year, were from fugitive sources, with about 90% of the fugitive emissions being from conventional oil and gas processing [2].

Methane emissions from these sources are typically dilute ($0.1 - 1.5\ v/v\%$) [5], and at ambient temperature and pressure. At low concentrations and flow-rates it becomes difficult to combust methane emissions using conventional methods. Methane, being a very stable compound with a tetrahedron structure, requires a high temperature to initiate the combustion reaction. A significant amount of heat energy would be required to bring the dilute methane gas to a sufficiently high temperature to sustain combustion.

2.2 Reduction of Emissions

Two options exist for the combustion of fugitive methane emissions; (1) homogeneous combustion, and (2) catalytic combustion.

2.2.1 Homogeneous Combustion

The most common use of homogeneous combustion in oil and gas applications involves the use of a flare. This method of eliminating fugitive emissions has been used for many years, as it can be cost effective. However, flaring is unpopular with the public, and obtaining flaring permits can be quite time consuming.

Dealing with various gasses produced from oil drilling operations often involves storing and mixing with other oils underground. To control the accumulation and to avoid the hazardous outcomes from excess storing, a relatively easy and cheap method of their elimination is to burn the gasses. Because of high temperature of the combustion, flaring can lead to producing other harmful substances such as NO_x, which is another pollutant of significant concern [2]. At low concentrations of the emissions, a support fuel may be required to assist with flaring of the emissions. This can also become economically unfeasible, by adding higher operating costs, and safety concerns, as well as increase greenhouse gases into the atmosphere. Homogeneous combustion is best conducted when the methane concentration is above 5%. As mentionned before, many methane emissions are dilute (below $1.5\% v/v$).

2.2.2 Catalytic Combustion

The second option for burning methane emissions is to use catalytic combustion. This is a flameless combustion process that uses a solid catalyst to promote the reaction. The first record of such combustion was recorded in 1818, when Sir Humphry Davy observed that methane reacted on a platinum wire without a flame, but enough heat was produced for the continuity of the reaction [1].

There are several advantages of using catalytic combustion. One of these

advantages is that relatively low inlet temperatures can be used, compared to those used for homogeneous combustion. Low concentrations of methane can be combusted without the use of any support fuel. This nearly eliminates the lower flammability limits for the combustion reaction and results in lower NO_x emissions. This form of combustion is limited by the inlet gas temperature and catalyst activity, which depends on the type of catalyst being used [1].

Catalysts are introduced to a system to increase the rate of reaction by lowering the activation energy. Two types of catalysts exist; (1) homogeneous catalysts, where the reactants and catalyst are in the same phase, and (2) heterogeneous catalysts, where the reactant is in a different phase than the catalyst [1]. Catalysts for the process of catalytic combustion are heterogeneous.

Both noble and non-noble metals can be used as catalysts for the combustion process. Catalysts such as platinum (Pt), palladium oxide (PaO), and iron oxide(Fe_2O_3), supported with other compounds such as aluminum oxide (Al_2O_3) and titanium oxide (TiO_2), have been used for catalytic combustion operations [6] [7] [8] [9] [10] [11] [4]. The use of perovskites(cheap transition medal based oxides) has also been reported for catalytic combustion processes [12].

The study of catalytic combustion for the elimination of waste gases has been ongoing for many years [13] [14] [15] [16]. Typical conditions involve lean methane streams at ambient temperatures. To increase the temperature of the feed gas, a pre-heating step is usually employed before the combustion reaction. Preheating methods include external heat sources, heat exchangers using the hot outlet gas, and using the thermal mass in the reactor by periodically switching flow directions. The first two methods mentioned can be associated with additional costs adjusting for increase in power consumption and pressure drop. The main advantage of the third option of periodic flow reversal is that its energy efficiency is greater than that of reactors with recuperative heat exchange [17].

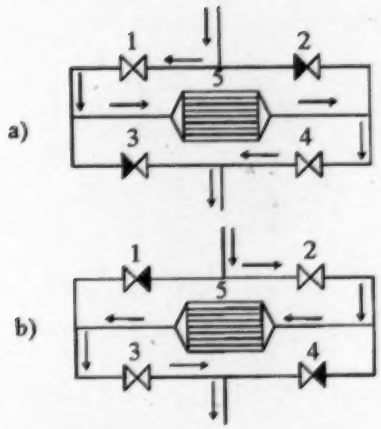

Figure 2.1: Reverse-flow reactor mechanism

2.3 Flow Reversal Reactor Concept

The technology of periodic reverse flow fixed bed reactor has been widely discussed [17] [18] [19] [20] [21] [22]. The use of the periodic flow reversal reactor was popularized by Matros and his co-workers for sulfur dioxide oxidation, catalytic incineration of volatile organic compounds, oxidation of lean methane, and reduction of NO_x [13] [16] [17] [11] [19]. It encompasses an array of aspects which are not only beneficial for energy requirements, but also for the reduction of harmful gasses in the environment, since heat can be extracted from this fixed bed reactor system [23] [15].

In a fixed bed flow reversal reactor, the inlet and outlets are not fixed. Instead, the inlet is periodically switched as the direction of the feed gas is switched between the two sides of the reactor. In a catalytic flow reversal reactor (CFRR), the front and end parts of the reactor act as a regenerative source, such that no external heat is required to sustain combustion. The forward and reverse flow concept is shown in Figure 2.1. Control valves are used to switch the direction of the flow. In Figure 2.1(a), opening valves 1 and 4 to allow the feed gas to flow from left to right, otherwise known as forward flow. To switch the direction to reverse flow, the valves 2 and 3 are opened, and the gas flows from right to left, as seen in Figure 2.1(b).

A full cycle refers to the completion of a forward and reverse cycle. One half-cycle is when either the forward or reverse cycle is completed. The switch-time is referred to the time taken for completing one half cycle. When each half-cycle is of the same duration, it is referred to as symmetric operation. If the flow directions have two different durations, it is known as an asymmetric operation. The full cycle duration is the sum of the times for forward and reverse flow times [19].

Figure 2.2 shows how the reverse flow mechanism can help trap the heat within the reactor. A possible axial temperature profile seen for unidirectional flow is shown in Figure 2.2(a). The inlet is cool and as the gas passes through the reactor, the combustion reaction takes place and heats the rest of the reactor. If the reactor loses more heat than is produced, over time, the thermal profile is pushed forward through the reactor, and the heat being generated escapes through the outlet, as seen in Figure 2.2(b). Since the gas is continued to be fed at low temperatures, the reactor cools, and over time the reactor is extinguished unless the gas is fed from the opposite direction, meaning the flow direction is switched. The heat at the outlet of the reactor can be used to pre-heat the feed and continue the combustion reaction. Switching the direction to reverse flow, shown in Figure 2.2(c), pushes the peak temperature toward the center of the reactor. Periodic switching allows for the "hot-spot" to remain in the center of the reactor as seen in Figure 2.2(e). Provided that the switch time is carefully chosen, and the reactor temperatures remain hot enough to sustain the reaction, an auto-thermal operation can be established. By periodically reversing the direction of flow, the stored energy is added to the feed stream, making it possible to achieve temperatures that are higher than the adiabatic temperature rise based on the fresh feed inlet temperature [19].

A well designed and operated reactor would be able to thermally sustain itself once there is sufficient heat present to initiate the reaction.

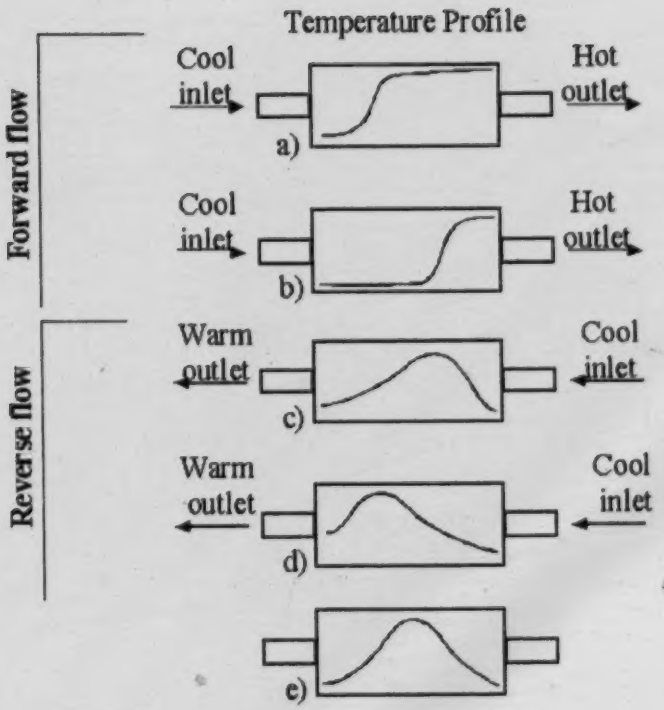

Figure 2.2: Heat trap effect cause by flow reversal

2.4 Inert Sections

Inert sections containing monoliths or packed beds can help to contain the heat within the reactor, leading to an auto-thermal operation by creating a heat-trap effect. These inert beds are often placed near both ends of the reactor and are present to heat the gas before it passes through the active catalytic bed section.

Before initiating the reaction with cold feed, the inert and active beds must be pre-heated, such that the active beds maintain temperatures that can initiate the reaction. Preheating of the inert and active sections can be done by using an external heat source, such as a heating blanket around the active section [24] [23]. Another method of preheating the materials is to pass hot air through the system, and use flow-reversal to ensure that both inert and active beds achieve sufficiently high temperatures. Once the active sections reach temperatures which can initiate the combustion reaction, the methane gas can then be introduced into the system, and the heat of combustion can be used to further increase the thermal energy of the reactor.

During the uni-directional operation, the left inert bed, which is initially hot due to pre-heating, cools down as the feed gas passes through. At the same time, the right inert bed heats up, as the combustion reaction takes place in the active zone, which is between the two inert beds. Once the flow direction is switched, the right inert bed cools down, while the left inert bed heats up [23]. Sufficient heat can be generated in the reactor such that thermal energy can be extracted through the mid-section of the reactor.

Types of inerts used in the reactor are chosen by the designer. Structured monoliths are widely used in the automotive industry as well for catalytic incineration [20]. Various shapes and materials are available for monoliths. Materials such as ceramics and metal alloys have been used [1]. Monoliths have a high surface to volume ratio, and result in a low pressure drop across a column. An even flow distribution can be established with monolith structures.

Packing the inert bed with spheres, Raschig rings, Berl saddles, etc., is another option for inert bed materials. Packed Denstone balls have been used

as inert material in reverse-flow reactors. A disadvantage of using a packed inert bed section is that the pressure drop across the column increases significantly. Comparing the pressure drop between inert ceramic monolith section with that of inert Denstone balls, showed that the pressure drop with the inert ceramic monolith was less by nearly one-tenth [25]. This increase in pressure drop with the packed bed inert increases the operating costs eventhough the thermal capacity of such packing is high.

2.5 Modeling of the Reactor

The reverse flow catalytic reactor has been modeled using one and two dimensional models to analyze reactor characteristics such as cycle period, bed length, and catalyst type [16] [26] [27] [28] [15]. Experimental results have used to validate the various types of proposed models.

Developing numerical models for periodic-flow reversal reactors is advantageous such that a better understanding of the system is achieved while reducing the number of experiments that might be conducted. A wide variety of experimental operations would help in the validation of a proposed numerical model for the system, and may determine an optimal design for flow reversal reactors. Once a model is validated, the reactor operation with new components, new dimensions, and new conditions can be tested at a lower cost than with experimentation.

One and two dimensional, discrete and continuous models have been developed, with homogeneous, pseudo-homogeneous, and heterogeneous model configurations [29] [30] [10] [31] [14]. Two dimensional models account for more of the dynamics present in the reverse-flow system rather than a one dimensional model [24]. In a one dimensional model, the radial and angular directions are ignored. A one dimensional model uses less computing time. Two dimensional models can simulate both the radial and axial effects in the reactor which may lead to better agreement with the experimental results.

Continuous models are more widely used over discrete models, as these models save computational effort, as well as show better agreement with ex-

perimental results [29]. Continuous models for a monolith assume that the gas and solid phases are locally and uniformly dispersed. In other words, there is no spatial distinction between solid and fluid. In essence, one uses a volume average property. Discrete models, on the other hand, model the complete structure at the particle size or channel size scale. Discrete models are computationally very expensive to solve and are, in practice, seldom used.

Homogeneous and heterogeneous models have been proposed for predicting the behaviour of reverse-flow reactors with monoliths in the inert beds, packed active beds as well as monolith active beds [32] [17] [33] [1]. Models that only consider one phase, or combine the solid and fluid phases, are referred to as homogeneous model. This type of model assumes that a parameter (temperature, concentration, etc.) at a point in the reactor is the same for both solid and fluid [24]. Heterogeneous models allow for the differences in temperature, concentration, etc. The phases are coupled through model equations, therefore, the two phases are considered.

Among many things, a major challenge in developing a model is to properly include the heat and mass transfer effects in the reactor. Heat transfer by radiation, convection, and conduction may be present in the system. Heat and mass transfer coefficients are one of the key parameters for a proper model. Sherwood and Nusselt dimensionless quantities, which quantify mass transfer effects, are well explained in Reference [34]. Heat transfer dimensionless quantities play a key role for both boundary conditions and accumulation of thermal energy in the reactor. Heat and mass transfer coefficients as well as the diffusion coefficient for catalysts are key parameters. For exothermic reactions, both of these numbers are required for two-phase models in order to fully characterize the system [35]. Reaction rates and effectiveness factors have been extensively studied for better prediction of the reactor system [32].

2.6 Objective

The purpose of this project was as follows:

- To study a catalytic solution for relatively high (greater than $100 kg/hr$) flow-rate sources of lean fugitive methane emissions. Examples of such sources are underground coal mines and tank filling operations.
- To study the effects of heat extraction and different inert sections used in the catalytic flow reversal reactor (CFRR) and their behaviour at different operating conditions.
- to validate a previously developed numerical model for the reactor with the new experimental results.

Chapter 3

Experimental and Modeling Methodology

3.1 Experimental Setup

The experiments were conducted on a pilot plant catalytic flow reversal reactor located at the CANMET Government of Canada labs at Varennes, Québec. Overall, the reactor consisted of two parallel reactor columns connected at the bottom by a U-bend. A schematic of the reactor is given in Figure 3.1 The diameter of the two reactor sections was $0.2m$, and each section is referred to as the left and right sides, or the 1^{st} and 2^{nd} reactor, respectively. The flow through the reactor was directed in either the forward or the reverse direction with the use of three-way valves at the top of each reactor. Forward flow refers to when the gas is flowing from reactor 1 to reactor 2. The reactor was made of hastelloy, and was thoroughly insulated to minimize thermal losses into the atmosphere. The reactor could be operated at temperatures not exceeding 1020^oC. Each reactor was approximately $1.28m$ in length from top cover to bottom cover.

3.1.1 Reactor Internals

The reactor internals consisted of the inert sections, active section, and open spaces. Three types of inerts were investigated; (1) ceramic monoliths, (2) metal monoliths, and (3) packed bed of Denstone balls. The inert sections aid in retaining the thermal energy within the active zone, thus minimizing heat

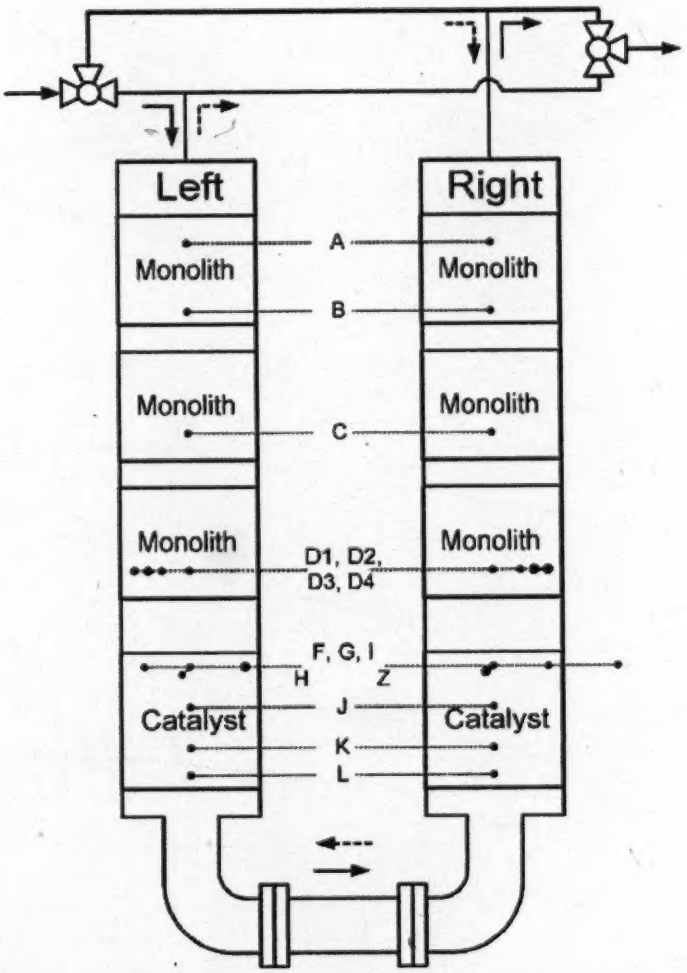

Figure 3.1: Schematic of reactor internals and thermocouple locations. Use of ceramic monoliths is illustrated.

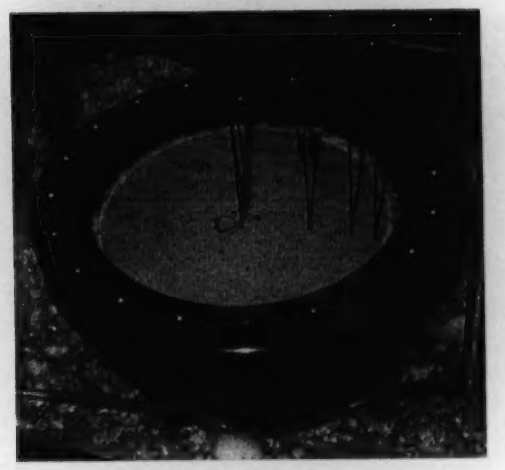

Figure 3.2: Photograph of ceramic monolith seen from the top of the reactor. Reactor diameter of $0.2m$

loss through the outlet. The air gaps allow mixing of the gas stream making the temperature more radially uniform.

Inert Sections

The total inert height remained the same at $0.7m$ for each inert type studied, however the actual number of inert sections within the reactor varied with different inert types. Regardless of the flow direction, the gas would pass through three inert ceramic monolith sections, each $0.205m$ in height, separated by a $0.035m$ void space, giving a total inert height of approximately $0.69m$. The ceramic was made up of 49% silicone oxide, 35.4% magnesium oxide, and 13.5% aluminum oxide, with 69% fractional open frontal area, and a bulk density of $530kg/m^3$. The monoliths had a surface area of $1340m^2/m^3$ and a hydraulic diameter of $2.108mm$ with square channel openings. Figure 3.2 shows the top of the reactor placed with ceramic monoliths. The inert ceramic monoliths were provided by Corning Environmental Technologies (USA), each weighing $2.94kg$.

The metal monolith configuration consisted of four inert metal monoliths, each $0.015m$ in height and separated by a $0.025m$ gap. The metal monolith was supplied by Performance Industries Incorporated, was made of SS430 metal,

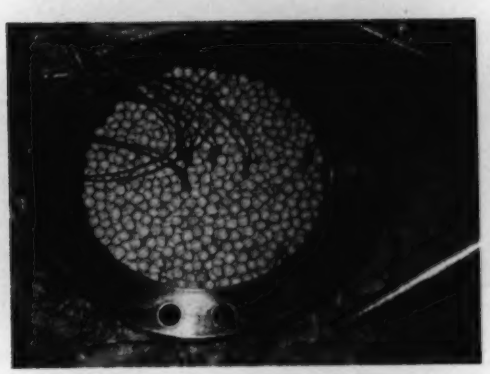

Figure 3.3: Photograph of Denstone balls from the top of the reactor

and had a surface area of over $2000m^2/m^3$. The monoliths had a bulk density of $532kg/m^3$, and a fractional open frontal area of 93%. The hydraulic diamter was $1.57mm$ and the channels were triangular in shape.

Denstone ball packing, provided by Norton Chemical Process Products Corporation(USA), was the third type of inert material studied, and was well packed to a total height of nearly $0.7m$ in each reactor. Figure 3.3 shows the reactor filled with Denstone balls. The Denstone balls consisted of approximately 67.4% silicone oxide, 24.1% aluminum oxide, and trace amounts of magnesium oxide, with a bulk density of $1440kg/m^3$, a void fraction of 0.40, and a surface area of $360m^2/m^3$. See Table 3.1

Active Section

The active sections of the reactor were packed with catalyst in the form of Raschig rings. The non-noble metal-oxide catalyst was evenly packed resulting in a total height of approximately $0.4m$ in each reactor.

Table 3.1: Characteristics of Inert Materials

	ρ_b	ϵ	a_v	k	ρC_p
	kg/m^3	-	m^2/m^3	W/mK	kJ/m^3k
Monolith Type:					
Ceramic	530	0.689	1340	1.46	440
Metal	532	0.92	2000	26.0	245
Denstone balls	1440	0.40	360	1.46	1500

3.1.2 Overall Operation

Air was supplied to the system via a compressor, and was monitored with a flow-meter located prior to the three-way valve. The methane gas, grade 1.3, was provided by BOC Gaz Canada. and was 93% methane in nitrogen. It was fed from standard gas cylinders.

Reactor Preheating

Initiation of the combustion reaction required pre-heating of the active catalyst beds. Preheating was carried out by feeding compressed air through the U-bend, which is between the two catalyst beds. The air compressed air to the U-bend between the two catalyst beds. The air passed through a heating element before entering the reactor. Thermocouples were placed in the heating element and in the catalyst bed. The set-point of the heating element was usually $800°C$ to $810°C$.

The air flow-rate through the preheating element was an important variable, as it determines the rate of heating of the reactor. Too high of an air flow-rate would not heat the compressed air enough before passing through the reactor bed. Consequently, too low of an air flow-rate would heat the air substantially, however, would take much too long to pass through the reactor, and instead tend to distribute heat to the pipe walls rather than to the reactor internals. For these experiments, the air flow-rate was set to $6.8kg/hr$ or $200SCFH$ (standard cubic feet per hour). A heat-trap effect was created by occasionally switching the direction of the air flow. This permitted the heating of both catalyst beds to sufficiently high temperatures to ensure the burning of methane. Once the reactor reached temperatures of around $400°C$, the preheating element was turned off, and methane was introduced into the system at relatively high concentrations, between 3% and 4% by volume. As the reactor temperatures increased even more, the desired regime of operation was established, and the experimental run was carried through.

Operation of Equipment

The desired concentration of methane and air velocity was set and fed to the reactor. The reactor was operated in either a forward direction (reactor 1 to 2) or reverse direction (reactor 2 to 1). A three-way valve was used to switch the direction of the flow. The term 'half-cycle' refers to the duration the reactor would run in one particular direction. Two half-cycles make one full cycle. The duration of the half cycles, or switch-time, was set in the computer-based control system. The value of the switch-time was determined by the operator, and would depend primarily on the superficial velocity of the gas along with the type of inert material. For high velocities, the residence time of the gas was low, and the cycle-time was short. Similarly, for low velocities, the cycle-time was longer. The heat capacities and thermal conductivities of the inert materials also played a role in determining a reasonable half cycle time. The objective was to maintain a high temperature in the active catalyst section, while keeping the exit temperatures fairly cool.

For higher methane concentrations, the heat that would accumulate within the reactor would be extracted through the U-bend between the two reactors. A valve was opened to create a certain pressure drop through an orifice plate placed in the mid-section of the reactor. A certain amount of air would flow out through the middle pipe and pass through a heat exchanger. The pressure drop reading was calibrated to the air flow-rate being extracted, thus an approximate fraction of extraction could be calculated. These calculations are shown in Appendix B.1.

3.1.3 Control and Data Acquisition

The reactor system was connected and controlled by a computer-based data acquisition system that measured the temperatures in the reactor and the gas flow-rate. The acquisition system was a custom software that transfered voltage readings into temperature and flow-rate data. The data would be stored at user-defined intervals of 1 to 5 seconds. At the end of the operation, the data were stored in a text file format.

The switch time was set into the control system by the user. The three-way switching valve, which determined the flow direction of the compressed air, was activated at the specified time interval. The airflow was measured by a Rosemount Micro-Motion apparatus, controlling the amount of air passing through the reactor.

The flow-rate of the methane gas was controlled by a flow-meter Type 1559A-050L, with a 30 SLM (standard litres per minute) range in methane, and a 4 channel controller model 247C, provided by MKS Instruments Inc (USA). The methane gas would pass from the cylinder through the 4 channel controller, where the desired methane output was set by the operator.

Gas Chromatograph

The methane concentration in the reactor was measured by sending gas samples to a gas chromatograph. Three sampling points were located in the system. Samples were taken before the inlet valve, after the outlet valve, and one at the middle section of the reactor. The gas chromatograph was a Hewlett Packard 5890 Series II system. It was modified by WASSON-ECE (USA company) to add a second oven on top of the GC to allow the columns in the WASSON oven to remain at a fixed temperature (135^oC in this case), while having the columns in the HP oven to undergo a programmed temperature increase.

Thermocouples

Thermal profiles in the inert and active sections were obtained using 33 thermocouples placed in the centreline and radial positions. Figure 3.4 shows the placement of the thermocouples in the reactor. The placement of the thermocouples remained the same for each type of inert material used. Sixteen thermocouples were placed along the centreline of the reactor, and twelve thermocouples were placed radially within the reactor. The remaining thermocouples were placed in the insulation, inlet and outlet positions. Thermocouple nomenclature was distinguished between the left and right reactors by the numbers 335 and 336, respectively, to indicate in which half of the reactor the

referred thermocouple is placed.

Figure 3.5 shows the locations of the thermocouples on a numerical scale corresponding to the axial length of the reactor.The thermocouple types were supplied by Thermo-Kinetics based in Québec.

In the inert section, the centreline and radial thermocouples were inserted from the top of the reactor. This can be seen from Figures 3.2 and 3.3, which are photographs of the top of the inert section. Centerline thermocouples were denoted by the letters A, B, C, and D1. Thermocouple A was placed closest to the top of the reactor, while thermocouple D1 was closest to the catalyst bed. Radial profiles in the inert sections were obtained by placing thermocouples D2, D3 and D4 (closest to the wall) in line with thermocouple D1 (closest to the center). These thermocouples were also inserted from the top of the reactor for both halves of the reactor system.

Thermocouples in the active packed bed section were placed through the sides of the reactor. The tip of the centreline thermocouples were inserted such that the tip of the thermocouples were in the centre of the packed bed. The centreline thermocouples in the active sections were denoted by the letters G, J, K and L. The radial profile in the left side reactor was recorded with thermocouples, F, G, H and I. Thermocouple G was placed in the centre, with thermocouples F, H and I placed approximately $9cm$ from the centre. Thermocouples F, G and H were aligned, and thermocouple I was displaced by 90^o. Similarly, the radial profile of the right side reactor was measured using thermocouples F, G, I, and Z. Thermocouples F, G, and I were placed at the same relative positions as in the left side reactor, however, thermocouple Z was installed in the insulation approximately $8cm$ from the outside of the reactor wall.

3.2 Numerical Model

The experimental conditions were modeled using a heterogeneous two-dimensional (in space) continuous numerical model, which was developed and refined by Salomons et. al. [24] [32]. The experimental results were used to validate and

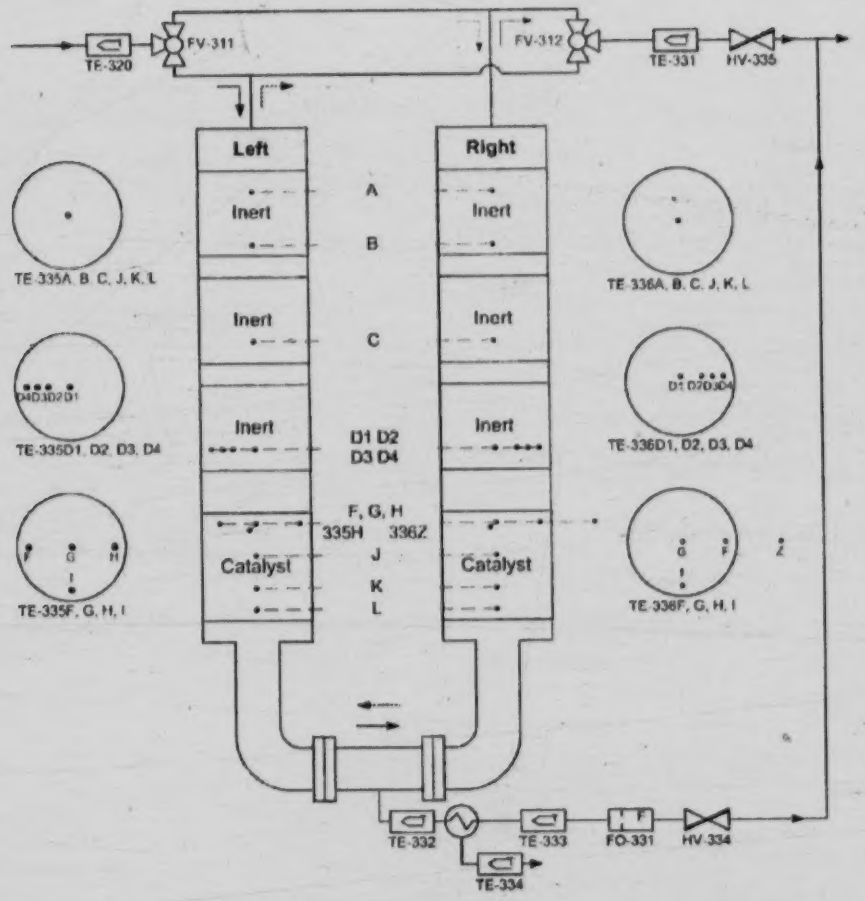

Figure 3.4: Schematic of reactor valves and thermocouple locations. Radially placed thermocouples are shown in the circles, and the gas withdrawal system is also shown

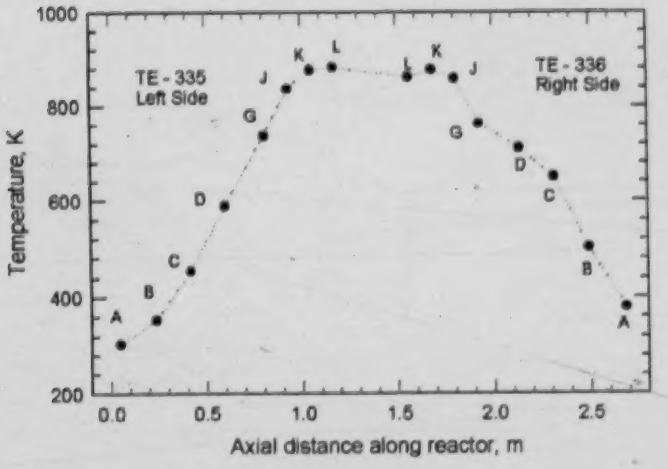

Figure 3.5: Locations of the centreline thermocouples placed in the reactor shown on a numerical scale

further develop the numerical model. The numerical simulator is written in such a way that any combination of inert and active packing types can be modeled. The modeling code was written in Fortran 95. Temperature and concentration profiles were stored in text format after the simulation of each half cycle. A full description of the model can be found in references [24] and [32]. A system of non-linear partial differential equations describing the system were numerically solved using the Galerkin finite element method.

3.2.1 Initial Conditions

The experimental initial conditions were interpolated by the simulator. Temperature readings obtained from the thermocouples within the reactor were linearly interpolated at each grid point for the reactor internals. Logarithmic interpolation was used for the reactor wall and insulation due to the solution of the conduction equation in cylindrical coordinates [32]. Centerline and radial temperature profiles for the fluid and solid were initially set to the same values.

3.2.2 Boundary Conditions

Owing to the symmetry of the reactor, all solid and fluid centerline fluxes were set to zero at the radial boundary. The solid phase axial boundary conditions were set to zero flux for both inlet and outlet energy balances. The axial fluid phase flux conditions were set to zero for the outlet mole and energy balances. Dirichlet conditions were imposed for the fluid phase equations at the inlet. External heat transfer was assumed to occur through radiation and convection.

3.2.3 Conservation Equations

Energy and mole balance equations for both the solid and fluid phases were developed assuming a pseudo-steady state for the gas phase in the transient model [32].

Mole Balance Equations

In the active packed bed and open sections, axial and radial mass transfer occurs by dispersion. Convection is responsible for mass transfer in the axial direction. The fluid phase mole balance, specific to methane, for active packed bed and open section is:

$$\frac{1}{r}\frac{\partial}{\partial r}\left(rD_{r,eff}C_f\frac{\partial Y_{CH_4,f}}{\partial r}\right)+\frac{\partial}{\partial z}\left(D_{a,eff}C_f\frac{\partial Y_{CH_4,f}}{\partial z}\right)- v_sC_f\frac{\partial Y_{CH_4,f}}{\partial z}-k_ma_vC_f\left(Y_{CH_4,f}-Y_{CH_4,s}\right)=0 \tag{3.1}$$

For the inert packed bed section, the mass transfer term drops off in the above equation.

The solid phase mole balance equation for methane is as follows:

$$\begin{aligned} k_ma_vC_f(Y_{CH_4,f}-Y_{CH_4,s}) &= (1-\epsilon)\eta(-R_CH_4) \\ &= (1-\epsilon)k_RC_sY_{CH_4,s} \end{aligned} \tag{3.2}$$

In the above equation, the rate of mass transfer in the solid phase to the solid surface equals the rate of reaction.

The fluid phase mole balance in the inert monolith section is described by:

$$\epsilon \frac{\partial}{\partial z}\left(D_{a,eff} C_f \frac{\partial Y_{CH_4,f}}{\partial z}\right) - v_s C_f \frac{\partial Y_{CH_4,f}}{\partial z} = 0 \tag{3.3}$$

This equation contains axial dispersion and advection effects.

Energy Balance Equations

The fluid phase energy balance for the active packed bed section includes axial flow, convection and conduction [32], and is modeled with the following equation:

$$\frac{1}{r}\frac{\partial}{\partial r}\left(r k_{rf,eff} \frac{\partial T_f}{\partial r}\right) + \frac{\partial}{\partial z}\left(k_{af,eff} \frac{\partial T_f}{\partial z}\right) - v_s \rho_f C_{p,f} \frac{\partial T_f}{\partial z} + h a_v (T_s - T_f) = 0 \tag{3.4}$$

For the fluid phase in the monolith section, it is assumed that radial energy dispersion is negligible. The equation is written as:

$$\epsilon \frac{\partial}{\partial z}\left(k_{a,eff} \frac{\partial T_f}{\partial z}\right) - v_s \rho_f C_{p,f} \frac{\partial T_f}{\partial z} + h a_v (T_s - T_f) = 0 \tag{3.5}$$

Solid phase energy balance equation includes terms for accumulation, axial and radial conduction, convection and heat generated by the reaction. The solid phase energy balance for both packed bed and monolith sections is as follows:

$$\frac{1}{r}\frac{\partial}{\partial r}\left(r k_{rs,eff} \frac{\partial T_s}{\partial r}\right) + \frac{\partial}{\partial z}\left(k_{as,eff} \frac{\partial T_s}{\partial z}\right) + h a_v (T_f - T_s) + (1-\epsilon)\Delta H_R \eta (-R_{CH_4}) = (1-\epsilon)\rho_s C_{p,s} \frac{\partial T_s}{\partial t} \tag{3.6}$$

For the inert monolith and inert packed bed sections, the reaction rate term is not included from Equation (3.6). The effective dispersion coefficients and thermal conductivities depend on the medium. See reference [32] for details.

3.2.4 Reaction Kinetics

The reaction kinetics were obtained from Aubé and Sapoundjiev [23] and were first order with respect to methane and zero order with respect to oxygen.

The effectiveness factor for an isothermal first order reaction in a flat plate is defined as:

$$\eta = \frac{\tanh(\phi)}{\phi} \tag{3.7}$$

The effectiveness factor indicates the relationship between the average reaction rate in the catalyst and the reaction rate at the surface conditions.

The Thiele modulus used for a first order reaction is generalized as:

$$\phi = L_C \sqrt{\frac{k_R}{D_{eff}}} \tag{3.8}$$

Where L_c is the characteristic length of the particles. The characteristic length is found by dividing the volume by the surface area.

The effective diffusivity is:

$$D_{eff} = \frac{D_K \epsilon}{\tau} \tag{3.9}$$

Equation (3.9) is the parallel pore model, where it is assumed that all pores in the catalyst are of the same size. In the equation, ϵ is the void fraction of the catalyst and τ is the tortuosity factor.

The effective diffusion coefficient for the porous catalyst pellets is expected to be dominated by Knudsen diffusion. The Knudsen diffusion coefficient is defined as:

$$D_K = 97 r_p \left(\frac{T}{M}\right)^{0.5} \tag{3.10}$$

Where T is the temperature (K), M is the molar mass of the diffusing element (g/mol), and r_p is the pore radius in m.

3.2.5 Physical Properties of the Fluid

The fluid was modeled as an ideal gas with molar and mass densities give by the following equations [32] :

$$C = \frac{P}{R_g T_f} \tag{3.11}$$

$$\rho_f = \frac{\bar{M} P}{R_g T_f} \tag{3.12}$$

A third-order polynomial function of temperature described the heat capacities for each gas species [1]. Viscosity and thermal conductivities were functions of temperature. The fluid velocity is defined in terms of a superficial velocity, v_s. This velocity is based on the actual fluid velocity, v in an empty cross sectional area at ambient conditions. The relationship of the two velocities is as follows:

$$v_s = v\epsilon \tag{3.13}$$

The pressure drop across the reactor was assumed to be negligible for this system, thus the velocity of the ideal fluid varied with temperature by the following equation:

$$v_s = v_{s,inlet}(\frac{T_f}{T_{f,inlet}}) \tag{3.14}$$

3.2.6 Heat and Mass Transfer Coefficients

Heat and mass transfer coefficients are important factors for both the monolith and the packed bed sections. The coefficients used in the numerical model are fully described in Salomons [24]. The interfacial area between the fluid and solid influences the rate of heat and mass transfer. The area to volume ratio for a monolith is given by:

$$a_v = \frac{4\epsilon}{D_H} \tag{3.15}$$

The hydraulic diameter and the void fraction of the monolith is used for this calculation. The hydraulic diameter is given by:

$$D_H = \frac{D_R}{\frac{3D_R}{2D_C}(1-\epsilon)+1} \tag{3.16}$$

Where D_R is the reactor diameter and D_C is the characteristic particle diameter, defined as follows:

$$D_C = 6\frac{V}{A} \tag{3.17}$$

The interfacial area for a packed bed incorporates the void fraction and the characteristic particle diameter. It is described in the following equation [32]:

$$a_v = \frac{6\,(1-\epsilon)}{D_C} \tag{3.18}$$

The heat transfer coefficient depends on the Reynolds and Prandtl numbers, while the mass transfer coefficient depends on the Reynolds and Schmidt numbers. These three dimensionless groups are defined by the following equations:

$$Re = \frac{v_s D_C \rho_f}{\mu} \tag{3.19}$$

$$Sc = \frac{\mu}{\rho_f D_{AB}} \tag{3.20}$$

$$Pr = \frac{C_p \mu}{k_f} \tag{3.21}$$

The molecular diffusion coefficient, D_{AB}, was calculated using the Fuller method, which uses diffusion volumes, temperature and pressure of the components to yield a result in units of m^2/s. The temperature dependent binary diffusion coefficient is given by [1]:

$$D_{AB} = 9.86 \times 10^{-10} T^{1.75} \tag{3.22}$$

The Sherwood and Nusselt numbers were also correlated to predict the mass and heat transfer effects, and are fully described in Salomons [24].

Chapter 4

Experimental Results

The experimental results obtained from the pilot plant CFRR are presented in three different categories for each of the three different inert types studied. It should be noted that the performance of the reactor is dependent on the initial conditions of the regime, which in turn depends on the reactor history. The reactor history depends on the pre-heating scheme or the previous experimental conditions. The rigorous pre-heating procedure would at times lead to thermal profiles with pronounced hot spots in one or both reactors. Setting an experimental regime with a unbalanced thermal profile would lead to either further hot spots in the reactor, or to the fairly even distribution of the temperature profile. Hot spots required special attention when setting the initial regime, as in that zone is where reaction occurs, thus continues to heat up further. It was important to make sure that the initial temperature profile would show an even accumulation of heat throughout the active sections. It is impossible to begin each experimental regime near the same initial temperature conditions. The comparison of different inert types is thus difficult, because the initial profiles determine the majority of the trends throughout the experiment.

Thermal energy was extracted from the reactor, by extracting mass, during several runs with each type of inert with 0.6% methane concentration. This process is referred to as heat extraction throughout this thesis. The resulting profiles depended on how much heat was being extracted versus how much was being generated and stored. When the amount of heat being extracted

was greater than that being generated, a general trend of cooling was seen in the axial temperature profile for each type of inert. The trend was such that the temperature of the inert sections would cool down, as the temperature of the catalyst bed rises, forming a bell shaped curve. The catalyst temperature would plateau to a certain temperature, and the axial temperature profile would begin to collapse from the top of the bell curve. Over time, this behaviour could lead to the extinction of the combustion reaction and cooling of the reactor. In some cases, the reactor reached a pseudo-steady state, where the amount of heat extracted was in harmony with the heat being generated.

In the following, the experimental results are discussed in detail.

4.1 Fractional Conversion of Methane

The analysis of the gas obtained from the mid-section and outlet streams, showed that the methane was fully combusted. The combustion reaction initiates when the temperature is above about $670K$. During the experimental operations, the reverse-flow reactor would be operating in conditions well above $670K$ in the catalyst section. The thermocouples in the catalytic beds read temperatures above $950K$, therefore, was understood that the methane is being completely converted. The few readings obtained by the GC for the system with each different type of inert show complete conversion of methane at the mid-section and outlet points.

4.2 Inert Ceramic Monolith

Six experiments were conducted with the inert ceramic monolith placed in the CFRR. Two of these experiments were conducted with heat extraction; the remainder without heat extraction. Methane concentrations of $0.2\%CH_4$, $0.6\%CH_4$, and $1\%CH_4$ were used. Superficial velocities of $0.3m/s$ and $0.7m/s$ were set for each methane concentration. The tests with methane concentration of 1% were difficult to control with the current system in the lab. A constant switch time for this methane concentration was unable to be established as the catalyst bed temperature would continuously rise toward excessive lev-

els. Overall, the inlet and outlet gas with the inert ceramic monoliths remained fairly cool at temperatures between $300K$ and $400K$. Low outlet temperatures indicated that most of the heat is being kept in the reactor because there is minimal heat losses through the outlet.

Experiments with methane concentrations of $0.2\%CH_4$ showed a cooling trend in the reactor over time, which indicates that the heat-trap effect is unable to conserve sufficient energy in the reactor to maintain the system at its initial temperatures.

Two superficial velocities, $0.3m/s$ and $0.7m/s$, were set at a methane concentration of $0.2\%CH_4$. Figure 4.1 shows the cooling trend with conditions at $0.3m/s$ superficial velocity and $0.2\%CH_4$ over 10 cycles, with a switch time of $300s$. The initial temperature profile showed hot spots being developed at this regime. However, for the same methane concentration and a superficial velocity of $0.7m/s$, with a switch time of $100s$ Figure 4.2 shows that a more stable initial profile, without hot spots, can lead to a stable regime throughout the experiment. This shows that the initial temperature, air velocity, and the cycle times strongly influence the subsequent behaviour.

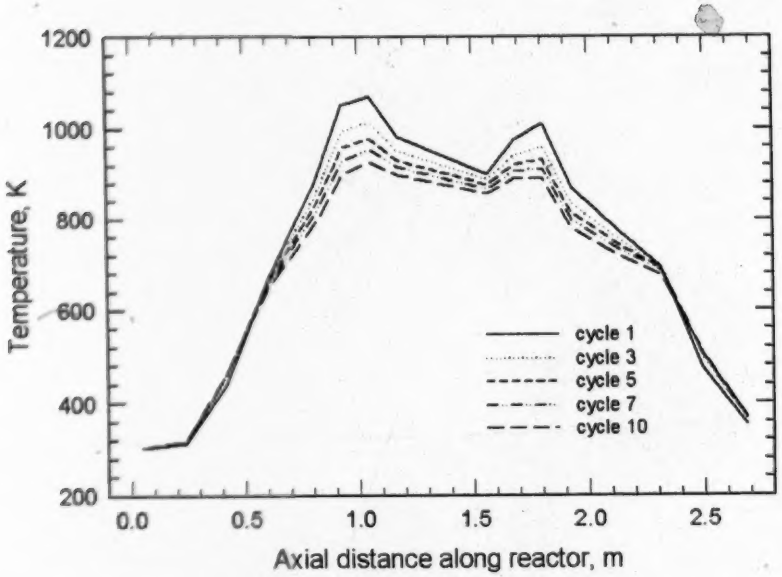

Figure 4.1: Ceramic monolith: Experimental axial forward flow temperature profiles. Multiple forward flow profiles for $0.2\%CH_4$ and $0.3m/s$ superficial velocity

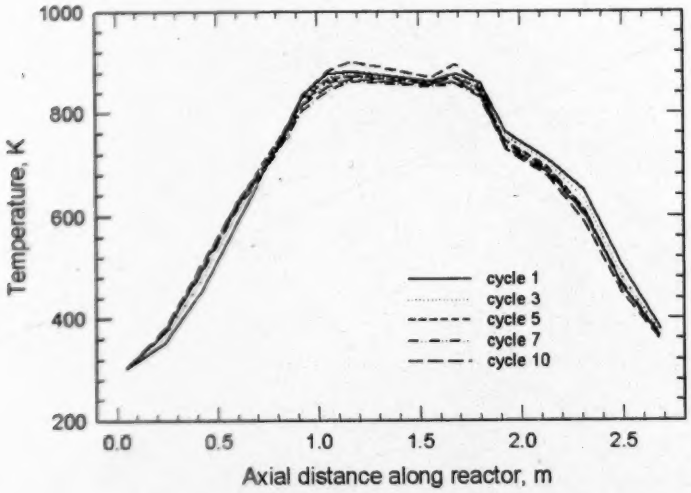

Figure 4.2: Ceramic monolith: Experimental axial forward flow temperature profiles. Multiple forward flow profiles for $0.2\%CH_4$ and $0.7m/s$ superficial velocity

At methane concentration of 0.6%, the heat in the reactor accumulated over time, as seen in Figure 4.3. The formation of dual localized hot spots in the catalyst bed is observed as more heat is generated in the reactor. A high methane concentration passing through the heated active zone, ensures high conversion, which eventually leads to high thermal energy released by the combustion reaction. The temperature in this zone would rise as methane is combusted during each half-cycle, and the hot spots would become more pronounced.

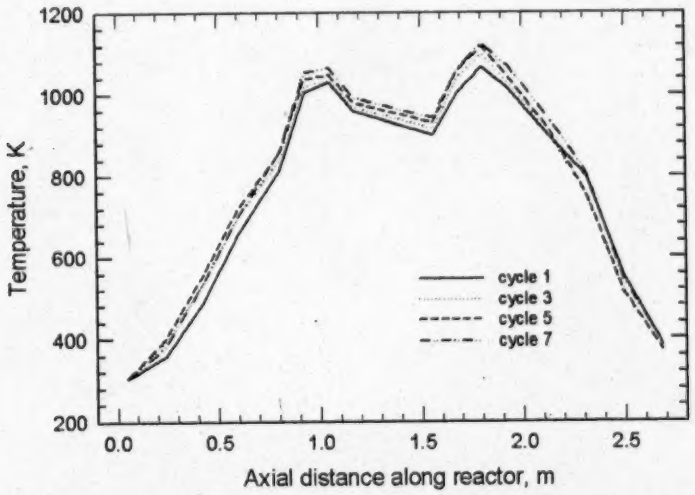

Figure 4.3: Ceramic monolith: Experimental axial forward flow temperature profiles. Multiple forward flow profiles for 0.6%CH_4 and 0.7m/s superficial velocity

As the three-way valve switched the direction of flow from forward to reverse, the axial thermal profile shifts along the reactor. This axial shift depends on the superficial velocity. At higher superficial velocities, the switch time was shorter, and lead to a shorter residence time in the reactor. Figure 4.4 shows the axial shift at a higher residence time, while Figure 4.5 shows the shift at a lower residence time. At a methane concentration of 0.6% with a superficial velocity of $0.3m/s$, the axial profile shifted by about $200K$ at thermocouple D1 in the first reactor. By increasing the superficial velocity to $0.7m/s$, thermocouple D1 shifted by nearly $300K$ in spite of the shorter switch time.

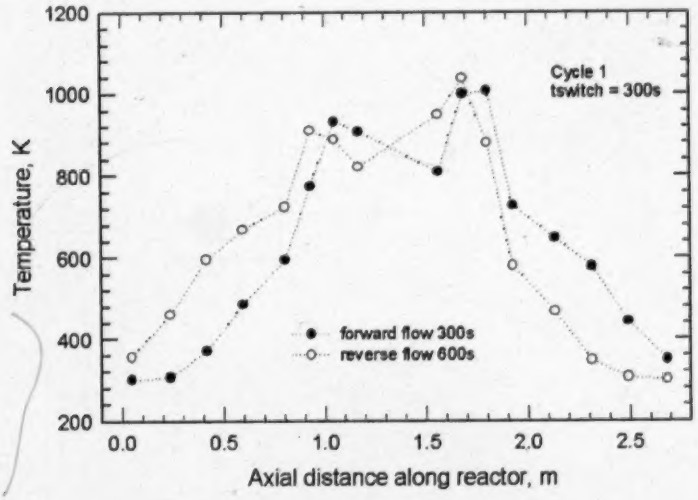

Figure 4.4: Ceramic monolith: Experimental axial temperature profile for one full cycle. Profile for cycle one at $0.6\%CH_4$ and $0.3m/s$ superficial velocity with switch time of $300s$

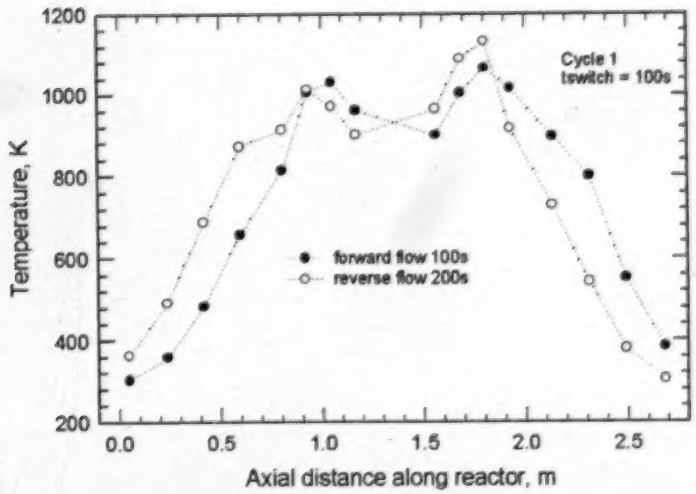

Figure 4.5: Ceramic monolith: Experimental axial temperature profile for one full cycle. Profile for cycle one at $0.6\%CH_4$ and $0.7m/s$ superficial velocity with switch time of $100s$

4.2.1 Inert Ceramic Monolith with Heat Extraction

Figure 4.6 shows the behaviour of the ceramic inert monolith with heat extraction with methane concentration of 0.6% and $0.3m/s$ superficial velocity. Prior to initiating heat extraction, the reactor was running without heat extraction at the same inlet conditions. After commencing extraction, the temperature in the mid-section, between thermocouples L in the first and second reactor, changes slowly, about $0.2K/s$. For the same curve, the front and ends of the reactor remain cool. Extracting heat from the mid-pipe causes the axial temperatures to decrease in the inert sections and increase in and between the catalyst sections. It is speculated that as the air is being extracted, the velocity in the remainder of the reactor is decreased. Since convective transfer dominates, the slower velocity allows for less convection, thus a decrease in temperature.

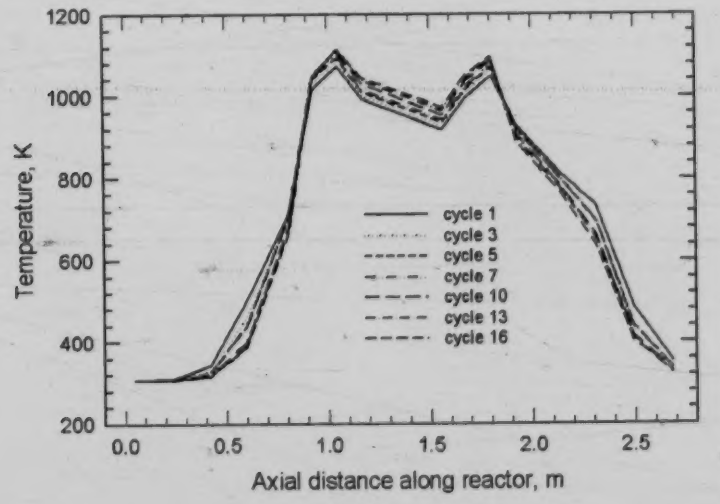

Figure 4.6: Ceramic monolith: Multiple experimental axial temperature profiles with heat extraction at $0.6\%CH_4$ and $0.3m/s$ superficial velocity with switch time of $350s$

It is possible to achieve a pseudo-steady state while extracting heat from the mid section. This can be seen in Figure 4.7, where the regime was set with a superficial velocity of $0.7m/s$ and 0.6% methane. This regime was set after brief heat extraction with varying switch times. The axial temperature profile

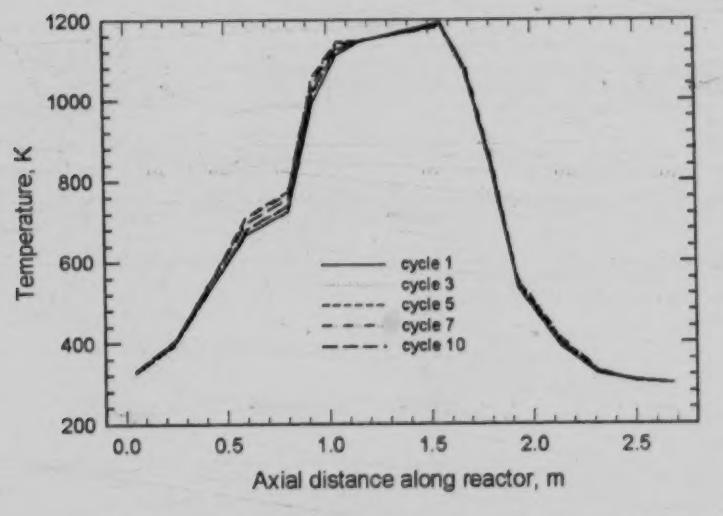

Figure 4.7: Ceramic monolith: Multiple experimental axial temperature profiles with heat extraction at $0.6\%CH_4$ and $0.7m/s$ superficial velocity with switch time of $130s$

changes minutely over 10 cycles. This indicates that the heat being generated and stored in the reactor is about the same as that being extracted. The ability to attain a pseudo-steady state operation by the balancing heat generation and extraction is key to successful operations in a practical application.

Figure 4.8 shows the results from extracting heat over time with 0.6% methane, a superficial velocity of $0.3m/s$ with a switch time of $350s$ in the forward direction. The previous conditions were at the same inlet conditions but without heat extraction. The change of shape in the axial temperature profile is seen in this figure, where after nearly five hours extracting heat, the inert sections show cooling and the active section shows heating.

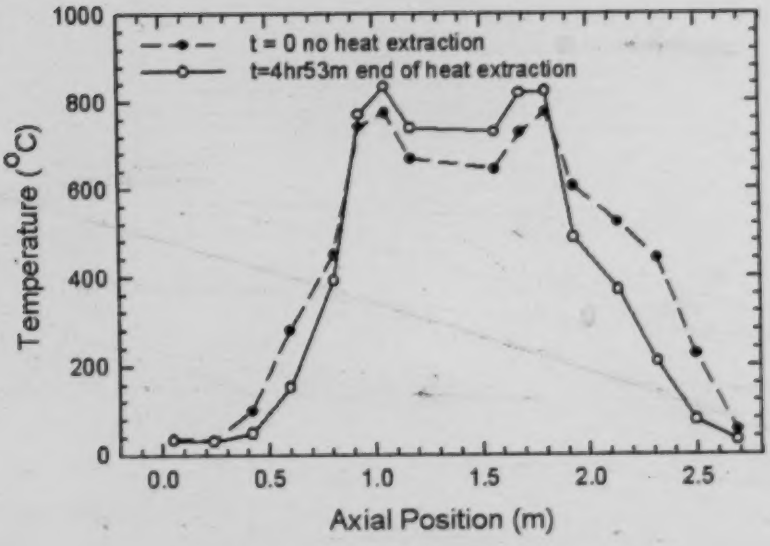

Figure 4.8: Ceramic monolith: Forward flow profiles showing heat extraction progression with $0.6\%CH_4$ and $0.3m/s$ superficial velocity with switch time of $350s$

4.3 Inert Metal Monolith

Eleven experiments were conducted with inert metal monoliths as a heat trap. Four experiments were conducted without heat extraction. Superficial velocities of $0.3m/s$, $0.7m/s$, $1m/s$, and $1.2m/s$ were set for each of the methane concentrations studied. The rate of propagation of the axial temperature profile was observed to be higher than that for ceramic inerts, which meant that shorter cycle times were used.

Figures 4.9 and 4.10 show about a $400K$ movement between the half cycles at thermocouple D1 in the first reactor over one half cycle. These figures show the first cycle of the operating conditions with a superficial velocity of $0.7m/s$ with methane concentrations of 0.6% and 0.2%, respectively. The temperature movement is nearly twice as much as what was seen with ceramic monoliths.

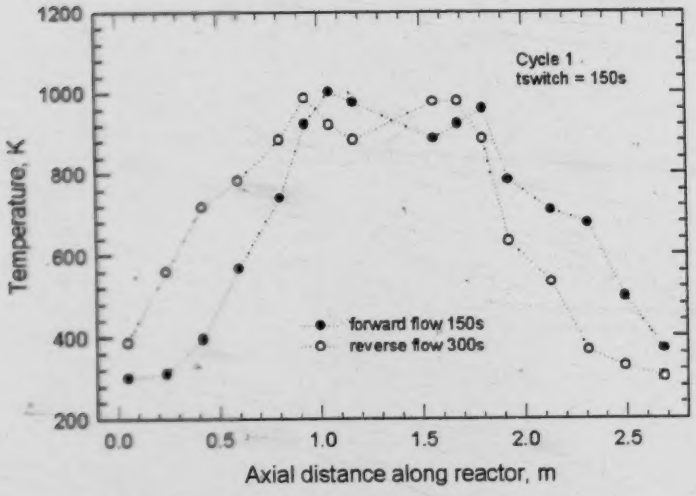

Figure 4.9: Metal monolith: Experimental axial temperature profile for one full cycle. Profile for cycle one at $0.6\%CH_4$ and $0.7m/s$ superficial velocity with switch time of $150s$

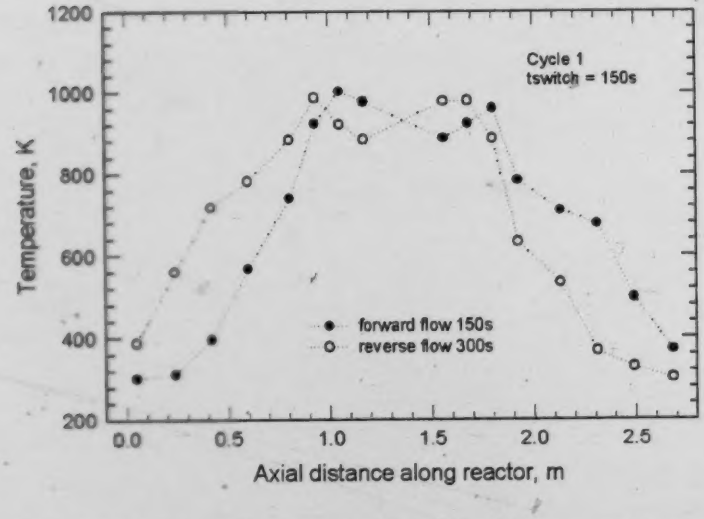

Figure 4.10: Metal monolith: Experimental axial temperature profile for one full cycle. Profile for cycle one at $0.2\%CH_4$ and $0.7m/s$ superficial velocity with switch time of $150s$

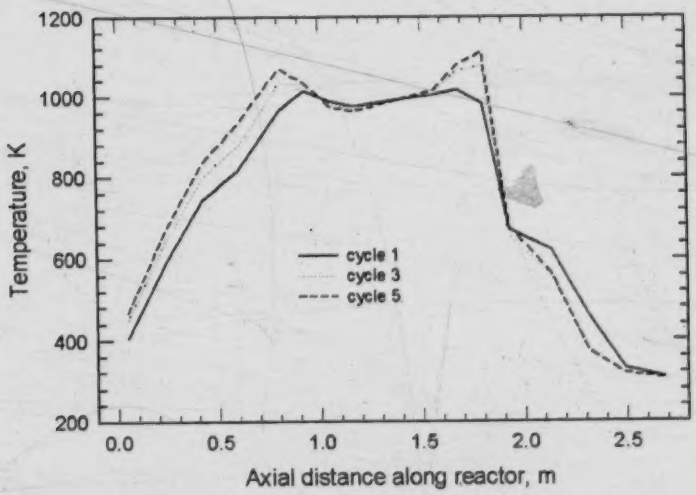

Figure 4.11: Metal monolith: Multiple experimental reverse flow axial temperature profiles at $0.6\%CH_4$ and $0.3m/s$ superficial velocity with switch time of $400s$

The outlet temperatures could reach nearly $400K$, which indicates that significant heat is being lost from the outlet. Heat escaping from the outlet is undesirable because the reactive bed can lose heat over time. Figure 4.11 shows the high temperatures attained at the reactor outlet along with some cooling in the mid-section.

At higher methane concentrations of $0.6\%CH_4$, the reactor would accumulate thermal energy in both the active and inactive zones, as seen in Figure 4.12. A pseudo-steady state was unreachable without heat extraction, as the reactor would continue to heat toward dangerously high temperatures in spite of the elevated heat loss from the exit. At this state, either the methane concentration was lowered, or heat extraction process was initiated.

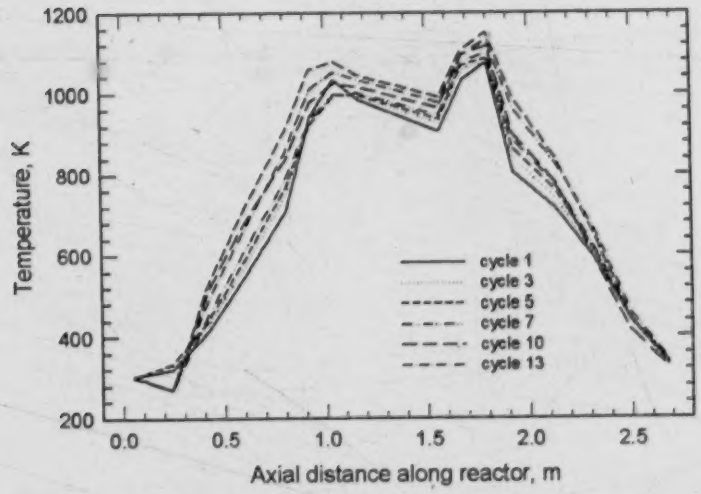

Figure 4.12: Metal monolith: Multiple experimental reverse flow axial temperature profiles at $0.6\%CH_4$ and $1m/s$ superficial velocity with switch time of $60s$

Lowering the methane concentration to 0.2% in the reactor with inert metal monoliths, the axial thermal profile cooled and reached toward a pseudo-steady thermal state. Figure 4.13 shows the above mentioned behaviour. This result follows the conditions of pre-heating with a methane concentration. Overall, lowering the methane concentration showed a decrease in the overall thermal state of the reactor.

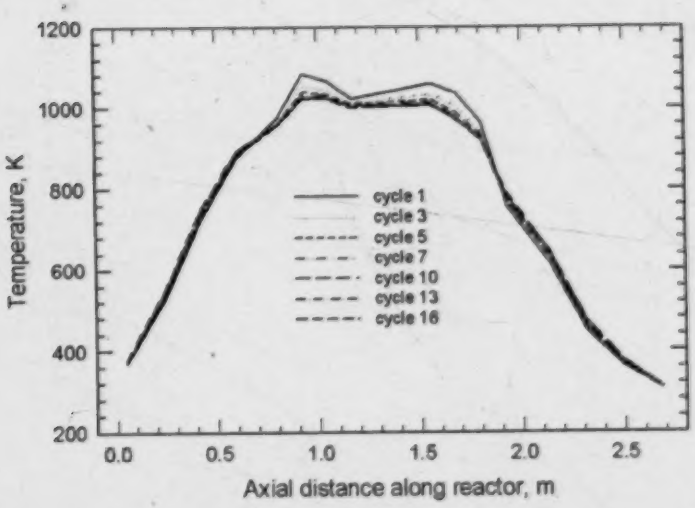

Figure 4.13: Metal monolith: Multiple experimental reverse flow axial temperature profiles at $0.2\%CH_4$ and $1.2m/s$ superficial velocity with switch time of $60s$

4.3.1 Inert Metal Monolith with Heat Extraction

Four experiments were conducted with heat extraction with the metal monolith. A methane concentration of 0.6% was set and the superficial velocities were varied from $0.3m/s$ to $1.2m/s$.

Figure 4.14 shows the conditions of 0.6% methane, at a high superficial velocity of $1.2m/s$, with a switch time of $60s$. It was observed that the outlet temperatures remained nearly $200K$ lower than without heat extraction. During heat extraction, the velocity of the gas passing through the second inert section decreases as the valve is opened in the mid-section of the reactor. The decrease in the velocity in the inert sections leads to a decrease in the outlet temperatures over time. Upon the heat extraction, the axial thermal profile would decrease mostly in the inert section at first, followed by a cooling of the active section, which is the same as the trend seen with the inert ceramic monoliths.

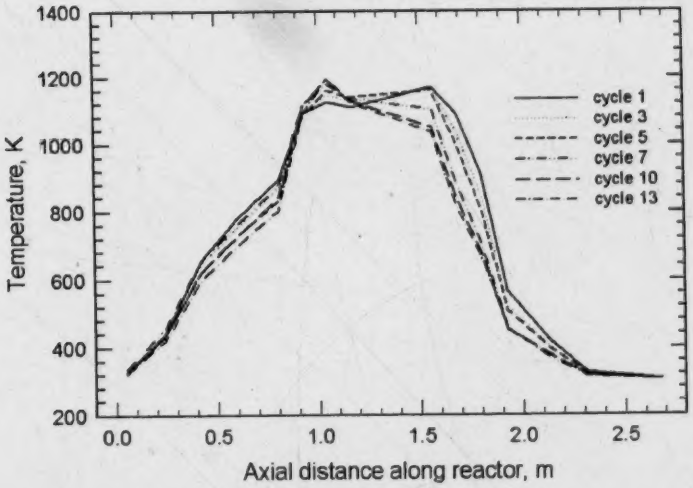

Figure 4.14: Metal monolith: Multiple experimental reverse flow axial temperature profiles with heat extraction at $0.6\%CH_4$ and $1.2m/s$ superficial velocity with switch time of $60s$

Figure 4.15 shows the axial temperature profile development with heat extraction with 0.6% methane, $0.7m/s$ superficial velocity, and a switch time of $150s$ over the span of 80 minutes. The initial condition was a pseudo-steady state without heat extraction. At time zero, heat extraction commenced. From this figure, it is clear that the inert sections cool while the active sections heat up during heat extraction.

Figure 4.16 shows the experimental temperature progression at the conditions of 0.6% methane, $0.7m/s$ superficial velocity, and switch time of $150s$. Comparison with Figure 4.14 ($0.6\%CH_4$ and $1.2m/s$ and switch time $60s$) shows the effect of operation conditions on the temperature changes. For example, at thermocouple L an increase in the superficial velocity from $0.7m/s$ to $1.2m/s$ combined with a reduced cycle time, resulted in a roughly two fold increase in the rate of temperature change.

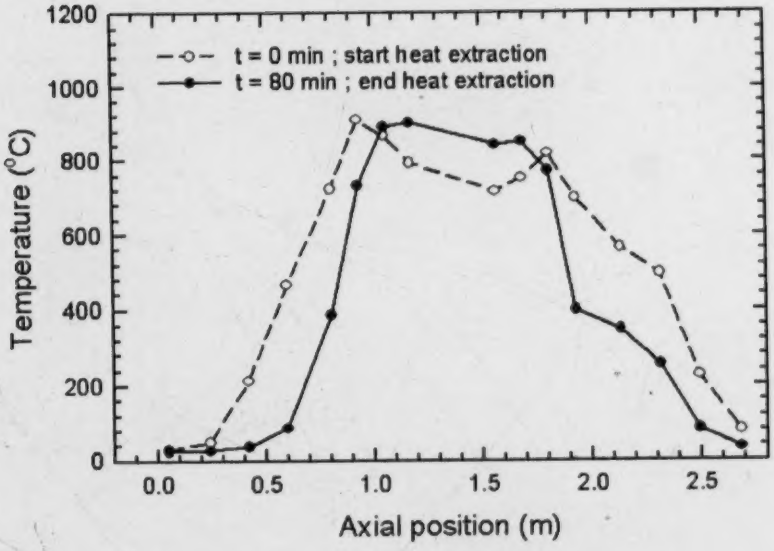

Figure 4.15: Metal monolith: Forward flow profiles showing heat extraction progression with $0.6\%CH_4$ and $0.7m/s$ superficial velocity with switch time of $150s$

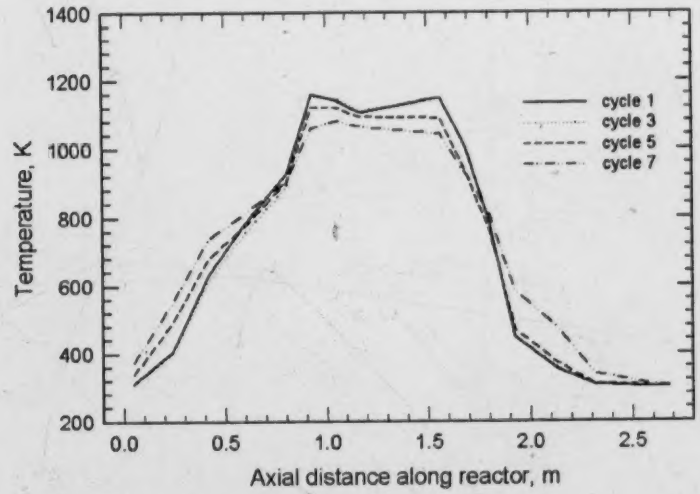

Figure 4.16: Metal monolith: Multiple experimental reverse flow axial temperature profiles with heat extraction at $0.6\%CH_4$ and $0.7m/s$ superficial velocity with switch time of $150s$

The axial profile shift from half-cycle to half-cycle also decreased as heat was being extracted from the system as seen in Figure 4.17. The initial condition was a pseudo-steady state without heat extraction.In this figure, the beginning of the heat extraction regime is shown where the axial temperature shift is approximately $300K$ at thermocouple D1 in the first reactor. By the end of the heat extraction regime, the shift at the same point is around $150K$, as seen in Figure 4.18.

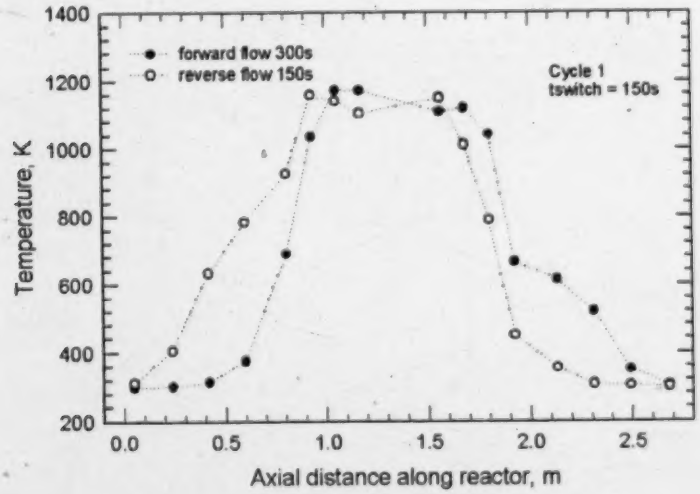

Figure 4.17: Metal monolith: Experimental axial temperature profile for one full cycle with heat extraction. Profile for first cycle at $0.6\%CH_4$ and $0.7m/s$ superficial velocity with switch time of $150s$

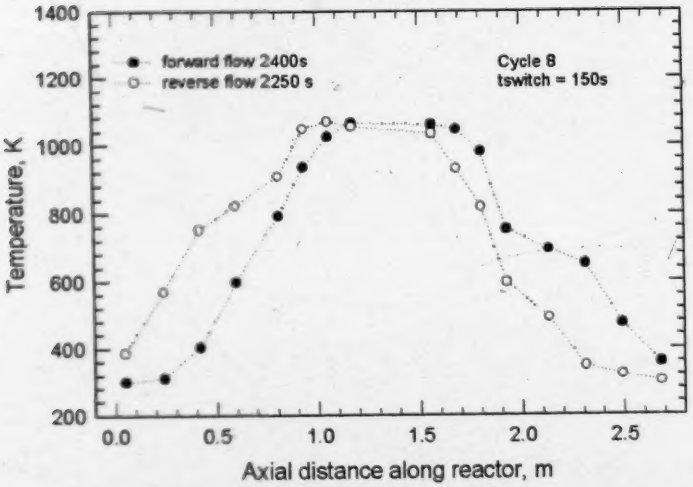

Figure 4.18: Metal monolith: Experimental axial temperature profile for one full cycle with heat extraction. Profile for 8^{th} cycle at $0.6\%CH_4$ and $0.7m/s$ superficial velocity with switch time of $150s$

4.4 Packed Denstone Ball Inert

Eight experiments were conducted without heat extraction, and four experiments with heat extraction for the reactor packed with Denstone balls placed in the inert sections. Two methane concentrations, 0.2% and 0.6%, were set for four different superficial velocities, $0.3m/s$, $0.7m/s$, $1m/s$ and $1.2m/s$. Experiments at 1% methane concentration were also attempted, however, as seen with the ceramic monolith inerts, the reactor was difficult to control, as the reactor temperature would rise to dangerous levels without being able to set a constant cycle time. Because of the high capacity for storing energy, the packed Denstone balls showed desirable behaviour of retaining the heat in the reactor.

At a methane concentration of 0.6%, the thermal energy in the reactor would increase over time. The reactive zones would increase in temperature while the inert sections would remain between ambient and about $500K$. The packed Denstone balls have a greater capacity for storing thermal energy, therefore, the front and rear ends of the reactor would remain cool over time

at temperatures nearing $300K$. The inert sections would trap the heat in the active zones and showed minimal movement as the direction of the flows were being switched. In Figure 4.19 it is seen that at a methane concentration of 0.6% and a superficial velocity of $0.7m/s$, the reactor would accumulate heat mostly in the active catalytic zone.

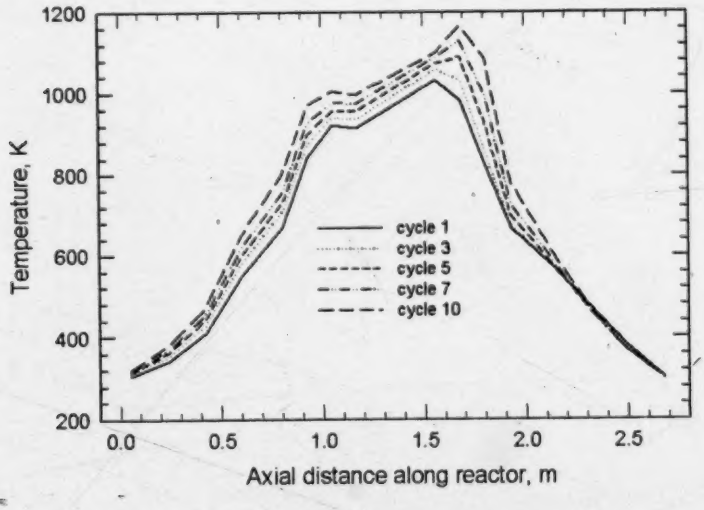

Figure 4.19: Denstone balls: Multiple experimental reverse flow axial temperature profiles at $0.6\%CH_4$ and $0.7m/s$ superficial velocity with a cycle switch time of $150s$

By decreasing the methane concentration, the axial thermal profile of the reactor showed a decrease in temperature in the catalytic zones. The heat from the active beds would dissipate into the inert zones, as seen in Figures 4.20, and thermal movement in the inert packed bed section was at a minimal at lower superficial velocities, as seen in Figure 4.21. Thermocouples A, B, C and D, would not change in temperature as much as the catalytic zones. This would indicated the heat being generated by the combustion reaction is being properly trapped in the reactive section.

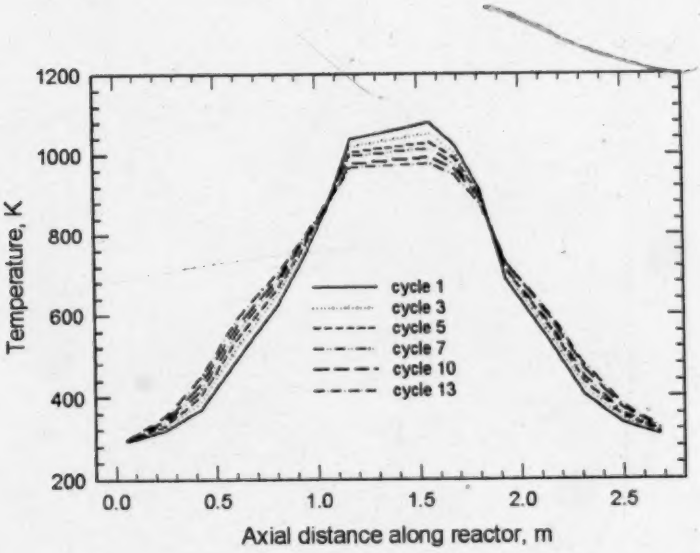

Figure 4.20: Denstone balls: Multiple experimental forward flow axial temperature profiles at $0.2\%CH_4$ and $1m/s$ superficial velocity with a cycle switch time of $60s$

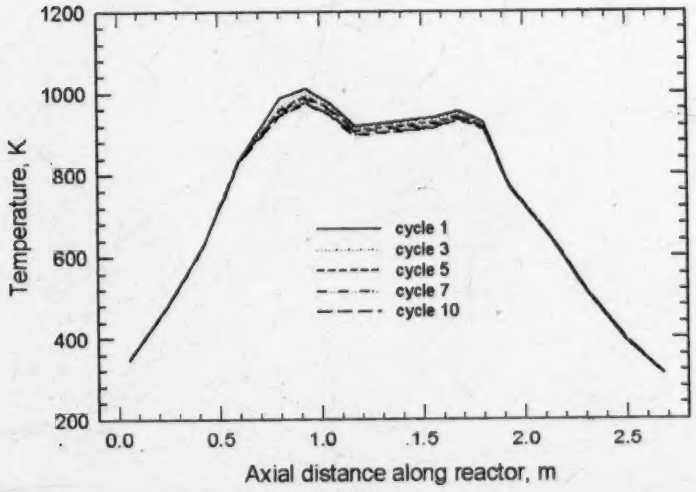

Figure 4.21: Denstone balls: Multiple experimental reverse flow axial temperature profiles at $0.2\%CH_4$ and $0.3m/s$ superficial velocity with a cycle switch time of $150s$

4.4.1 Denstone Ball Inert with Heat Extraction

Experiments with heat extraction were conducted for a methane concentration of 0.6%, at superficial velocities of $0.7m/s$, $1m/s$, and $1.2m/s$. A heat extraction experiment was also conducted for conditions with no methane being fed into the reactor with a superficial velocity of $0.7m/s$.

At a methane concentration of 0.6%, upon extracting thermal energy, the axial thermal profile exhibited the same behaviour as seen with the ceramic and the metal monoliths with heat extraction. The inert sections cool while the active section increases in temperatures until a certain point, after which the active section also begins to cool. Figure 4.22 clearly shows the behaviour of cooling in the inert sections, and heating in the active sections.

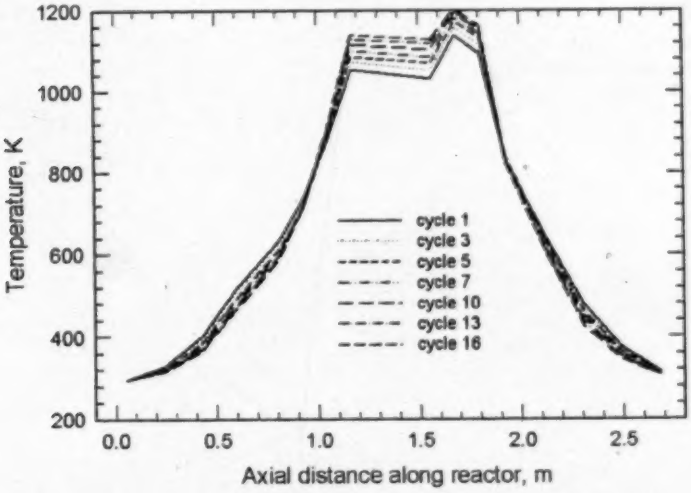

Figure 4.22: Denstone balls: Multiple experimental forward flow axial temperature profiles at $0.6\%CH_4$ and $0.7m/s$ superficial velocity with a cycle switch time of $130s$

Figure 4.23 shows the axial thermal profile over time for conditions at 0.6% methane and a high superficial velocity of $1.2m/s$. The axial temperature profile begins to decrease in the inert sections, as mentioned before,however the catalyst section seems to maintain the reaction at a pseudo-steady state.

At a superficial velocity of $0.7m/s$, the methane valve was shut off for the duration of around 13 cycles, while heat was continuously being extracted

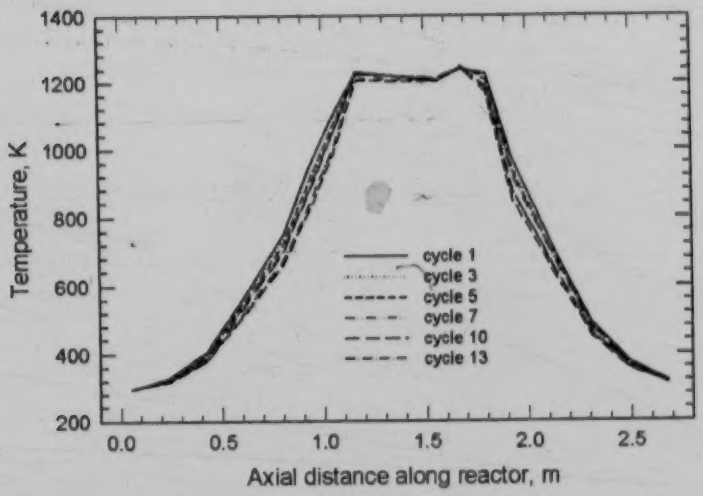

Figure 4.23: Denstone balls: Multiple experimental forward flow axial temperature profiles with heat extraction at $0.6\%CH_4$ and $1.2m/s$ superficial velocity with a cycle switch time of $100s$

through the U-bend. In this case, all of the thermocouples in the reactor showed an increasingly rapid cooling, as seen in Figure 4.24.

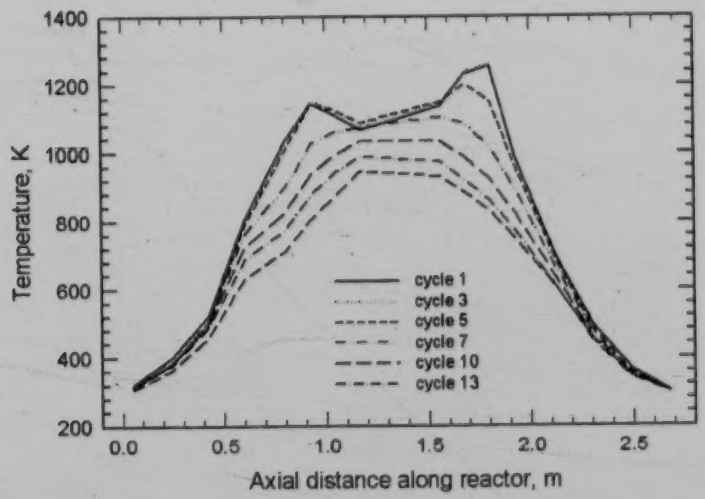

Figure 4.24: Denstone balls: Multiple experimental reverse flow axial temperature profiles with heat extraction at $0\%CH_4$ and $0.7m/s$ superficial velocity with a cycle switch time of $150s$

Without feeding methane through the reactor, the combustion reaction was impossible, thus the reactor began to distribute the heat remaining in the reactor through each half-cycle. The minor hot spots that were initially present in the thermal profile disappeared as the reactor continued to cool. Thermocouple K in the first reactor showed no cooling for the first three cycles, and by the fifth cycle, the thermocouple showed a cooling of $1000K$. Within 13 cycles, thermocouple K in the first reactor cooled by about $400K$.

In the inert Denstone packing, the thermocouples also recorded a reduction in temperatures, however, the cooling was less rapid than seen in the active sections. Thermocouple C in the first reactor cooled about $100K$ over 13 cycles. The reactor experienced rapid cooling from each successive half cycle, thus, after each half-cycle, the reactor cools further. The rapid cooling causes the axial thermal profile to increasingly sway. The sway displaces the cross-over point, which is where the forward and the reverse cycle axial profiles meet at a certain point. The cross over point between the two profiles shifted from being in the center of thermocouples L, as seen in Figure 4.25, to being further in the catalyst bed in the second reactor as seen in Figure 4.26.

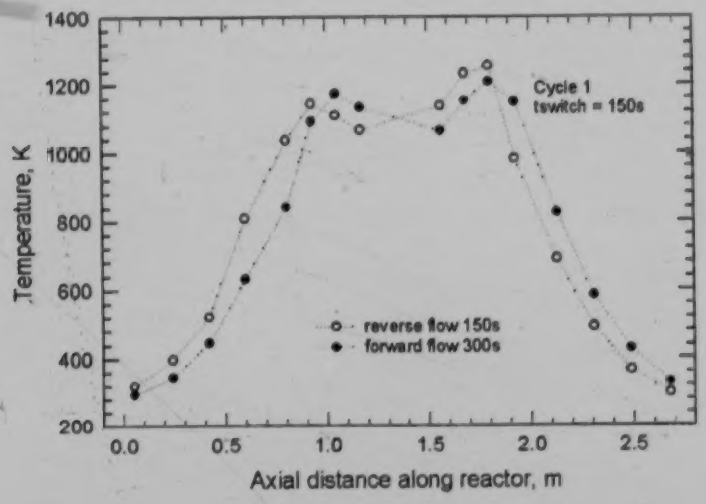

Figure 4.25: Denstone balls: Experimental axial temperature profiles for first cycle with heat extraction at $0\%CH_4$ and $0.7m/s$ superficial velocity with a cycle switch time of $150s$

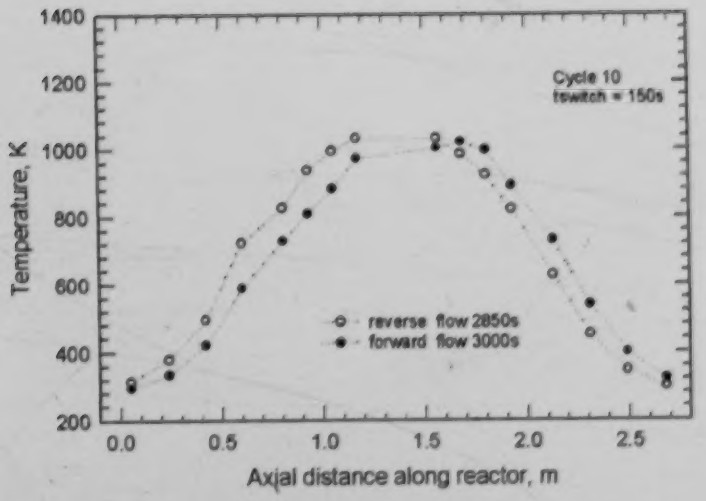

Figure 4.26: Denstone balls: Experimental axial temperature profiles for the 10^{th} cycle with heat extraction at $0\%CH_4$ and $0.7m/s$ superficial velocity with a cycle switch time of $150s$

4.5 Radial Gradients of the Inert Types

The radial temperature profiles shown in the inert sections are described in this section. Radial thermal gradients may affect the conversion of methane since there may be lower temperatures away from the centre of the reactor. In the monolith sections, radial heat transfer is dominated by conduction through the walls of the channels, while with the packed bed, radial fluid mixing also occurs.

Figure 4.27 shows the temperatures recorded by the radially placed thermocouples in the ceramic inert section in the left-hand-side. Two out of four of the profiles shown on this graph describe the beginning and end of the operating regime of 0.6% methane and $0.7m/s$ superficial velocity without heat extraction, and the remaining are for conditions with heat extraction.

Here it is seen that the radial gradients are fairly linear with the highest temperature being recorded near the wall at thermocouple D4. The thermal mass of the reactor is significant as a thick layer of insulation is placed around the reactor wall. Over time, the thermal energy in the reactor travels out-

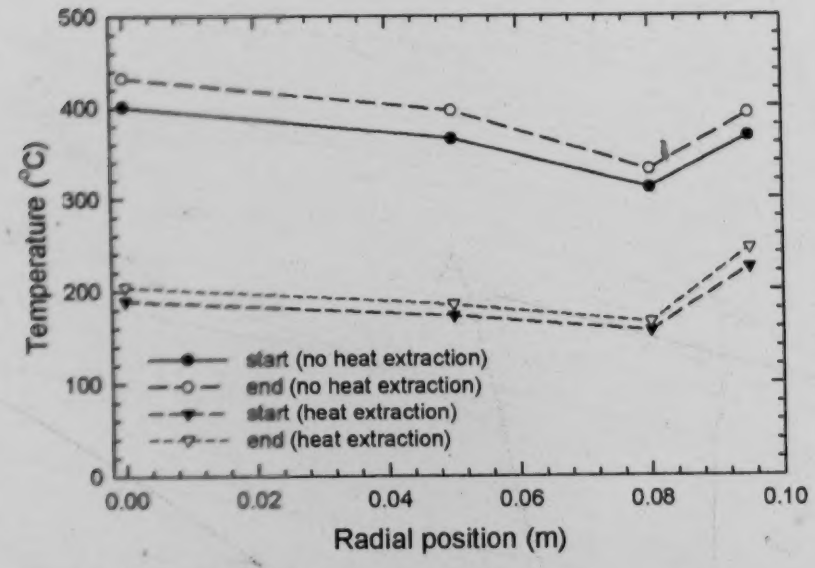

Figure 4.27: Experimental radial temperature profiles in the inert ceramic monolith in the left-hand-side reactor during experimental conditions of $0.6\%CH_4$ and $0.7m/s$ superficial velocity

ward toward the reactor wall, and is accumulated in the insulation. Once the insulation reaches a temperatures that is higher than that of the radial thermocouples, the thermal energy is distributed back into the reactor through convection.

Figure 4.28 shows the radial gradients recorded in the left side inert ceramic monolith section as one cycle progressed. These results are at conditions of $0.6\%CH_4$ and $0.7m/s$ superficial velocity and a switch time of $100s$, starting from the beginning of the fifth cycle, moving forward in time to the beginning of the sixth cycle. From this graph the movement of the radial gradients is seen to be significant. The temperatures near the wall increases by about 100^oC. As the cool gas enters the left side reactor, the radial gradient becomes more linear along with an increase in temperature. By the end of the half cycle, the radial gradient shows significant heating throughout. As the second half cycle progresses, the radial temperatures begin to cool, and by the end of the full cycle, the thermal position of the radial points return to nearly the temperatures observed at the beginning of the previous cycle.

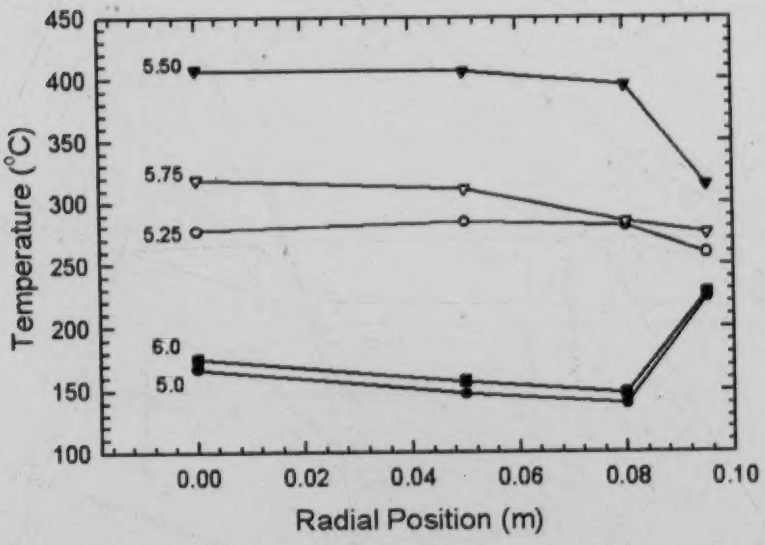

Figure 4.28: Experimental radial gradients in the inert ceramic monolith in the left side reactor for one full cycle during experimental conditions of $0.6\%CH_4$ and $0.7m/s$ superficial velocity

At the beginning of the cycle from left to right, the wall temperature is greater than the temperature at the centre. At the half-cycle point, the wall temperature becomes less than that of the centre temperature. This is better seen in Figure 4.29 where the temperature progression over many full cycles is shown at the same conditions of 0.6% methane and inlet velocity of $0.7m/s$.

Figure 4.30 shows the radial thermal gradients for the experimental conditions of $0.6\%CH_4$ and $0.7m/s$ superficial velocity with the metal monoliths Here the three thermal profiles indicate the beginning of the regime without heat extraction, the point where heat extraction was activated, and at the end of the regime with heat extraction, respectively.

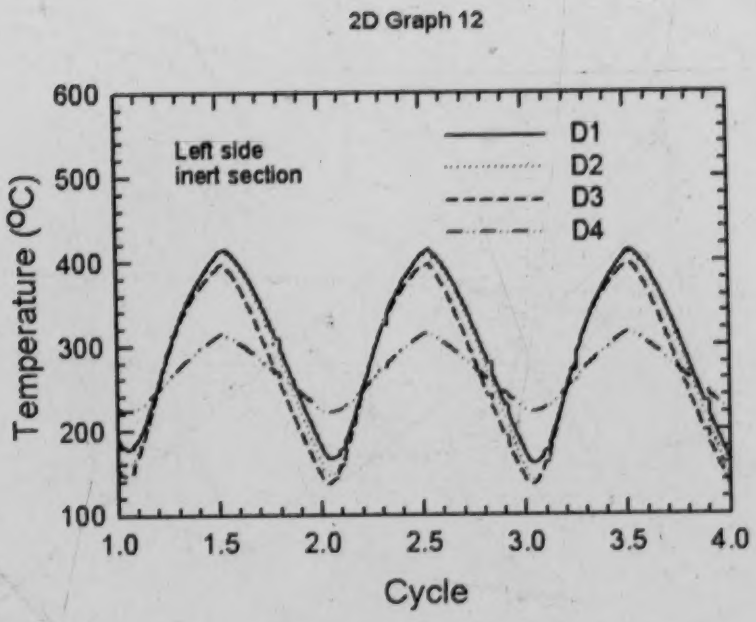

Figure 4.29: Experimental radial gradients in the inert ceramic monolith in the left side reactor for three full cycles during experimental conditions of $0.6\%CH_4$ and $0.7m/s$ superficial velocity

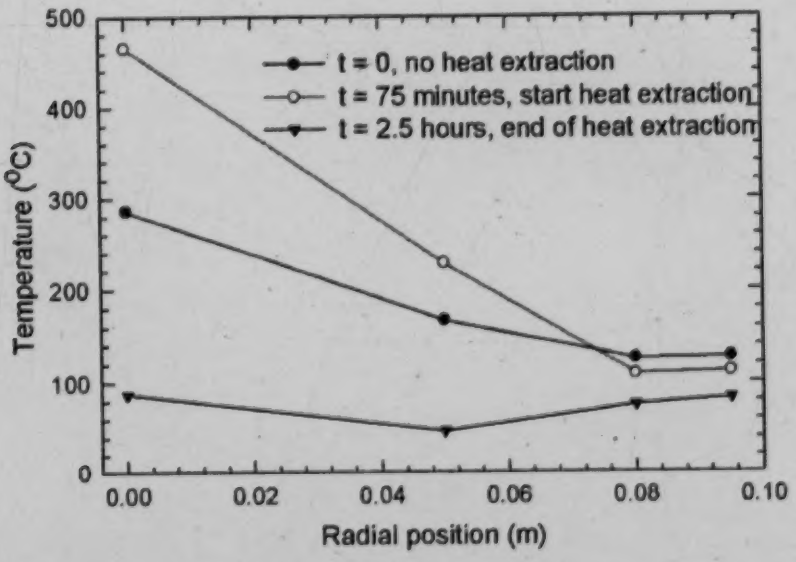

Figure 4.30: Experimental radial temperature profiles in the inert metal monolith of the left-hand-side reactor during experimental conditions of $0.6\%CH_4$ and $0.7m/s$ superficial velocity

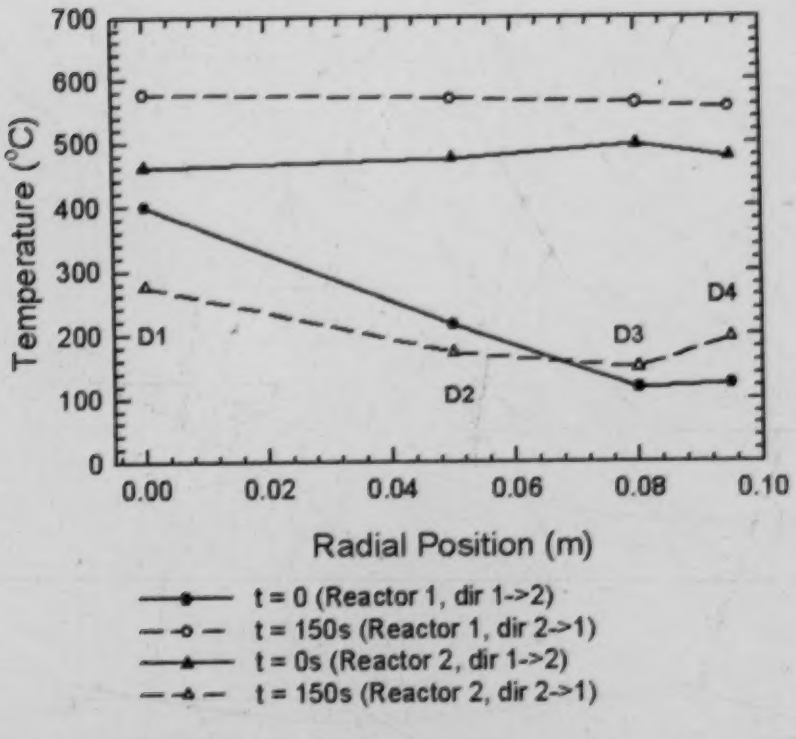

Figure 4.31: Experimental radial temperature profiles for one half cycle in the inert metal monolith in both reactors during experimental conditions of $0.2\%CH_4$ and $0.7m/s$ superficial velocity

The radial gradients in the metal monoliths show more variation over time. This dynamic behaviour was also seen in the axial temperature profiles. Figure 4.31 shows the radial gradients present in both left and right reactor inert sections for the conditions of 0.2% methane and $0.7m/s$ superficial velocity at a switch time of $150s$ during one half cycle. It is seen that when the reactor is flowing from 1 to 2, or left to right, the left side reactor is cooler near the middle and the wall, while the right side reactor stays hot throughout. When the flow direction is switched to being from right to left, or 2 to 1, the radial temperatures in the right remain hot, while the left radial temperatures remain cool. Overall, the right side reactor shows higher temperatures and the left side reactor shows lower temperatures. This could be due because of the amount of thermal energy stored in the insulation around each reactor.

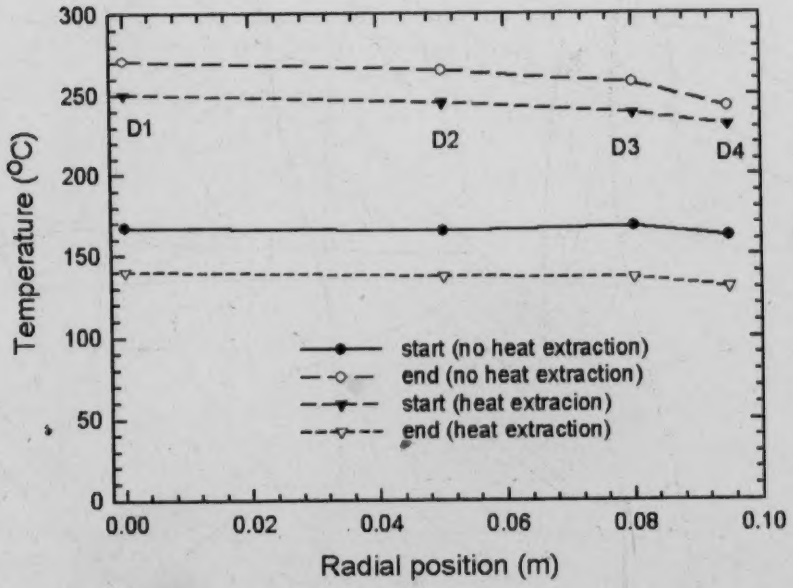

Figure 4.32: Experimental radial temperature profiles in the inert Denstone balls in the left-hand-side reactor during experimental conditions of $0.6\% CH_4$ and $0.7 m/s$ superficial velocity

The radial thermal profiles in the Denstone balls was found to be more evenly distributed from the centre to the reactor wall. The densely packed Denstone balls create an effective heat trap for the system because of its greater capacity for storing heat energy. Figure 4.32 shows the radial thermal profile of the inert section in the left-hand-side reactor for experimental conditions of 0.6% methane concentration and $0.7 m/s$ superficial velocity.

The radial thermal profiles show that the Denstone balls were able to create a uniform radial temperature profile. The radial profiles in the monoliths were more dynamic, which proves that the reactor system includes both radial and axial effects.

4.6 Discussion

The experimental results show the behaviour of the reverse-flow reactor with ceramic monoliths, metal monoliths, and Denstone balls as inert materials. Heat extraction was conducted with each of these materials at a methane concentration of 0.6% and various superficial velocities.

One of the most important observations found through the experiments was that the history of the reactor plays an important role in the behaviour of the reactor. Each previous operating regime effected the results for the subsequent runs. Even if the methane concentration and air velocity were identical for two runs, the reactor was unable to attain the same thermal state for both conditions, during the time of the experimental run. This makes comparison of the results difficult. From the few GC results obtained, it was observed that the methane was fully combusted at the middle and outlet of the reactor. Temperatures of well above $900K$ in the active section allowed for complete conversion of the methane.

The ceramic monoliths showed fairly stable behaviour for inlet methane concentrations of 0.2% and 0.6%. Low methane concentrations of 0.2% lead to the overall reduction of heat, or extremely slow heating in the reactor. The outlet temperature remains near ambient, therefore it might be possible that the heat trap effect is unable to conserve enough energy in the reactor at such low methane concentrations. A higher methane concentration of 0.6% lead to an increase in reactor temperature, such that over time, heat could be extracted from the experiment. The inlet temperatures remained ambient, and the outlet temperatures showed an increase from ambient to nearly $100K$ above ambient. This increase could be due to the effects of the switching time and the physical properties (thermal conductivity, and thermal capacity) of the ceramic material. Overall, a greater shift in temperature is observed as the superficial velocity is increased. From the results with the inert ceramic monoliths, it was seen that radial thermal gradients also experience heating and cooling within one cycle. This would indicate that among many other things, the switch time also has an effect on the radial temperature gradients.

The metal inert monoliths showed more movement in the temperatures than that seen with the ceramic monoliths. This could be due to the higher thermal conductivity of the metal monolith. The capacity for storing heat for the metal material is fairly low, therefore more temperature movement would be expected. As seen with the ceramic monoliths, at a methane concentration of 0.2%, the reactor showed cooling overall, and at a higher methane concentration of 0.6%, the reactor showed an overall heating. The heating rate with the metal inert monoliths was higher than that of the ceramic monoliths.

There was more movement with the inert metal monoliths, therefore, the cycle times had to be adjusted to be shorter than that set for the ceramic, as to minimize heat escaping from the outlet. The higher outlet temperatures could be a result of a slightly longer switch time than required. The radial gradients in the metal monolith sections showed greater temperature movement over time, than what was seen in the ceramic monolith. As mentioned before, this could be due to the high thermal conductivity of the material. The radial profile was somewhat linear with coolest temperatures being at the wall.

The Denstone balls showed similar results to the ceramic monoliths, as in the low methane concentration of 0.2% resulted in overall cooling, and a methane concentration of 0.6% showed an overall heating in the reactor system. Eventhough the Denstone ball material is a type of ceramic, its ability for thermal storage is nearly 3 times greater than that of the ceramic monolith. This was visible from the operation of the experiments as the outlet temperatures with Denstone balls remained cooler than those of the ceramic monoliths. The outlet temperatures with the Denstone ball packing would remain fairly cool, and the increase or decrease in temperatures within the reactor were at a steady pace. The radial gradients showed a very flat profile, which would indicate that the radial gradients vary less than what was seen with the ceramic and the metal monoliths.

With each type of inert, extracting heat from the system resulted in a cooling in the inert section and heating in the active section. The heat was being extracted from the middle of the two active beds, thus the catalyst sections became hotter over time. The rate of the cooling in the reactor with

heat extraction, would depend on the amount of heat being extracted as well as the physical properties of the material. Because the inert sections become cooler, the inlet gas is eventually unable to reach a temperature to allow for the combustion reaction. Thus the temperature profile in the reactor would begin to decrease uniformly. A pseudo-steady state while extracting heat can be reached, provided that the heat generated and stored is nearly the same as that being extracted. Therefore, the amount of heat being extracted is an important design parameter. Detailed optimization of this parameter is required, however is beyond the scope of this project. The metal monoliths temperatures changed the fastest among the three inert types, followed by the ceramic monoliths and Denstone balls.

The radial gradients not only depended on the inert material, but are also affected by the amount of thermal energy which is stored in the insulation of the reactor. If the insulation is hotter than the inert, then the heat from the insulation will help heat the reactor, and when the reactor is hotter than the insulation, heat from the reactor helps to increase the temperature of the insulation.

Chapter 5

Simulation Model Validation

The experiments conducted with the CFRR were used to verify the numerical simulator developed by Salomons and Hayes [24] [32]. This simulator was previously verified with only ceramic inert monoliths, and not with any other type of inert or with heat extraction. This chapter presents results obtained for the model validations conducted for each type of inert inserted in the CFRR. A comparison of experimental and simulated temperature profiles is presented throughout this chapter.

For simulations involving extraction of heat, the mass flow rate ratio of the inlet gas with the that of the extracted gas determined the heat extraction ratio of the system. For example, for a superficial velocity set to $0.3m/s$, which is a mass flow rate of $40kg/hr$, and though calculations shown in Appendix B, the flow-rate through the mid-pipe is determined to be $8kg/hr$, the heat extraction ratio would be $8kg/hr/40kg/hr$, or 0.2. There could be some experimental error associated with this calculation, however the exact amount is unavailable as the error of the flow-meter is undetermined. The heat extraction ratio is what allowed the simulator to determine by how much the flow-rate should change through the U-bend.

A sensitivity analysis was also conducted on the numerical model, where the effect of the amount of heat extraction was varied for a particular experiment to its effects on the system. A parameter analysis is presented in this chapter. The effect of cycle times and methane concentration on the behaviour of the reactor system is presented.

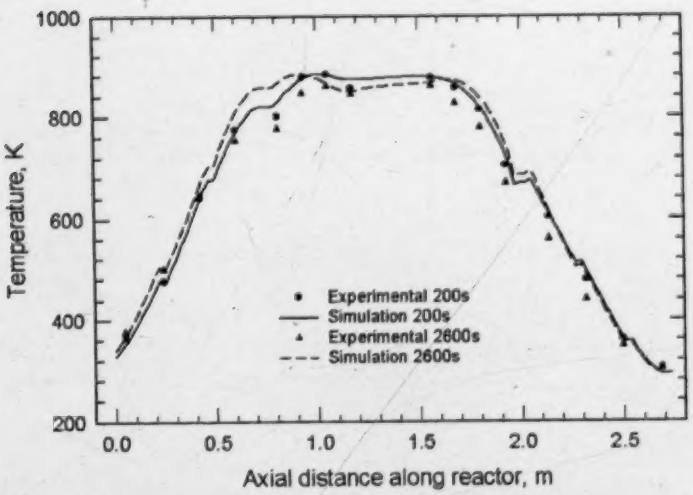

Figure 5.1: Ceramic monolith: Model and Experimental results for axial reverse flow temperature profile at $0.2\%CH_4$ and $0.7m/s$ superficial velocity. Profiles shown for the beginning and end of the simulation

5.1 Ceramic Monolith Inert

The numerical simulations conducted for the inert ceramic monolith showed good agreement with the experimental results. The experimental trends were well predicted by the numerical model provided that the initial conditions showed small or no hot spots.

For the experiment with $0.7m/s$ superficial velocity and 0.2% methane, the numerical simulator behaved much like the experimental system. From Figure 5.1, it is seen that the temperature profile obtained from the simulator match those obtained through the experiments for 24 switchings. The initial temperature profile for this run was free of irregular hot spots.

However, with the case with 0.6% methane and a superficial velocity of $0.3m/s$, the simulation results diverge from the experimental results as time increases. Figure 5.2 clearly shows this behaviour. The initial temperature conditions for this regime included a hot spot in the second reactor, where the temperature in the second active section was about $100K$ above that of the fist reactor. The numerical simulator must have encountered difficulties

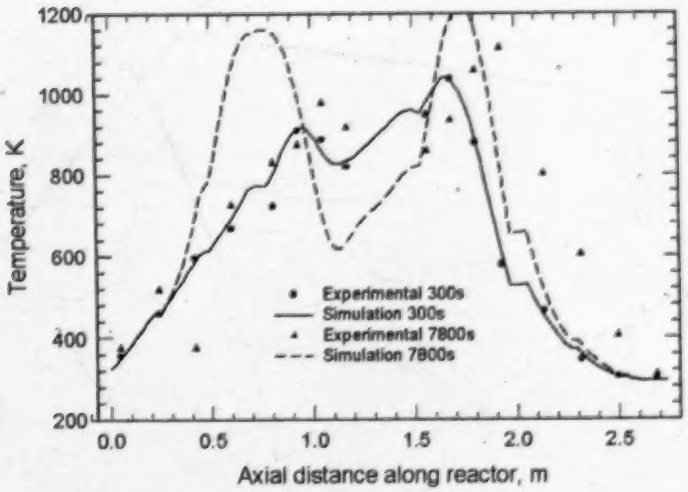

Figure 5.2: Ceramic monolith: Model and Experimental results for axial reverse flow temperature profile at $0.6\%CH_4$ and $0.7m/s$ superficial velocity. Profiles shown for the beginning and end of the simulation

calculating the heat accumulation in the reactor, and as seen in Figure 5.3, showed extremely pronounced peaks being formed in the reactor by the fifth end of the fifth cycle. This indicates that the simulator is unable to process irregular temperature profiles.

The temperature trends of heating or cooling were well predicted by the simulator. At lower methane concentrations, the simulator predicted a cooling in the reactor, and for higher methane concentrations, heating of the reactor was seen. Figure 5.4 shows experimental and simulation results for the beginning and the end of the regime with 0.2% methane and a superficial velocity of $0.3m/s$ during forward flow.

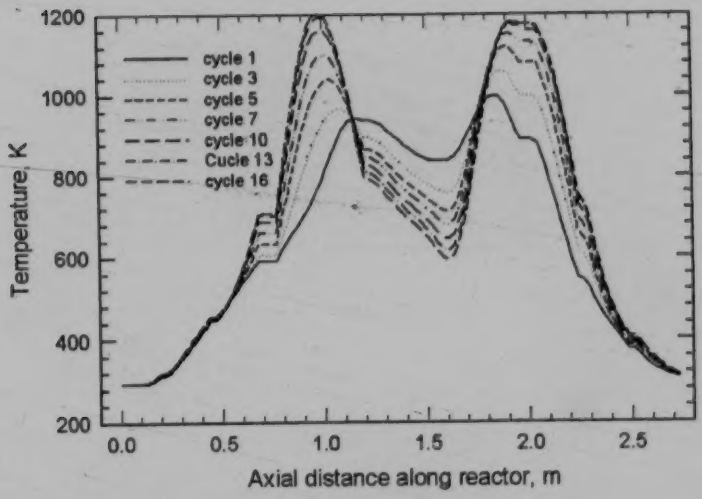

Figure 5.3: Ceramic monolith: Model results for multiple axial reverse flow temperature profiles at $0.6\%CH_4$ and $0.3m/s$ superficial velocity.

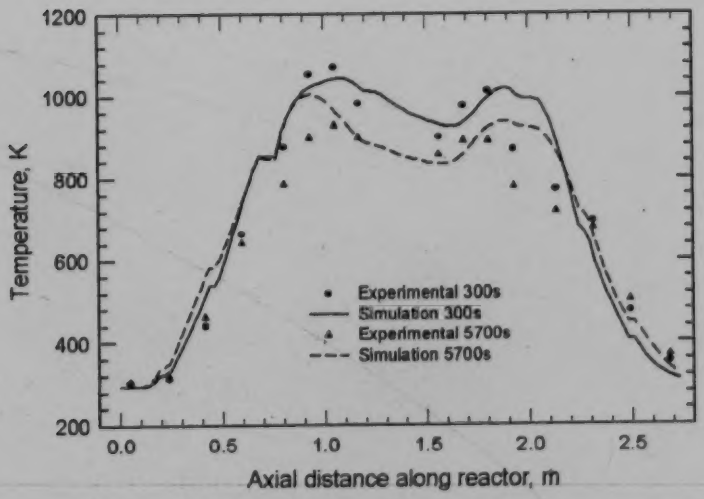

Figure 5.4: Ceramic monolith: Model and Experimental results for axial forward flow temperature profile at $0.2\%CH_4$ and $0.3m/s$ superficial velocity. Profiles shown for the beginning and end of the simulation

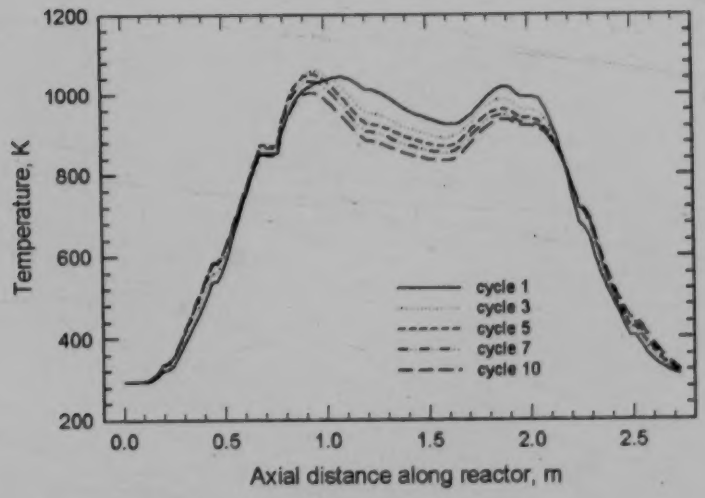

Figure 5.5: Ceramic monolith: Simulated axial forward flow temperature profiles. Multiple forward flow profiles for $0.2\%CH_4$ and $0.3m/s$ superficial velocity

The temperatures of the inert sections, thermocouples A, B, C, and D1, are in agreement with those predicted by the simulator. Thermocouples G, J, and in the active section are over predicted by the simulator, while thermocouple L show similar temperatures for both the model predictions and the experimental results. The thermal trend of overall cooling in the reactor that was seen in the experimental results, Figure 4.1, was also present from the numerical simulator, Figure 5.5.

Similarly, the thermal trend of overall heating in the reactor for the conditions of 0.6% methane and $0.7m/s$ superficial velocity was seen both in the experimental case, Figure 4.3, as well as in the case of the simulator, Figure 5.6.

Figure 5.7 shows that the simulator can effectively predict the trend and the instantaneous axial temperature profile in agreement with the experimental temperature profile and trend at the conditions of $0.6\%CH_4$ and $0.7m/s$ superficial velocity. The temperatures in the inert bed are matched very well by the simulator. The temperatures in the active bed are a little over-predicted, however, the points where heat accumulation occurs most are emphasized.

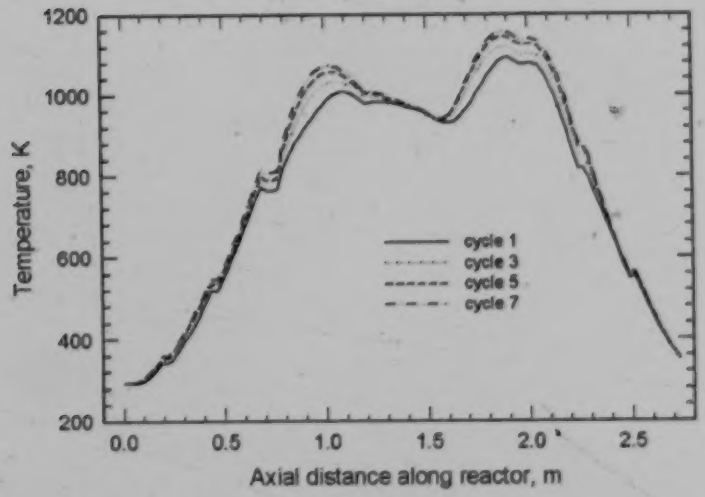

Figure 5.6: Ceramic monolith: Simulated axial forward flow temperature profiles. Multiple forward flow profiles for $0.6\%CH_4$ and $0.7m/s$ superficial velocity

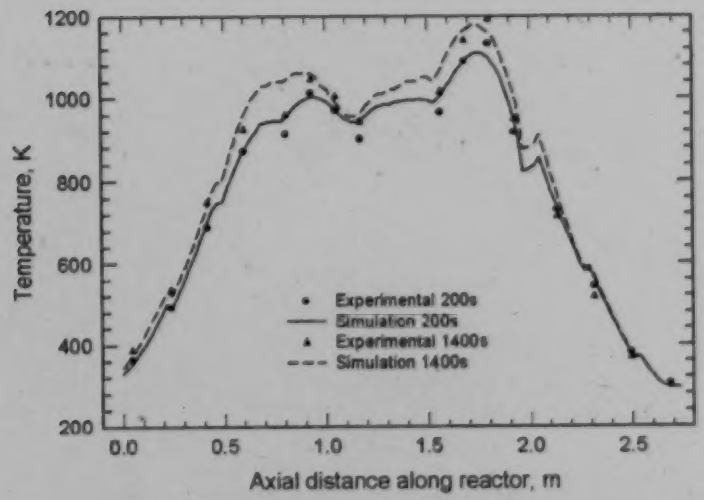

Figure 5.7: Ceramic monolith: Simulated and experimental axial reverse flow temperature profiles for $0.6\%CH_4$ and $0.7m/s$ superficial velocity, switch time $100s$

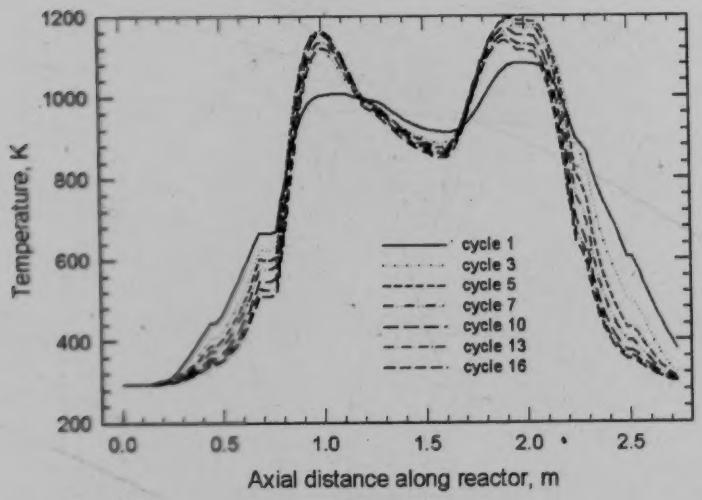

Figure 5.8: Ceramic monolith: Simulated axial forward flow temperature profiles with heat extraction. Multiple forward flow profiles for 0.6%CH_4 and 0.3m/s superficial velocity

Simulations conducted with heat extraction predicted the experimental trend of cooling in the inert section of the monolith, and heating in the catalytic bed. Figure 5.8 shows that over time, the inert monolith section cools while the active beds heat up. This results is for conditions at 0.6% methane concentration and a superficial velocity of 0.3m/s. As previously mentioned, the initial temperature condition plays a key role in the behaviour of the reactor and the numerical simulator.

For the experimental conditions with 0.6% methane and 0.7m/s superficial velocity, the experimental results showed that the system reaches a pseudo-steady state of operations. Figure 5.9 shows minimal cooling in the active catalyst bed and inert sections. This may show that the pilot plant reactor has the capability of storing more heat than that assumed in the numerical model.

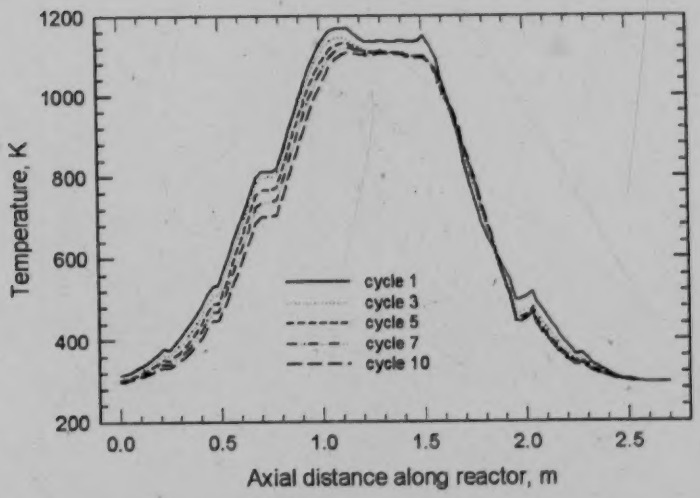

Figure 5.9: Ceramic monolith: Simulated axial reverse flow temperature profiles. Multiple reverse flow profiles for $0.6\%CH_4$ and $0.3m/s$ superficial velocity

The simulator over-predicted the temperatures achieved in the second active section through which the gas passes. Figure 5.10 shows reverse flow axial profiles for both experimental and simulation results at the beginning and the end of the flow regime of 0.6% methane concentration and $0.3m/s$ superficial velocity. The inert and active section temperatures were fairly well predicted for the first reactor the gas passes through, however the active packed bed temperatures are overshot by the simulator for the second reactor the gas is passed through. The temperature overshoot is seen in the first reactor in Figure 5.11, which shows the forward flow results for the same experimental regime.

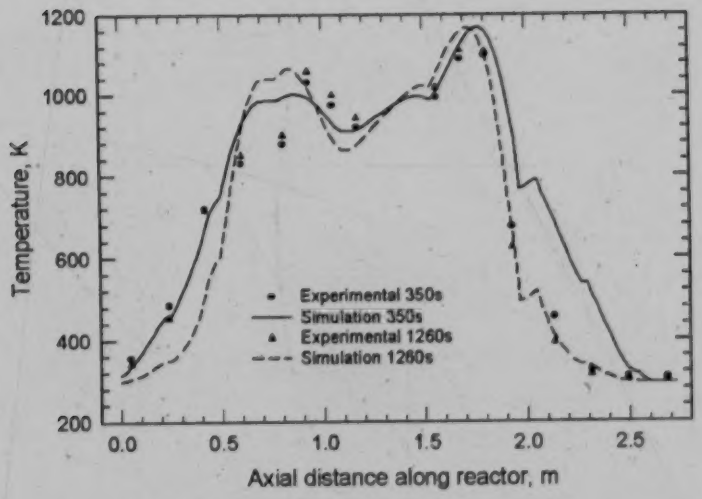

Figure 5.10: Ceramic monolith: Model results for axial reverse flow temperature profile at $0.6\%CH_4$ and $0.3m/s$ superficial velocity with heat extraction.

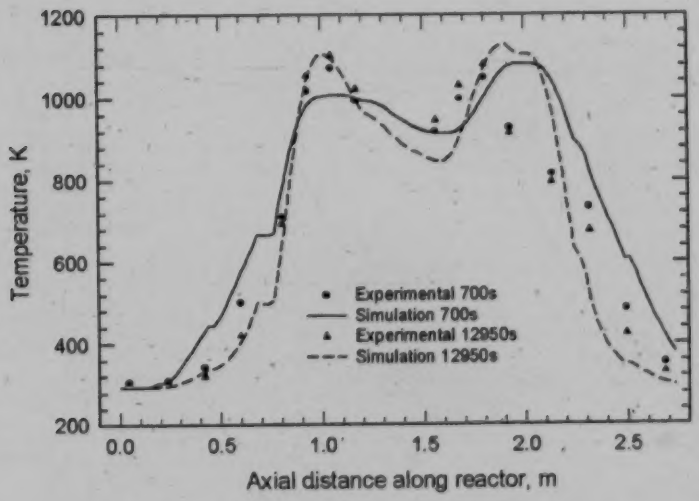

Figure 5.11: Ceramic monolith: Model results for axial forward flow temperature profile at $0.6\%CH_4$ and $0.3m/s$ superficial velocity with heat extraction.

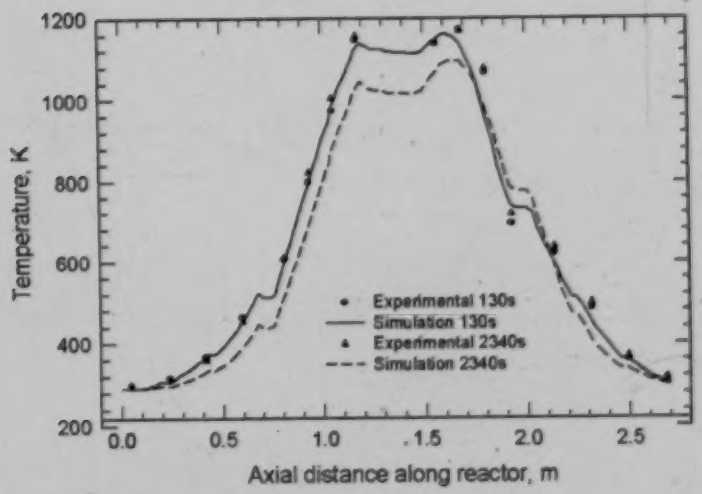

Figure 5.12: Ceramic monolith: Model results for axial reverse flow temperature profile at $0.6\%CH_4$ and $0.7m/$ superficial velocity with heat extraction

If there is error in the heat extraction ratio, the simulator would overpredict the cooling occurring in the reactor. The forward flow results comparing the experimental and simulator temperatures in Figure 5.12, show that the model was able to predict the axial temperatures at the beginning of the run, however as time moves forward, by the end of the run, the simulator shows more cooling than what was seen in the experimental conditions. Again, this may lead to the conclusion that the CFRR reactor is able to contain more thermal energy than modeled in the simulator.

5.2 Metal Monolith Inert

The numerical model showed good agreement with the experimental results for the cases with inert metal monoliths placed as heat traps. As seen in the experimental results, the high conductivity of the metal material allows for greater movement of the axial profiles between each half cycle. Figure 5.13 shows that the beginning and end of the experimental operating conditions were well predicted by the numerical model in the forward flow direction.

The high temperatures achieved at the outlet of the reactor for the exper-

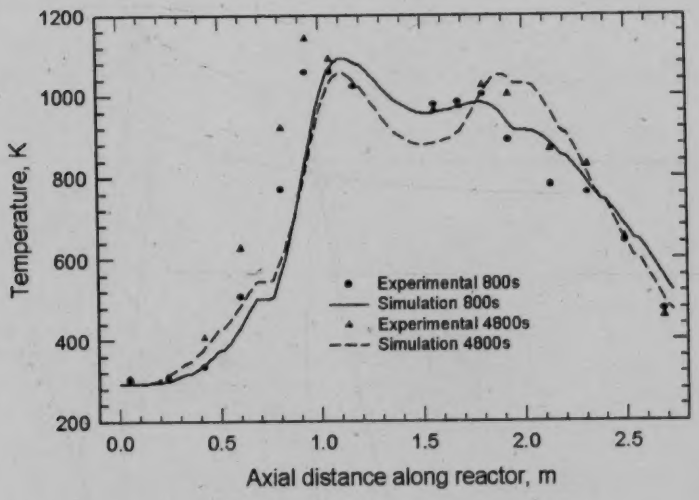

Figure 5.13: Metal monolith: Model results for axial forward flow temperature profile at $0.6\%CH_4$ and $0.3m/$ superficial velocity

imental conditions of 0.6% methane concentration and a superficial velocity of $0.3m/s$. At a higher superficial velocity of $1.2m/s$, and a methane concentration of 0.6%, the simulator over-predicted the outlet temperatures, and the axial temperatures were predicted to be cooler in the model than in the reactor. The experimental temperature trends of the inert monolith section matched well with the model trends, where inert temperatures in the first rector would cool down, while the temperatures in the second reactor would heat up, as the gas passes from the first to the second half of the reactor.

Decreasing the methane concentration also decreased the thermal energy in the active section of the reactor. Simulating the experiment with 0.2% methane concentration and superficial velocity of $1.2m/s$, the lower methane concentration allows for cooling of the reactor, however the simulator over-predicts cooling in the second reactor through which the gas passes, as seen in Figure 5.14. The experimental results from Figure 4.13 in Chapter 4 also shows cooling in the reactor, however results also show a pseudo-steady state of operation. This indicates that the model accounts for more cooling, or less thermal energy storage than that shown in by the experimental reactor.

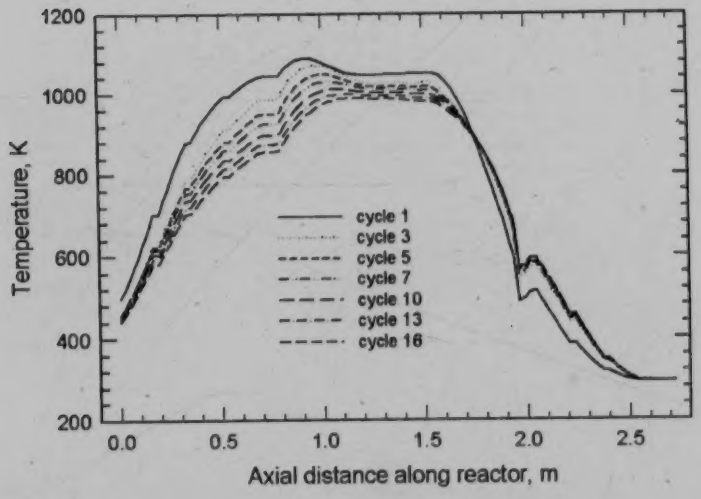

Figure 5.14: Metal monolith: Multiple simulated reverse flow axial temperature profiles at $0.2\%CH_4$ and $1.2m/s$ superficial velocity

The heat extraction simulations predicted the trends seen in the experimental results. The heat extraction experiment conducted with 0.6% methane concentration and a low superficial velocity of $0.3m/s$ resulted in a cooling of in the inert sections, and pseudo steady-state temperatures in the active section. In Figure 5.15, the model shows that over time, the inert sections cooled, while retaining the heat in the active section, which matches the experimental results shown in Figure 5.16.

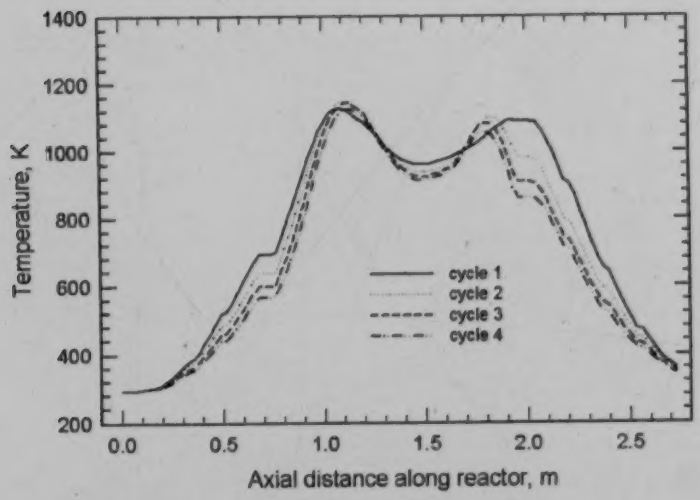

Figure 5.15: Metal monolith: Multiple simulated axial temperature profile with heat extraction. Forward flow profiles at $0.6\%CH_4$ and $0.3m/s$ superficial velocity with switch time of $400s$

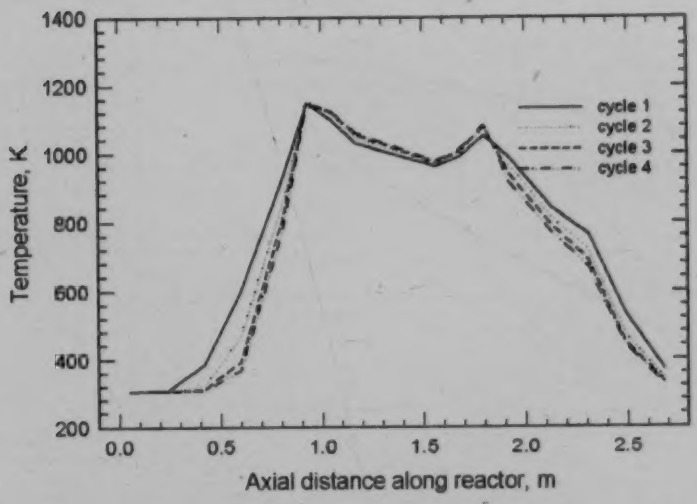

Figure 5.16: Metal monolith: Multiple experimental axial temperature profile with heat extraction. Forward flow profiles at $0.6\%CH_4$ and $0.3m/s$ superficial velocity with switch time of $400s$

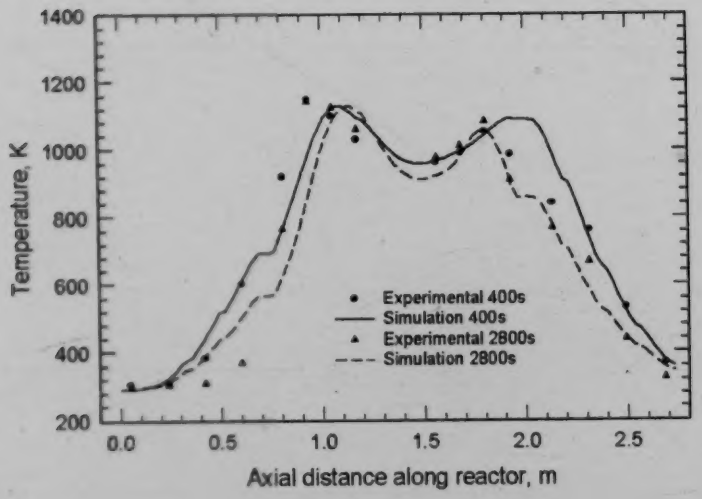

Figure 5.17: Metal monolith: Comparison of experimental and simulated axial temperature profiles for the forward flow direction at the beginning and end of the run. Profiles for cycle one at $0.6\%CH_4$ and $0.3m/s$ superficial velocity with switch time of $400s$

The comparison of experimental and simulation results for reverse flow at the beginning and end of the operating regime of 0.6% methane concentration and $0.3m/s$ superficial velocity is shown in Figure 5.17. The experimental and model temperatures match up quite well, however, as seen before, the outlet model temperature is over-predicted by about $40K$.

At a higher superficial velocity of $1.2m/s$ and a methane concentration of 0.6% with heat extraction, the model results showed further cooling than seen in the experimental results. Figure 5.18 shows both experimental and model results for forward flow at the beginning and end of the operating regime spanning over about 30 cycles. The experimental points at the end of the regime show higher temperatures in the active sections than the model predictions. The temperatures in the inert sections are matched in the first reactor through which the gas passes, however, the temperatures in the second inert section are under-predicted.

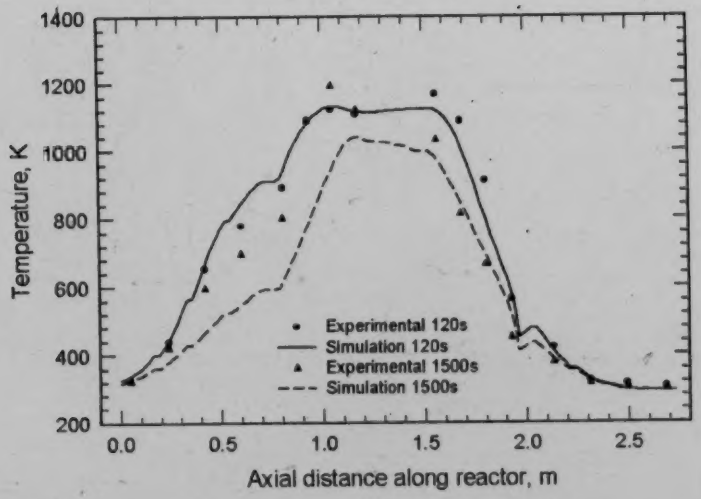

Figure 5.18: Metal monolith: Comparison of experimental and simulated reverse flow axial temperature profiles with heat extraction at $0.6\%CH_4$ and $1.2m/s$ superficial velocity

5.3 Packed Denstone Ball Inert

The first result presented for the validation of the model with inert Denstone balls is with a methane concentration of 0.2% and a superficial velocity of $0.7m/s$. Figure 5.19 shows that the model and experimental temperatures for the inert packed bed sections are in good agreement with one another. The active bed sections are slightly under-predicted by the model. Cooling occurs in both experimental and simulator results, however the model shows up to $60K$ cooler temperatures in the active section of the reverse-flow reactor.

Figure 5.20 shows the experimental multiple forward cycles while Figure 5.21 shows temperatures predicted by the model for the same operating conditions. Both figures show that over a span of 10 cycles, the active bed of the reactor showed up to $100K$ cooling in the catalyst bed, however the inert sections remained cool and at a pseudo-steady state of operation.

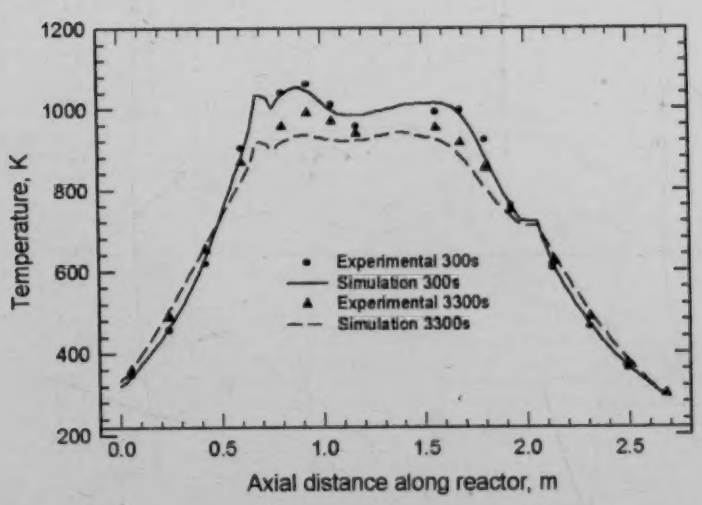

Figure 5.19: Denstone balls: Comparison of experimental and simulated reverse flow axial temperature profiles at $0.2\%CH_4$ and $0.7m/s$ superficial velocity

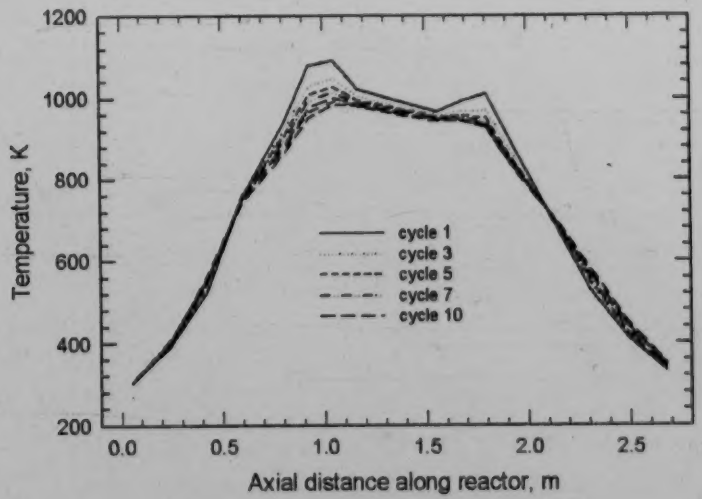

Figure 5.20: Denstone balls: Multiple experimental forward flow axial temperature profiles at $0.2\%CH_4$ and $0.7m/s$ superficial velocity with a cycle switch time of $150s$

At a higher superficial velocity of $1m/s$ and low methane concentration of 0.2%, the active sections show a cooling for both experimental and simulator results, while the inert sections show less movement in temperature over time,

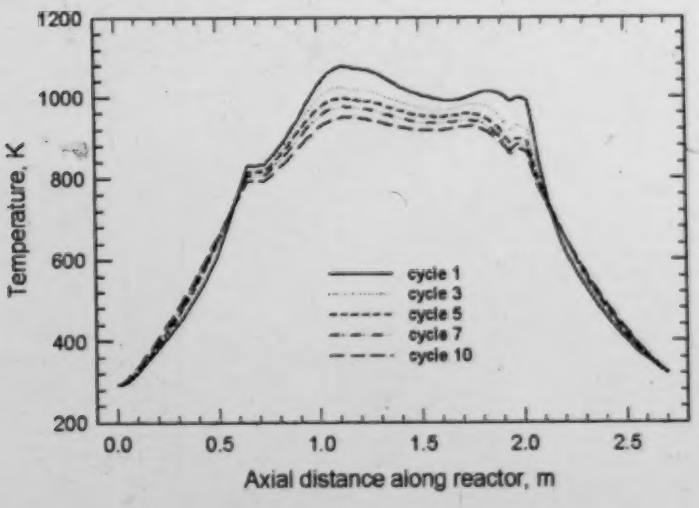

Figure 5.21: Denstone balls: Multiple simulated forward flow axial temperature profiles at $0.2\%CH_4$ and $0.7m/s$ superficial velocity and cycle switch time of $150s$

as seen in Figure 5.22. The thermal trend in the reactor over 10 cycles, modeled by the simulator seen in Figure 5.23, shows the same behaviour as seen in Figure 4.20, with cooling in the active bed section, and slow heating of the inert Denstone ball section. The model predicts the cooling trend in the reactor for a low methane concentration at both low and high superficial velocities.

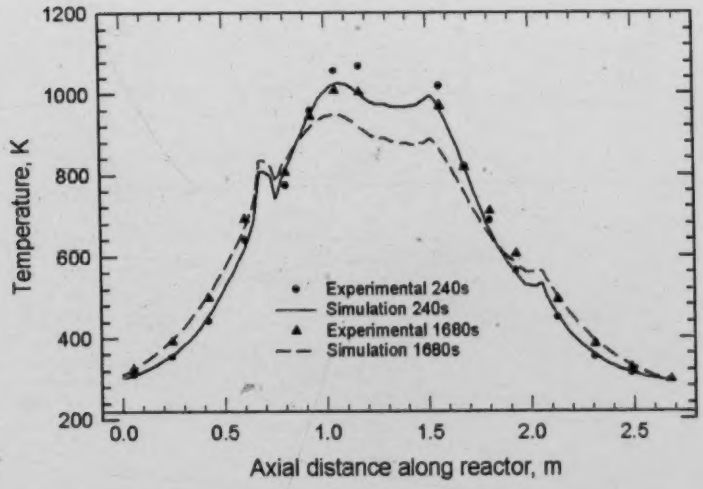

Figure 5.22: Denstone balls: Comparison of experimental and simulated reverse flow axial temperature profiles at $0.2\%CH_4$ and $1m/s$ superficial velocity

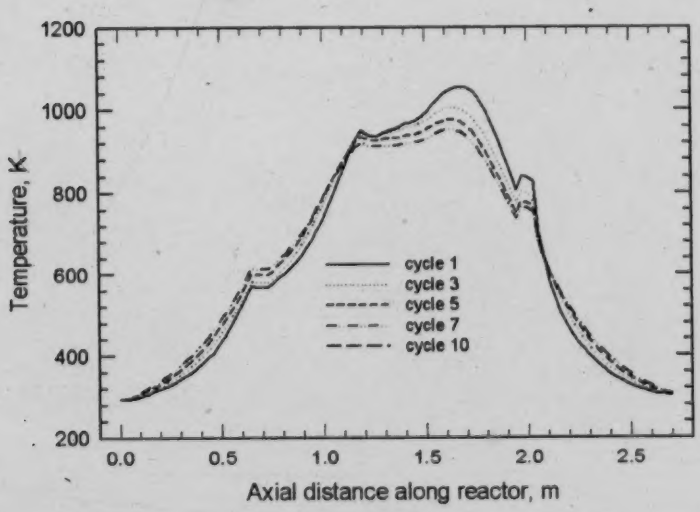

Figure 5.23: Denstone balls: Multiple simulated forward flow axial temperature profiles at $0.2\%CH_4$ and $0.7m/s$ superficial velocity and cycle switch time of $60s$

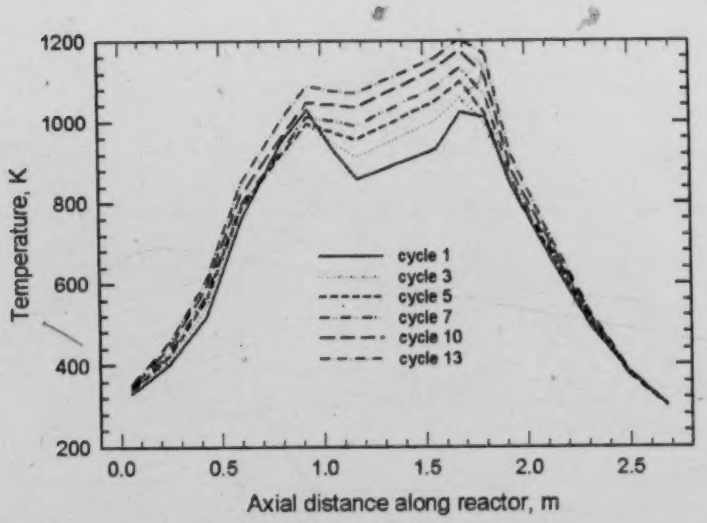

Figure 5.24: Denstone balls: Multiple experimental reverse flow axial temperature profiles at $0.6\%CH_4$ and $1.2m/s$ superficial velocity with a cycle switch time of $100s$

A higher methane concentration of 0.6% and $1.2m/s$ superficial velocity increased the temperature in reactor, however, the simulator predicted a lower temperature rise than was observed experimentally. Figure 5.24 shows that the heat accumulation in the active section is very significant, however, Figure 5.25 shows a slower accumulation of heat energy in the active bed section. The simulator showed a heat accumulation rate of nearly 17 times less than that seen in the experiments.

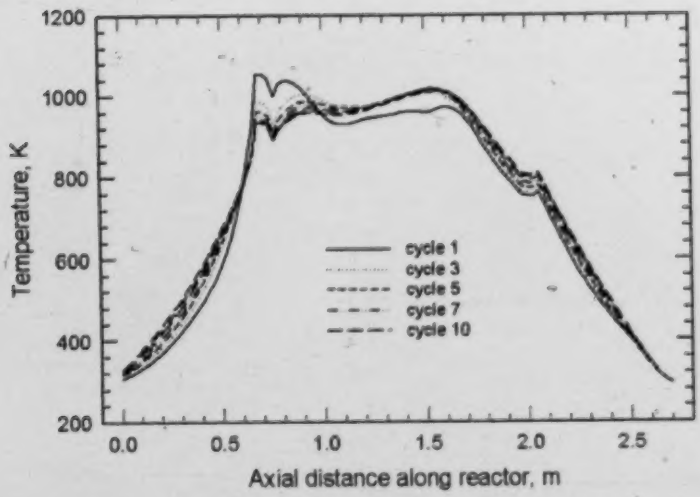

Figure 5.25: Denstone balls: Multiple simulated reverse flow axial temperature profiles at 0.6%CH_4 and $1.2m/s$ superficial velocity and cycle switch time of $100s$

The temperatures in the inert packed bed sections are modeled favourably as seen in Figure 5.26 for the axial temperatures during the beginning and end of the operating regime. This figure also shows that by the end of the run, the model under-predicted the temperature between $60K$ to $100K$ in the active section. At a lower superficial velocity of $0.3m/s$ and methane concentration of $0.6m\%$, the simulator predicted the experimental results.

Figure 5.27 shows that throughout the experimental run in the forward direction, the simulator temperature results matched well with the active and inert section. At the end of the regime, the simulator missed more experimental temperature points than at the beginning of the regime, which means that the model predicts better at lower times, or less cycles.

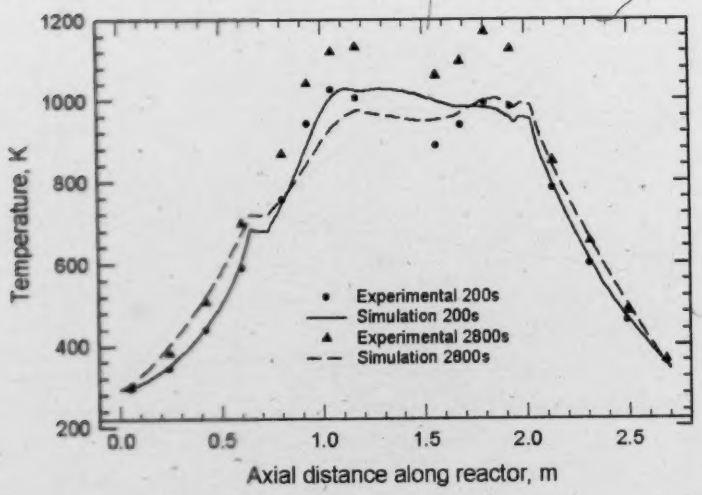

Figure 5.26: Denstone balls: Comparison of experimental and simulated reverse flow axial temperature profiles at $0.6\%CH_4$ and $1.2m/s$ superficial velocity

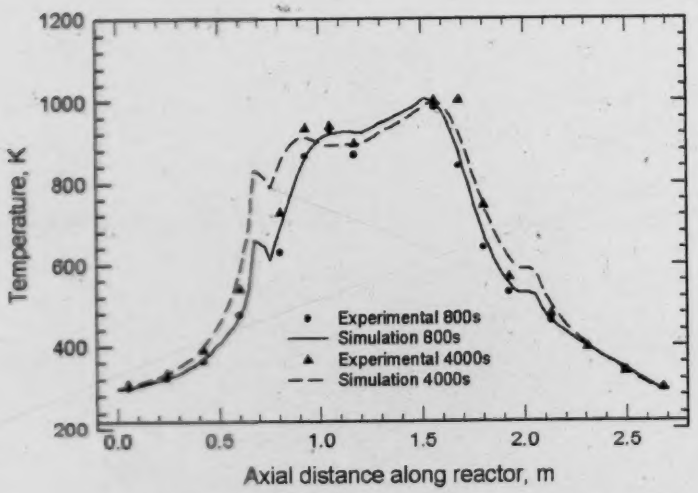

Figure 5.27: Denstone balls: Comparison of experimental and simulated reverse flow axial temperature profiles at $0.6\%CH_4$ and $0.3m/s$ superficial velocity

The inert beds showed more accumulation of heat from the model than from the experimental results. Figure 5.28 shows the axial profiles from cycles 1, 3, and 5 resulting from the model, and Figure 5.29 shows the experimental results. Both show a heating trend throughout the reactor, while the endpoints remained cool at nearing $300K$.

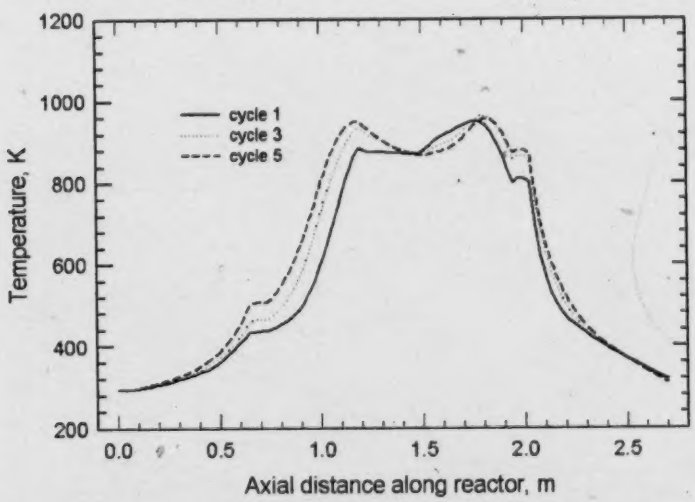

Figure 5.28: Denstone balls: Multiple simulated reverse flow axial temperature profiles at $0.6\%CH_4$ and $0.3m/s$ superficial velocity and cycle switch time of $400s$

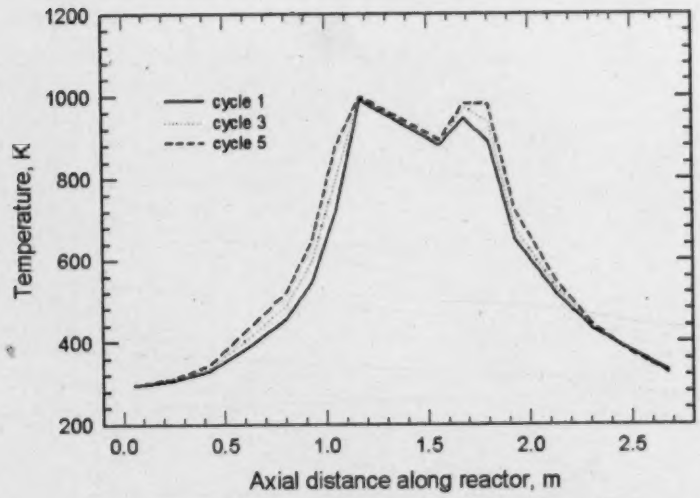

Figure 5.29: Denstone balls: Multiple experimental reverse flow axial temperature profiles at $0.6\%CH_4$ and $0.3m/s$ superficial velocity with a cycle switch time of $400s$

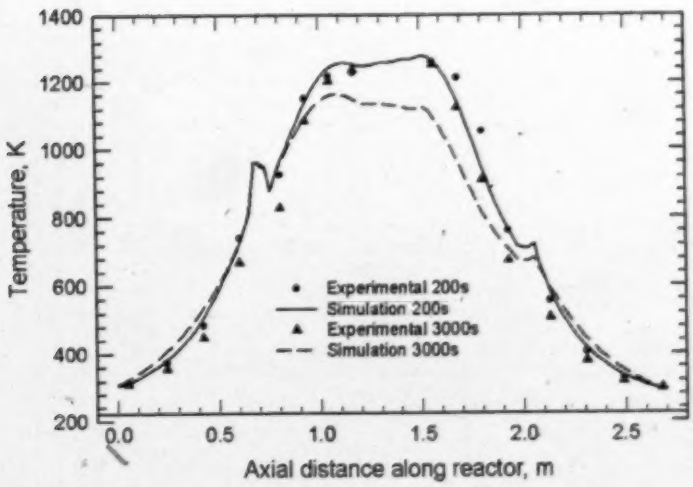

Figure 5.30: Denstone balls: Comparison of experimental and simulated reverse flow axial temperature profiles with heat extraction at $0.6\%CH_4$ and $1.2m/s$ superficial velocity with a cycle switch time of $100s$

Introducing heat extraction into the system generated model temperature results with rapid cooling in the reactor. For the system with 0.6% methane concentration and a superficial velocity of $1.2m/s$, Figure 5.30 shows that by the end of the operating regime, the simulator temperatures cooled between $60K$ and $90K$ more than the experimental active section temperatures. The inert packed bed sections remained at a stable state throughout the simulated run over 16 cycles as seen in Figure 5.31. This figure also presents the cooling of the active section, particularly the second reactor while flowing in the forward direction.

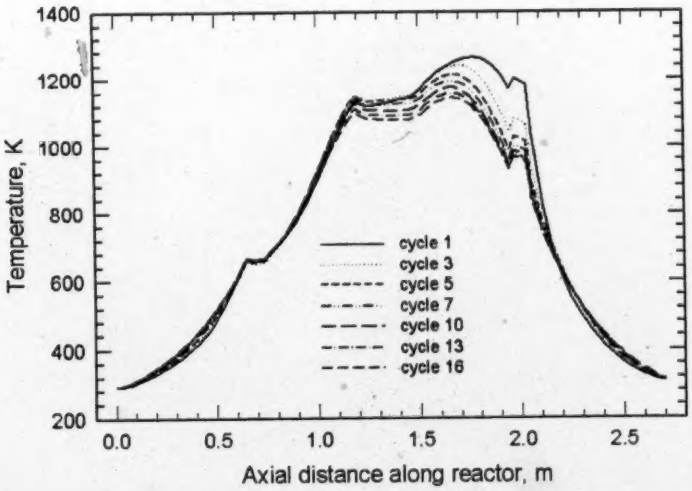

Figure 5.31: Denstone balls: Multiple simulated forward flow axial temperature profiles at $0.6\%CH_4$ and $1.2m/s$ superficial velocity and cycle switch time of $100s$

5.4 Sensitivity Analysis - heat extraction

A sensitivity analysis was conducted on the amount of heat extraction modeled by the numerical simulator. The experimental conditions of no methane and superficial velocity of $0.7m/s$ and a heat extraction ratio of approximately 0.1 was used for this analysis. The elimination of methane from the system eliminates the effects of the combustion reaction. The only heat that is distributed in the reactor is that which remained upon the turning off of methane. Two heat ratios, 0.1 and 0.3 were simulated for this condition. The simulator modeled a much faster cooling of the reactor than the experimental results showed. Figure 5.32 shows the experimental temperatures and the simulated temperatures after the 5^{th} cycle. The model results show the same temperature trend, however a heat extraction ratio of 0.3 cools up to $130K$ faster than the profile developed from a heat extraction ratio of 0.1. Both axial profiles have under-predicted temperatures in the, however the temperatures in the inert sections are favourably modeled by the simulator.

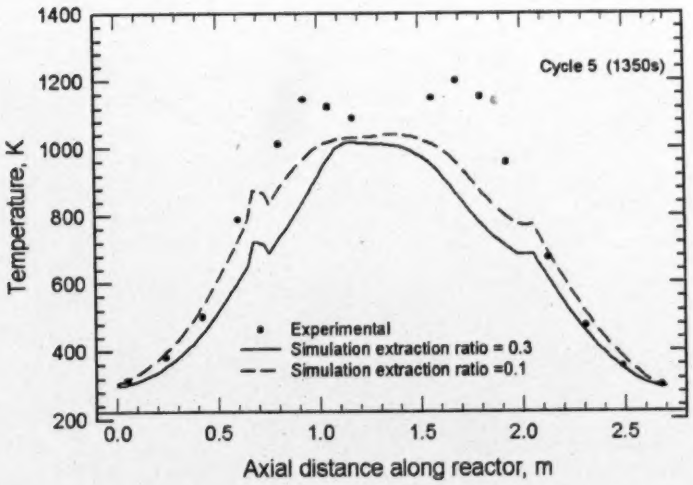

Figure 5.32: Comparison of different heat extraction ratios at the 5^{th} cycle. Experimental and simulated forward flow axial temperature profiles with heat extraction at $0\%CH_4$ and $1.2m/s$ superficial velocity with a cycle switch time of $100s$

By the 10^{th} cycle, it is seen in Figure 5.33 that the simulated axial temperature profile at a ratio of 0.1 showed closest results to the experimental temperature points.

Increasing the heat extraction ratio causes the temperature profile of the reactor to cool at a faster rate, however it has no effect on the shape of the axial profile.

5.5 Parameter Analysis

Parameter analysis was conducted on the simulator by changing the residence time through the reactor and by changing the methane concentration. Both the cycle time and the superficial velocity was varied independently for the experimental conditions with the inert ceramic monoliths.

5.5.1 Cycle Time and Velocity

The experimental conditions with a methane concentration of 0.6% methane and $0.7m/s$ superficial velocity was chosen. The experimental switch time was

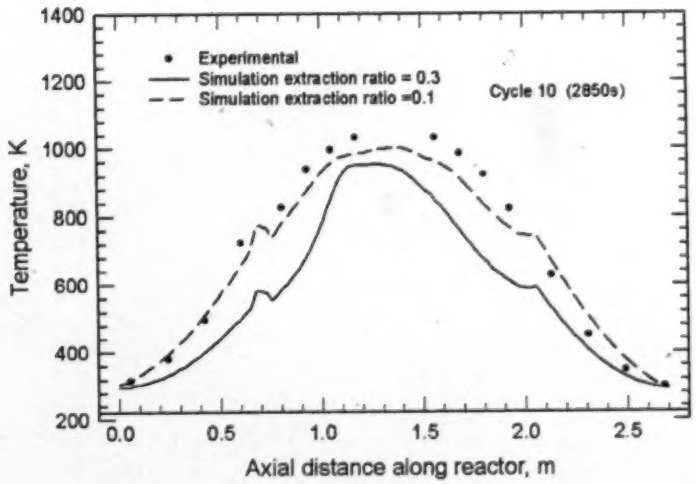

Figure 5.33: Comparison of different heat extraction ratios at the 10^{th} cycle. Experimental and simulated forward flow axial temperature profiles with heat extraction at $0\%CH_4$ and $1.2m/s$ superficial velocity with a cycle switch time of $100s$

set to $100s$, and was varied by the simulator to 200 and 400. The results are shown in Figure 5.34.

With each increasing cycle time, the axial temperature profile in the reactor was shifted or pushed further along the reactor. The peaks in the reactor showed an increased displacement with each increase in cycle time. The gas has more residence time at a higher switch time, which leads to pushing the thermal profile further in the direction of flow. The outlet temperature also increases, which indicates a greater heat loss from the endpoint of the reactor. This is an unfavourable condition as it is desired to keep the heat energy near the active sections of the reactor. An extreme case of increasing the cycle time would be an infinite cycle time. This extreme case can be referred to as a case without flow reversal, where it is assumed that over time the thermal energy in the reactor escapes through the outlet, which eventually extinguishes the reactor.

The same experimental conditions were chosen to examine the effect of different superficial velocities of $1m/s$ and $2m/s$, at the experimental switch

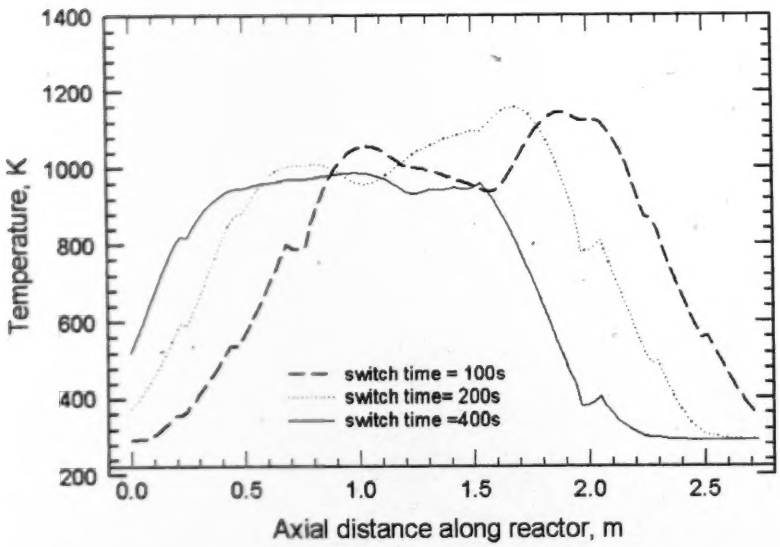

Figure 5.34: Comparison of different cycle switch times at the 5^{th} cycle. Simulated reverse flow axial temperature profiles at $0.6\%CH_4$ and $0.7m/s$ superficial velocity

time of $100s$. Figure 5.35 shows the comparison of three different superficial velocities, $0.7m/s$, $1m/s$, and $2m/s$.

With increasing superficial velocity, the thermal profile shifts further toward the outlet. The same behaviour is seen with an increasing cycle switch time. Both of these variables effect the gas residence time, thus have the same effect on the axial temperature profile of the reactor.

5.5.2 Methane Concentration

Methane concentration was varied for the experimental initial conditions of 0.2% methane concentration and a superficial velocity of $0.7m/s$ with a switch time of $100s$. The methane concentration was increased to 0.8% and 1.5%, respectively. Figure 5.36 shows the increasing amount of heat energy that is generated in the reactor as the methane concentration increases.

Increasing the methane concentration in the feed, will increase the thermal energy being generated through the combustion reaction. Consequently, the active packed bed sections will heat up much more rapidly.

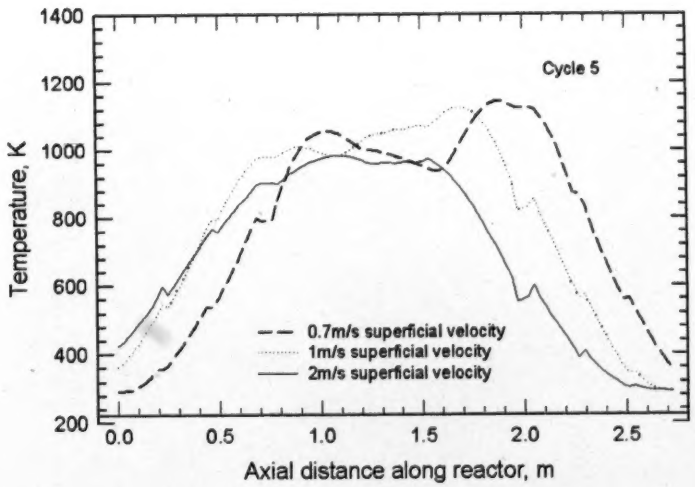

Figure 5.35: Comparison of different superficial velocities at the 5^{th} cycle. Simulated reverse flow axial temperature profiles at $0.6\%CH_4$ and switch time of $100s$

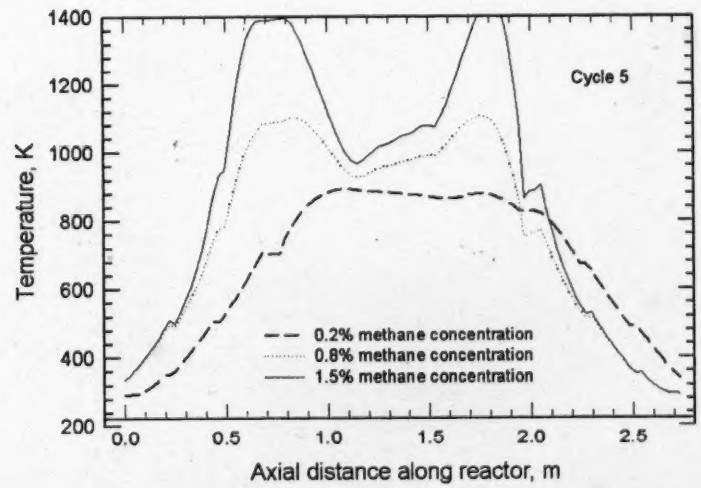

Figure 5.36: Comparison of different methane concentrations at the 5^{th} cycle. Simulated reverse flow axial temperature profiles at a superficial velocity of $0.7m/s$ and switch time of $100s$

5.6 Discussion

The previously developed simulator used to model the reverse-flow reactor showed that it is capable of predicting the trends in the reactor and, in most cases, able to predict the temperatures in the reactor. The simulator results obtained with each of the three different types of inert were mostly in agreement with the experimental results for cases with and without heat extraction.

The heating trend at high methane concentrations of 0.6%, and the cooling trend at low methane concentrations of 0.2%, were predicted by the model for all three inert types studied. Further increase in the methane concentration, up to 1% resulted in the formation of extreme hot spots within a short amount of time, predicting that the reactor would reach to very high temperatures at higher methane concentrations.

For cases with increased superficial velocities, the simulator had a tendency to over-predict the temperatures. In reality, the reactor system is three-dimensional. Perhaps the two-dimensional axially symmetric assumption is only valid until a certain point. A three-dimensional numerical model might be able to predict the temperatures more accurately. One and two dimensional models have been verified using experimental results, however, upon the development of a three-dimensional numerical model, further information can be gathered to understand the behaviour of the CFRR.

From the simulator results, it was seen that the initial profile played an important role for the predictions of the experiment. At more stable initial profiles, the model could easily predict the experimental results. However, with irregular initial temperature conditions (high superficial velocities, higher methane concentrations), the model would become less accurate and predict extreme behaviour that were not seen in the experimental results. Perhaps, a modification in how the simulator interpolates the initial conditions could lead to better agreement with the experimental results. At the same time, more experimental results measurements are required for the verification.

In some cases with heat extraction operations, the experimental results were under-predicted by the simulator, which might indicate that there is

more thermal mass in the pilot plant than that modeled in the simulator. It could be that the amount of thermal energy in the insulation of the reactor is more than what is assumed in the model. Further development to account for this possible missing thermal mass might show better agreement between the simulator and experimental results.

Chapter 6

Conclusions and Recommendations

The reverse-flow catalytic combustion technology is favourable for lean methane emissions at low feed temperatures. The flow-reversal concept is able to successfully preheat the feed gas, and contain the heat within the reactor, which eventually leads to an auto-thermal state of operation, provided that the reactor is initially heated.

Maintaining a high reaction temperature allows for complete combustion. Generally, higher methane concentrations lead to higher reactor temperatures. For methane concentrations of around 1% or more, the operation without heat extraction led to excessive temperatures.

6.1 Experimental Conclusions

Inserting the ceramic monoliths into the inert section of the reactor showed that the axial temperature profile would rise at a manageable pace. This could be due to the low thermal conductivity of the ceramic material. The outlet temperatures of the reactor would remain at fairly cool temperatures, provided the switch-time of each half cycle was properly chosen as to retain the heat within the middle of the reactor. The radial temperature profiles showed a fairly even distribution from the centre to the wall in the inert bed.

With the inert metal monoliths,the temperatures showed increased movement throughout the cycles. The material's high thermal conductivity and

low capacity for storing heat energy, resulted in a faster rate of heating at high methane concentration. Heat would easily be lost through the outlet of the reactor, as higher outlet temperatures were achieved at cycle switch times that are comparable to those used with the inert ceramic monolith. With this inert type,the catalytic beds reach high temperatures more rapidly, thus heat can be extracted sooner. If metal inert monoliths are used as a heat trap in the reactor, then shorter cycle times will have to been implemented as there are greater axial and radial temperature gradients present with this type of material. Shorter cycle time means shorter gas residence time, which could lead to less methane conversion in the active section.

The Denstone balls showed favourable behaviour for trapping the heat in the active sections of the reactor, control of the reactor, and keeping the outlet temperatures nearly at ambient. The capacity for thermal storage is greatest with the Denstone balls, thus the majority of the heat generated by the combustion reaction was contained well within the reactor. The radial temperature gradients were mostly flat, which shows an even temperature distribution in the inert sections. The major downfall with using a densely packed bed for an inert section is the high pressure drop that is developed across the reactor.

6.2 Heat Extraction Conclusions

In order to effectively extract thermal energy from the reactor while remaining in the auto-thermal state of operation, high temperatures in both the active and inert sections are favourable. Also, the amount of hot air being extracted must be carefully chosen such that the reactor remains hot. The behaviour of the axial thermal profiles during heat extraction was shared between each of the three inert types. With the extraction of heat, the inert beds would begin to cool as the active bed begins to heat up slowly until the inert beds are unable to heat the feed gas to a high enough temperature. Once this occurs, the active bed section begins to drop, and the thermal profile shows cooling. Over a very long period of time, the reactor would reach extinction. Heat

accumulation in the reactor depends on the type of inert being used. In order for pseudo-steady state operation for the reactor, the heat extraction ratio would depend on the inert type as well as the operating conditions (methane concentration, residence time, etc.).

6.3 Simulation Conclusions

The simulator that was developed for a reverse-flow reactor produced temperature profiles which were, as a whole, in agreement with the experimental results. The generic layout of the model code made it possible to study the behaviour with different inert types and operating conditions. The simulator results matched the heating and cooling trends seen with the pilot-plant reactor.

The simulations conducted with the inert ceramic monolith, inert metal monolith and inert packed Denstone balls, were in agreement with the experimental results for both high and low superficial velocities and methane concentrations. The model predicted heating of the reactor at higher methane concentrations, and cooling of the reactor at lower concentrations of methane. In the case of more dynamic operating conditions, such has high superficial velocities, high methane, shorter cycle times, the reactor would tend to slightly over-predict some temperatures in the reactor.

One of the most interesting behaviours of the simulator was that the initial temperature conditions of the operation would have an effect on the stability of the modeled temperatures. When the initial temperature profile was clear of hot spots, simulator would shows lightly less agreement with the experimental temperatures. With more stable initial temperature profiles, the model favourably predicted the experimental trends and behaviour.

The effect of increasing the methane concentration showed that the reactor temperature would rapidly increase to a dangerous state once the methane concentration exceeds about 1%. The effect of increasing the cycle time resulted in a greater heat loss through the outlets of the reactor. This same result was seen as the effect of increasing the superficial velocity of the feed. The major

advantages with using a numerical simulator is that operating conditions can be studied without excessive investment of time, money and energy.

Between the three different inert types, the simulator showed best agreement with the inert ceramic monoliths and the Denstone balls. With the results generated with the simulator, it is concluded that the model is able to produce satisfactory experimental results, given the accuracy and assumptions in the model.

6.4 Recommendations and Future Work

Further work with the numerical model and with the pilot plant are required to eventually attain a better understanding of the system. Modifications in the model will lead to more accurate predictions, while further experimental work and data will aid in verifying the reverse flow model. Some recommendations and suggestions for future work for both the experimental and simulator work is presented in the following subsections.

6.4.1 Experimental

To successfully contain the heat energy generated by the methane combustion reaction, the inert packed Denstone balls prove to show the most favourable behaviour experimentally. However, due to the high pressure drop associated with packed columns, the inert ceramic monolith is the next favourable choice for the inert bed section. The metal monoliths lead to a very dynamic system, which can become difficult to control, however are able to conduct thermal energy at a much faster rate, which can keep the catalytic beds active.

A possible inert bed configuration could be by using two or more inert types at different sections of the inert bed. For example, since the Denstone balls prevent heat from escaping, a portion nearing the entrance and exits of the reactor can be packed with Denstone balls. Because the metal monoliths are easily able to conduct thermal energy, they can be placed near the active zones of the reactor, while placing the inert ceramic monolith between in Denstone balls and metal monolith. Studying the effects of mixed inert types would

be beneficial and may lead to an optimal configuration for trapping the heat, fully combusting methane, and keeping the pressure drop of the reactor at a minimal.

Safety controls for the operation of the experimental reactor is are essential. For the case of the reverse-flow reactor, it is difficult to determine a tuning method to yield high fractional conversion, low emissions, and heat storage. The operating conditions which will result in extracting the most thermal energy may be different that the conditions for obtaining highest conversion of methane. A method for determining an optimal switch time and amount of heat extraction is yet to be developed, since these two are critical operating parameters. The optimization of the critical parameters has yet to be explored. A process control system has yet to be established for the reverse-flow catalytic combustion reactor.

The behaviour of the reverse-flow reactor on a large scale, rather than a pilot scale, would show if the reactor would remain stable at a larger scale. The effect of the cycle time on a reactor with an increased diameter and length is unknown. In reality, a constant flow of methane might be difficult to achieve. Knowledge of how long the reactor will be able to sustain the heat already in the reactor would help with the introduction of this technology to industrial and farm uses. Also the purity of the feed methane can vary with each application. Developing a reactor that will properly suit the environment and the surrounding conditions has yet to be investigated.

6.4.2 Simulator suggestions

The initial temperature profile, which the simulator used to begin its predictions, seemed to have an effect on the outcome of results. The stability of the initial profile was key for the stability of the model predictions. This would indicate that the reading of the initial profiles is very important. Perhaps the method in which the simulator interprets the initial conditions could be modified to help solve this problem.

There were instances when the simulator over-predicted the cooling in the reactor. It seems as though the pilot scale reactor is storing more thermal

energy than is predicted by the model. Modification in the code to account for this missing thermal mass may lead to better predictions of the experimental results.

Thus far, one and two dimensional numerical models have been verified with the CFRR. From what is observed, the model predicts the trends fairly accurately. A three-dimensional model might increase the accuracy of the predictions. An accurate numerical simulator is critical to further understanding the reverse-flow technology. The development of the reverse-flow reactor may lead to an economically efficient, environmentally beneficial, and widely used option for the combustion of lean methane mixtures.

Bibliography

[1] R.E. Hayes and S.T. Kolaczkowski. *Introduction to Catalytic Combustion.* Gordon and Breach Science Publishers, Reading, UK, 1997.

[2] Government of Canada. http://www.ec.gc.ca/pdb/ghg_home_e.cfm. last visited: September 22, 2003.

[3] Science Daily. http://www.sciencedaily.com/releases/2002/10/021010065923.htm. last visited: September 22, 2003.

[4] V.A. Sazonov, Z.R. Ismagilov, and N.A. Prokudina. Catalytic combustion of lean methane-air mixtures. *Catalysis Today*, 47:149–153, 1999.

[5] H. Sapoundjiev. Catalytic combustion of lean methane emissions in reactor with flow reversal operation. Environmentally Friendly Gas Technologies, 2000.

[6] Y.S. Oh, T.Y.Song, and S.J.Yoo. A study of the catalytic combustion of methane on Pd/Al_2O_3 prepared by Sol-gel method. Environmentally Friendly Gas Technologies, 2000. 2nd Canadian-Korean joint workshop.

[7] Y.S. Seo, N.J. Chung, and S.J. Cho. Surface and gas reaction of the premixed lean mixture in a catalytically stabilized combustor. Environmentally Friendly Gas Technologies, 2000. 2nd Canadian-Korean joint workshop.

[8] S. Kang and N. Jeong. Investigation of a high temperature catalytic burner to reduction furnace. Environmentally Friendly Gas Technologies, 2000. 2nd Canadian-Korean joint workshop.

[9] R. Spinicci and A. Tofanari. A study of the catalytic combustion of methane in non-steady conditions. *Applied Catalysis*, 227:159–169, 2002.

[10] A.L. Boehman. Radiation heat transfer in catalytic monoliths. *AIChE Journal*, 44(12):2745–2755, December 1998.

[11] B. Liu, M.D. Chekel, R.E. Hayes, M. Zheng, and E. Mirosh. Transient simulation of a catalytic converter for a dual fuel engine. *Canadian Journal of Chemical Engineering*, 78:557–568, 2000.

[12] K. Song, S.D. Kim, and S. Kang. Utilization of pervoskites in catalytic combustion. Environmentally Friendly Gas Technologies, 2000. 2nd Canadian-Korean joint workshop.

[13] Y.Sh. Matros and G.A. Bunimovich. Reverse-flow operation in fixed bed catalytic reactors. *Catalysis Reviews: Science and Engineering*, 38(1):1–68, 1996.

[14] C. Sapundzhiev, G. Grozev, and D. Elenkov. Non-steady state catalytic decontamination of waste gases. *Chemical Engineering Technology*, 14:209–212, 1991.

[15] G.G. Grozev and C. Sapundzhiev. Modelling of the reversed flow fixed bed reactor for catalytic decontamination of waste gases. *Chemical Engineering Technology*, 20:378–383, 1997.

[16] G. Eigenberger and U. Nieken. Catalytic combustion with periodic flow reversal. *Chemical Engineering Science*, 43(8):2109–2115, 1988.

[17] U. Nieken, G. Kolios, and G. Eigenberger. Fixed-bed reactors with periodic flow reversal: experimental results for catalytic combustion. *Catalysis Today*, 20:335–350, 1994.

[18] J.W. Geus and J.C. van Giezen. Monoliths in catalytic oxidation. *Catalysis Today*, 47:169–180, 1999.

[19] S. Salomons, R.E. Hayes, M. Poirier, and H. Sapoundjiev. Flow reversal reactor for the catalytic combustion of lean methane mixtures. *Catalysis Today*, 83:59–69, March 2003.

[20] J.L. Williams. Monolith structures, materials, properties and uses. *Catalysis Today*, 69:3–9, 2001.

[21] T.N. Haynes, C. Georgakis, and H.S. Caram. The design of reverse flow reactors for catalytic combustion systems. *Chemical Engineering Science*, 50(3):401–416, 1995.

[22] B. Glödelckler, G. Kolios, and G. Eigenberger. Analysis of a novel reverse-flow reactor concept for autothermal methane steam reforming. *Chemical Engineering Science*, 58:593–601, 2003.

[23] F. Aubé and H. Sapundjiev. Mathematical model and numerical simulations of catalytic flow reversal reactors for industrial applications. *Computers and Chemical Engineering*, 24:2623–2632, 2000.

[24] S. Salomons. Modelling the Behaviour of a Reverse-Flow Catalytic Reactor for the Combustion of Lean Methane. Master's thesis, University of Alberta, Edmonton, Alberta, 2003.

[25] M. Poirier, H.Sapoundjiev, S. Salomons, and R.E. Hayes. Pressure drop reduction by using monolith in a pilot-scale flow reversal reactor. In 17^{th} *Canadian Symposium on Catalysis, Vancouver*. Natural Resources Canada, June 2002. conference presentation.

[26] Shorter Communications. Analysis of catalytic reactor operation with periodic flow reversal. *Chemical Engineering Science*, 46(1):361–367, 1991.

[27] W.R. Smith and L.N. Bobrova. Mathematical modelling of a reverse flow reactor with catalytic surface dynamics. *Chemical Engineering Science*, 57:393–407, 2002.

[28] M. Cittadini, M. Vanni, and A.A. Barresi. Transient behaviour and start-up of periodic flow reversal reactors for catalytic decontamination of waste gases. *Chemical Engineering and Processing*, 41:431–443, 2002.

[29] G. Groppi and E. Troconi. Continuous vs discrete models of nonadiabatic monolith catalysts. *AIChE Journal*, 42(8):2382–2387, August 1996.

[30] G. Groppi, E. Troconi, and P. Forzatti. Mathematical models of catalytic combustors. *Catalysis Reviews: Science and Engineering*, 41(2):227–254, 1999.

[31] K. Zygourakis. Transient operation of monolith catalytic converters: A two-dimensional reactor model and the effects of radially nonuniform flow distributors. *Chemical Engineering Science*, 44(9):2075–2086, 1989.

[32] S. Salomons, R.E. Hayes, M. Poirier, and H. Sapoundjiev. Modelling a reverse flow reactor for the catalytic combustion of fugitive methane emissions. *Computers and Chemical Engineering*, June 2003.

[33] G. Groppi and E. Troconi. Simulation of structured catalytic reactors with enhanced thermal conductivity for selective oxidation reactions. *Catalysis Today*, 69:63–67, 2001.

[34] F.P. Incropera and D.P. DeWitt. *Fundamentals of heat and mass transfer*. John Wiley & Sons, Inc., USA, 4 edition, 1996.

[35] N. Gupta and V. Balakotaiah. Heat and mass transfer coefficients in catalytic monoliths. *Chemical Engineering Science*, 56:4771–4786, 2001.

Appendix A

List of Experiments and Simulations

A.1 List of Experiments

Table A.1: **Experiments conducted without heat extraction**

Inert material	$v\ (m/s)$	$mol\%CH_4$	**switch time** (s)
Ceramic monolith	0.3	0.2	300
	0.3	0.6	300
	0.7	0.2	100
	0.7	0.6	100
Metal monolith	0.3	0.6	400
	0.7	0.2	150
	0.7	0.6	150
	1.0	0.2	60
	1.0	0.6	60
	1.2	0.2	60
	1.2	0.6	60
Denstone balls	0.3	0.2	150
	0.3	0.6	400
	0.7	0.2	150
	0.7	0.6	150
	1.0	0.2	120
	1.0	0.6	120
	1.2	0.2	100
	1.2	0.6	100

Table A.2: **Experiments conducted with heat extraction**

Inert material	$v\ (m/s)$	$mol\%CH_4$	**switch time** (s)
Ceramic monolith	0.3	0.6	350
	0.7	0.6	130
Metal monolith	0.3	0.6	400
	0.7	0.6	150
	1.0	0.6	60
	1.2	0.6	60
Denstone balls	0.7	0.6	130
	0.7	0	150
	1.0	0.6	120
	1.2	0.6	100

A.2 List of Simulations Conducted

Table A.3: **Simulations conducted with ceramic monoliths**

simulation	$v\ (m/s)$	$mol\%CH_4$	**switch time** (s)
without heat extraction			
0029	0.3	0.2	300
0030	0.7	0.2	100
0031	0.3	0.6	300
0032	0.7	0.6	100
with heat extraction			
0048	0.3	0.6	350
0049	0.7	0.6	130
with no equivalent experiments			
0032ts1	0.7	0.6	200
0032ts2	0.7	0.6	400
0032v1	1.0	0.6	100
0032v2	2.0	0.6	100
0030m1	0.7	0.8	100
0030m2	0.7	1.5	100

Table A.4: **Simulations conducted with metal monoliths**

simulation	$v\,(m/s)$	$mol\%CH_4$	switch time (s)
without heat extraction			
0038	0.7	0.6	150
0045	0.7	0.2	150
0046	0.3	0.6	400
0058	1.0	0.2	60
0059	1.0	0.6	60
0060	1.2	0.6	60
0061	1.2	0.2	60
with heat extraction			
0054	0.7	0.6	150
0055	1.0	0.6	60
0056	1.2	0.6	60
0057	0.3	0.6	400

Table A.5: **Simulations conducted with Denstone balls**

simulation	$v\,(m/s)$	$mol\%CH_4$	switch time (s)
without heat extraction			
0033	0.3	0.6	400
0034	0.7	0.6	150
0035	0.7	0.2	150
0036	0.3	0.2	150
0039	1.0	0.6	120
0040	1.0	0.2	120
0041	1.2	0.6	100
0042	1.2	0.2	100
with heat extraction			
0044	0.7	0.0	150
0050	0.7	0.6	130
0052	1.0	0.6	120
0053	1.2	0.6	100

Appendix B

Calculations used during experiments

B.1 Heat extraction calculation

The equations used for heat extraction calculations are presented here, and were found by previous correlations. These calculations are conducted after opening the manual heat extraction valve.

flow-rate of extracted air

First the flow-rate of air through the middle pipe is calculated in units of m^3/h using the following equation:

$$air\,flow\,(m^3/hr) = \sqrt{94.34 \times PDI\,331 + 4.4} \tag{B.1}$$

where $PDI\,331$ is the pressure caused by the orifice place situated after the heat exchanger.

The density of the air passing by the orifice is calculated by the following equation:

$$\rho\,(kg/m^3) = 1.292 \times \left(\frac{273.15\,K/°C}{273.15 + TE\,333}\right) \times \left(\frac{407.2 + PI\,334}{407.2\,inH_2O/atm}\right) \tag{B.2}$$

where $TE\,333$ is the temperature of the air ($°C$) after is passes through the heat exchanger, and $PI\,334$ is the pressure reading across the reactor in units of inH_2O.

The air flow-rate is converted into units of kg/hr using the density by:

$$\dot{m}\,(kg/hr) = airflow\,(m^3/hr) \times \rho\,(kg/m^3) \tag{B.3}$$

Through previous correlations, it was found that the actual flow-rate of air was 15% lower than the calculated flowrate. The following correction had to be made, which gives the actual flow-rate of air being extracted through the U-bend.

$$corrected\,\dot{m}\,(kg/hr) = 0.85 \times \dot{m}\,(kg/hr) \tag{B.4}$$

heat extraction ratio

The ratio of air being extracted with the air being fed into the reactor is found by the following relation.

$$heat\ extraction\ ratio = \frac{flow - rate\ of\ extracted\ air}{flow - rate\ of\ inlet\ air} \tag{B.5}$$

energy balance calculations

A calculation for estimating the amount of energy being fed into the reactor is done by the following equation:

$$\dot{E}_in\,(kJ/hr) = Q_{CH_4} \times \Delta H_n \times 0.651\,g/L \tag{B.6}$$

where Q_{CH_4} is the volumetric flow-rate(L/hr) of methane in the inlet, and ΔH_n is the enthalpy of combustion of methane (kJ/g).

The energy being extracted from the mid-section was estimated by the following equation:

$$\dot{E}_out\,(kJ/hr) = corrected\,\dot{m} \times C_p \times (T_{out} - T_{in}) \tag{B.7}$$

B.2 Calculating air velocities

The following equations show how the mass flow-rate of the compressed air was converted into a superficial velocity. The apparent velocity, assuming the reactor is empty and at ambient temperature was found by using the internal

diameter, D_R, of the reactor column, $0.197m$. The internal area of the empty reactor was found as follows:

$$\begin{aligned} A &= \frac{\pi D_R^2}{4} \\ &= \frac{\pi(0.197m)^2}{4} \\ &= 0.0305\,m^2 \end{aligned} \tag{B.8}$$

The density of compressed air at 20^oC and $1atm$ was $1.205\ kg/m^3$. The mass flow-rate of air was converted to a volumetric flow-rate using the density.

$$\begin{aligned} \dot{v}\,(m^3/hr) &= \frac{\dot{m}\,(kg/hr)}{\rho\,(kg/m^3)} \\ &= \frac{100\ kg/hr}{1.205\ (kg/m^3)} \\ &= 82.99\,m^3/hr \end{aligned} \tag{B.9}$$

The volumetric flow-rate is then divided by the internal area of the column, and appropriate unit conversions are used to obtain the superficial velocity ,v_s, in units of m/s.

$$\begin{aligned} v_s &= \frac{\dot{v}\,(m^3/hr)}{A\,(m^2)} \times \frac{1\ hr}{3600\ s} \\ &= \frac{82.99\,m^3/hr}{0.0305\,m^2} \times \frac{1\ hr}{3600\ s} \\ &= 0.756\,m/s \end{aligned} \tag{B.10}$$

Therefore, at ambient conditions, when the reactor is empty, the following relation applies for the compressed air.

$$100\,kg/hr = 82.99\,m^3/hr = 0.756\,m/s \tag{B.11}$$

This ratio was used to convert the mass flow of air into a superficial velocity. For example, if the inlet air flow rate for an experiment was set to $40kg/hr$, through the application of ratios, the corresponding superficial velocity would be $0.30m/s$.